

Analyses of gene regulatory networks
involved in murine oocyte formation

福田 胡桃

博士（理学）

総合研究大学院大学

生命科学研究科

遺伝学専攻

平成30（2018）年度

**Analyses of gene regulatory networks
involved in murine oocyte formation**

Fukuda, Kurumi

Doctor of Philosophy

Department of Genetics

School of Life Science

SOKENDAI

(The Graduate University for Advanced Studies)

Contents

1. Abstract2
2. Gene symbols and abbreviation6

Chapter I: Requirement of the 3'-UTR-dependent suppression of DAZL in oocytes for pre-implantation mouse development

3. Introduction9
4. Results12
5. Discussion21

Chapter II: Analysis of pre-granulosa cell progenitor differentiation in primordial follicle formation

6. Introduction25
7. Results29
8. Discussion43
9. Material and Methods in Chapter I48
10. Material and Methods in Chapter II57
11. Table legends63
12. References67
13. Acknowledgements74
14. Figures75

1. Abstract

Mammalian oogenesis consists of two genetically distinct events. One is meiosis, which starts in germline cysts in embryonic ovaries, and the other is folliculogenesis occurred after birth (Fig.1). The latter process is initiated by the event termed primordial follicle formation in neonatal ovaries, by which germline cysts are separated and oocytes are enclosed by their supporting somatic cells, pre-granulosa cells. The interaction between germ cells and granulosa cells is known to be important to generate functional oocytes. However, the underlying mechanisms remain elusive.

In my thesis study, I addressed the mechanisms of oogenesis after birth via two different perspectives regarding germ cells and somatic cells. In Chapter I, I described my investigation of the function of a germ cell-specific factor, DAZL, in the postnatal ovary, and in Chapter II, I discussed my analysis of gene expression changes in somatic cells focusing on the pre-granulosa cell lineage during primordial follicle formation.

In Chapter I, I focused on an RNA-binding protein implicated in the translational promotion, DAZL, which is known to be a critical factor for meiotic progression and is expected to play a role in folliculogenesis. First, I examined *Dazl* function in the postnatal ovary by generating postnatal oocyte-specific *Dazl* knockout mice. However, I unexpectedly found that the *Dazl* gene is dispensable for oocyte

differentiation in postnatal ovaries as mutant females were fertile and produced a normal number of pups. In addition, DAZL protein expression was not detected in the postnatal ovary, whereas *Dazl* mRNA was continuously observed, suggesting that DAZL is post-transcriptionally suppressed after birth.

Next, I asked whether DAZL translation was suppressed via its 3'-UTR sequence. To address this question, I removed the *Dazl* 3'-UTR sequence and examined DAZL expression. As a result, DAZL expression was increased in the 3'-UTR-deleted transgenic ovaries, even postnatally, suggesting that DAZL translation is suppressed in a 3'-UTR-dependent manner. Furthermore, the increased DAZL expression caused the mothers to have a reduced litter size due to the failure of pre-implantation development, indicating that the 3'-UTR-dependent suppression of DAZL in postnatal oocytes may be required for pre-implantation mouse development. Based on these results, I concluded that the proper switching of DAZL expression from “on” in the embryonic stage to “off” in the postnatal stage is essential to produce the next generation.

In Chapter-II, I described my transcriptome analyses of pre-granulosa cell progenitors in wild-type and germ cell-deficient ovaries using a FACS method that selectively isolated *Lgr5*-positive developing pre-granulosa cells. Through these comparative analyses, I identified increased and decreased genes associated with

pre-granulosa cell differentiation. The most marked changes I found during primordial follicle (PF) formation were the significant downregulation of Wnt and TGF- β signaling pathway genes, and the upregulation of Notch and PI3K pathway genes. Although *Lgr5*-positive pre-granulosa progenitors developed in the absence of germ cells, the timing of pre-granulosa cell differentiation is influenced by oocytes, suggesting that crosstalk between germ cells and *Lgr5*-positive cells is important for the differentiation of pre-granulosa cells. Thus, I further classified the genes showing increased or decreased expression during PF formation as germ cell-dependent or -independent. Based on this classification, gene upregulation was largely dependent on germ cells, whereas the downregulated genes, which comprised putative factors involved in the retention of germline cysts, were regulated in both germ cell-dependent and -independent manners. These results provide insight into the gene regulatory networks functioning in differentiating pre-granulosa cells during primordial follicle formation. Moreover, they will help further analyses to identify unknown factors required for pre-granulosa cell differentiation.

Taken together, my study revealed dynamic changes from the embryonic to postnatal stages during oocyte development such as *DAZL* expression regulation in oocytes and gene expression changes during pre-granulosa cell differentiation in

somatic cells. By focusing on different events related to oocyte development, as described in Chapters I and II, my study helps clarify the complicated regulatory mechanisms at the transcriptional and post-transcriptional levels necessary for generating a functional oocyte.

2. Gene Symbols and Abbreviation

Gene Symbols:

Chapter I

Cpeb1: Cytoplasmic polyadenylation element binding protein 1

Pumilio1: Pumilio RNA-binding family member 1

Maskin: CPEB-associated factor Maskin

Msy2: Minisatellite Y 2

Dazl: Deleted in azoospermia-like

Foxl2: Forkhead box L2

Gdf9: Growth differentiation factor 9

Nanos2: Nanos C2HC-type zinc finger 2

Tex19.1: Testis expressed gene 19.1

Tpx2: TPX2, microtubule-associated

Cdc20: Cell division cycle 20

Arid1a: AT rich interactive domain 1A

Bub1b: BUB1B, mitotic checkpoint serine/threonine kinase

Suz12: SUZ12 polycomb repressive complex 2 subunit

Chapter II

Rac1: Rac family small GTPase 1

Stat3: signal transducer and activator of transcription 3

Jag1: jagged 1

Bmp15: bone morphogenetic protein 15

Nobox: NOBOX oogenesis homeobox

Kit: KIT proto-oncogene receptor tyrosine kinase

Figla: folliculogenesis specific basic helix-loop-helix

Lgr5: leucine rich repeat containing G protein coupled receptor 5

Nanos3: nanos C2HC-type zinc finger 3

Mvh: DEAD (Asp-Glu-Ala-Asp) box polypeptide 4

K8: keratin 8

Igf1r: insulin-like growth factor I receptor

Notch2: notch 2

Notch1: notch 1

Hey1: hairy/enhancer-of-split related with YRPW motif 1

Dmrt1: doublesex and mab-3 related transcription factor like family A1

Heyl: hairy/enhancer-of-split related with YRPW motif-like
Nrarp: Notch-regulated ankyrin repeat protein
Smad3: SMAD family member 3
Bmp2: bone morphogenetic protein 2
Fst: follistatin
Id2: inhibitor of DNA binding 2
Id3: inhibitor of DNA binding 3
Nog: noggin
Snai2: snail family zinc finger 2
Acvr1c: activin A receptor, type IC
Wnt2b: wingless-type MMTV integration site family, member 2B
Gprc5b: G protein-coupled receptor, family C, group 5, member B
Cthrc1: collagen triple helix repeat containing 1
Scyl2: SCY1-like 2
Caprin2: caprin family member 2
Shisa6: shisa family member 6
Mycl: v-myc avian myelocytomatosis viral oncogene lung carcinoma derived
Arnt2: aryl hydrocarbon receptor nuclear translocator 2
Klf13: Kruppel-like factor 13
Nr0b1: nuclear receptor subfamily 0, group B, member 1
Bhlhe41: basic helix-loop-helix family, member e41
Pbx3: pre B cell leukemia homeobox 3
Sp5: trans-acting transcription factor 5
Zfp52: zinc finger protein 52
Rfx5: regulatory factor X, 5 (influences HLA class II expression)
Tcf12: transcription factor 12
Sox11: SRY (sex determining region Y)-box 11
Zfp503: zinc finger protein 503
Grk5: G protein-coupled receptor kinase 5
Tiam1: T cell lymphoma invasion and metastasis 1
Daam1: dishevelled associated activator of morphogenesis 1
Celal: chymotrypsin-like elastase family, member 1

Abbreviation

Chapter I

RT-qPCR: quantitative reverse transcription-polymerase chain reaction

ICBs: intercellular bridges

PF: primordial follicle

PrF: primary follicle

SF: secondary follicle

AF: antral follicle

cKO: conditional knockout

BAC: bacterial artificial chromosome

RBPs: RNA-binding proteins

MII: meiosisII

ZFN: Zinc Finger Nuclease

TALEN: Transcription activator-like effector nuclease

CRISPER/Cas9: Clustered Regularly Interspaced Short Palindromic Repeats/CRISPR associated nucleases

Chapter II

PF: primordial follicle

Pre-G: pre-granulosa cells

Lgr5-GFP: Lgr5-GFP-Ires-CreERT2

OE: ovarian epithelial

FACS: fluorescence-activated cell sorter

DEGs: differentially expressed genes

FSH: follicle stimulating hormone

Chapter I: Requirement of the 3'-UTR-dependent suppression of DAZL in oocytes for pre-implantation mouse development

3. Introduction

The production of functional oocytes is an essential process in the female ovary, by which genetic information is passed to the next generations. For successful oocyte development, gene expression needs to be precisely regulated according to the developmental stages and environmental cues such as gonadotropic hormones. Oocytes that fail to regulate proper gene expression are degenerated during their development or are unable to proceed with embryonic cleavage even if they are fully developed [1]. Therefore, unveiling mechanisms controlling the quality of oocytes is a crucial issue to understand the molecular basis of female reproduction.

Post-transcriptional gene regulation mediated by RNA-binding proteins is an important molecular mechanism involved in this process. An evolutionarily conserved and well-documented post-transcriptional event is the translational suppression and storage of maternal mRNAs with shorter poly (A) tails [2]. Although the genome is actively transcribed and proteins are produced during oocyte growth, transcription become inactive in full-grown oocytes and stored maternal mRNAs are used for protein

synthesis in early zygote development [3]. These processes are orchestrated by a battery of relevant RNA-binding proteins, including cytoplasmic polyadenylation element binding proteins (CPEB), maskin, and other germ cell-specific RNA-binding proteins [4,5,6,7]. In addition to the oocyte maturation process, germ cell-specific RNA-binding proteins are also responsible for multiple processes in oogenesis. For instance, CPEB1 and Pumilio1 are involved the progression of meiotic prophase I in the embryonic ovary[8,9], and MSY2 is involved in follicle development after birth in mice [10,11], suggesting the significant contribution of post-transcriptional gene regulation throughout oogenesis.

Deleted in azoospermia-like (DAZL) is a member of the evolutionarily conserved DAZ family of RNA-binding proteins that acts as a translational activator in mice [12]. Biochemical and structural analyses showed that DAZL binds to the U-rich sequences of its target's 3'-UTR [13,14,15]. Genetic analyses revealed that DAZL is indispensable for gametogenesis in both males and females [16,17,18]. As DAZL is reportedly required for sexual differentiation of primordial germ cells, progression of meiotic prophase I in embryonic female germ cells [19], and for the progression of meiosis in maturing oocytes [20], it is believed that DAZL is involved in female germ cell development throughout oogenesis. However, the role of DAZL in follicular

oocytes remains unknown, because *Dazl*-deficient oocytes die due to the failure of meiotic initiation in the embryonic ovary [16,21]. Moreover, although the previous immunohistochemical analysis demonstrated that DAZL was expressed in both embryonic and follicular oocytes in postnatal ovaries [16], it was also noted that DAZL signals were not detectable by western blotting in ovaries 1 to 2 weeks after birth [22]. Therefore, further analysis is required to clarify contradiction of DAZL function and expression in postnatal ovary.

In this study, I investigated DAZL expression in embryonic and postnatal ovaries, and found that DAZL was translationally suppressed in a 3'-UTR-dependent manner in follicular oocytes. Genetic analysis by knocking out the *Dazl* gene in a follicular oocyte-specific manner indicated that *Dazl* is dispensable for follicular growth, maturation, and fertilization. On the other hand, the 3'-UTR-dependent suppression of DAZL in follicular oocytes is required for the progression of normal pre-implantation development. Our data clarify the previously ambiguous expression pattern of DAZL in the postnatal ovary, and simultaneously demonstrate the significance of the post-transcriptional suppression of DAZL in follicular oocytes.

4. Results

DAZL is post-transcriptionally suppressed in postnatal oocytes

To examine *Dazl*/DAZL expression in detail, I performed quantitative reverse transcription-polymerase chain reaction (RT-qPCR) and western blotting analyses using ovaries from embryos until juvenile stages (Fig. 2A and B). RT-qPCR data showed that *Dazl* mRNA was constantly expressed and expression fluctuations were less than 1.6-fold among all stages investigated (Fig. 2A). On the other hand, the amount of DAZL protein markedly changed during oocyte development (Fig. 2B). Although it was abundant in embryonic ovaries, with the strongest expression at embryonic day (E) 15.5, the expression declined in newborn ovaries. Afterwards, DAZL expression further declined and was hardly detectable in 1- and 2-week ovaries, which is consistent with previous descriptions in one paper [22].

As DAZL expression significantly decreased in the newborn ovary and onward, I next asked whether this reduction in DAZL was correlated with the formation of primordial follicles. In the embryonic ovary, oocytes are connected each other by intercellular bridges (ICBs). Within a few days after birth, ICBs are broken and each oocyte is enclosed by pre-granulosa cells, resulting in the formation of primordial follicles [23]. Thus, I examined the expression changes of DAZL in perinatal ovaries by

immunostaining DAZL together with a granulosa cell marker, forkhead box protein L2 (FOXL2), from E18.5 to 1week (W) ovaries. Strong DAZL signals were observed in most oocytes until the day of birth (P0), when a large number of oocytes were still connected each other. However, at one day after birth (P1), its expression began to decrease in some oocytes (Fig. 2C, open arrowheads). The expression of DAZL was further decreased at two days after birth (P2), at which point, many oocytes formed primordial follicles (Fig. 1C, yellow arrowheads) and exhibited weaker DAZL expression than cystic-oocytes (Fig. 1C, white arrowheads). Thereafter, the weakened DAZL expression was observed in 1-week ovaries. These data suggest that DAZL is decreases in oocytes coinciding with the development of primordial follicles.

DAZL is not required for oogenesis in the postnatal ovary

Both immunostaining and western blotting analyses revealed that DAZL was decreased in oocytes shortly after birth, which raised the possibility that DAZL is dispensable for follicular development. To test this possibility, I used conditional *Dazl* knockout (cKO) strategy (Fig. 3A). *Dazl*^{fl^{ox}} mice were crossed with a postnatal oocyte-specific Cre mouse line, *Gdf9-iCre*, which expresses improved Cre recombinase from P2 oocytes [24]. The *Dazl* gene was successfully disrupted by *Gdf9-iCre*, as evidenced by

RT-qPCR and western blotting, in which both *Dazl* mRNA and DAZL protein were hardly detectable in *Dazl* cKO ovaries (Fig. 3B and C). I also confirmed that our *Dazl* KO (*Dazl*^{1lox}) allele was a exon-deleted and non-functional allele, since the phenotype of (*Dazl*^{1lox/1lox}) females showed similar defect to previously reported *Dazl*-null mice (Fig.4A and B)[16]. On histological analysis, *Dazl* cKO ovaries as well as control ovaries contained both primordial and growing follicles (Fig. 5A). Notably, cKO ovaries did not have any significant differences in the number of primordial or growing follicles (Fig. 5B). These data suggest that DAZL is dispensable for the survival and growth of follicular oocytes.

In order to evaluate the reproductive capability of *Dazl* cKO oocytes, I next crossed *Dazl* cKO females with wild-type (WT) males. I found that *Dazl* cKO females were fertile and produced a normal number of pups (Fig. 5C). The average litter size delivered from *Dazl* cKO females (11.3±0.62) was almost identical with that from WT (12.0±2.83). I also confirmed that all progeny delivered by *Dazl* cKO females were heterozygotes for the *Dazl*^{1lox} allele (n=258). These results were surprising because a previous report stated that *Dazl* knockdown in MII oocytes results in the defective progression of the oocyte to zygote transition due to the defective formation of meiotic spindle [20]. However, MII oocytes derived from *Dazl* cKO females did not have

abnormal spindle morphology (Fig. 5D). These data indicate that DAZL is not required for the maturation of oocytes or subsequent fertilization.

DAZL is suppressed in a 3'-UTR dependent manner

In embryonic male germ cells, *Dazl* is post-transcriptionally suppressed in a 3'-UTR-dependent manner by a male-specific RNA-binding protein, NANOS2 [25]. As DAZL decreases in postnatal ovaries, it is possible that *Dazl* is also post-transcriptionally suppressed in a 3'-UTR-dependent manner by unidentified mechanisms in follicular oocytes. In order to test this possibility, I used our bacterial artificial chromosome (BAC)-carrying transgenic mouse line, in which the FLAG tag was inserted at the C-terminus of *Dazl* and the *Dazl* 3'-UTR was flanked with *Frt* sequences (*Dazl 3F*, Fig. 6A upper) [25]. The significance of the *Dazl* 3'-UTR for its expression was assessed by crossing the BAC transgenic female with a *Rosa-Flp* male (*Dazl 3F;Flp*, Fig. 6A lower). RT-qPCR showed that the amount of *Flag-Dazl* mRNA was increased in both *Dazl 3F* and *Dazl 3F;Flp* ovaries in P0 to 3W (Fig. 6B), in which the effect of removing the 3'-UTR was observed. Similarly, the total *Dazl* expression level (*Flag-Dazl* + endogenous *Dazl*) was increased after birth although the difference between *Dazl 3F* and *Dazl 3F;Flp* was not significant except for the P0 ovary (Fig. 6B and C). In contrast,

FLAG-DAZL expression analyzed by western blotting was greatly increased after birth only in *Dazl 3F;Flp* (Fig. 6D). FLAG-DAZL (filled arrowheads) decreased in *Dazl 3F* ovaries from P0 onward, which was consistent with the reduction in endogenous DAZL (open arrowhead), its expression was continuously observed in P0, 1W, and 2W ovaries when the 3'-UTR was removed. Quantification of FLAG-DAZL expression revealed that its expression increased 20-fold in *Dazl 3F;Flp* at P0 (Fig. 6E). Although it is possible that FLAG-DAZL expression observed in P0 ovary in *Dazl 3F;Flp* could be due to the increased or stabilized mRNA expression, the FLAG-DAZL expression at 1W and 2W may be caused by the efficient translation of DAZL. The results of western blotting were also supported by immunostaining. Both total- and FLAG-DAZL expression was strongly observed in *Dazl 3F; Flp* ovaries (Fig. 6F and Fig. 7), whereas their expression levels in WT and *Dazl 3F* ovaries were comparable with those in *Dazl* cKO ovaries. Furthermore, strong DAZL expression was observed in all stages of follicular oocytes in *Dazl 3F; Flp* ovaries (Fig. 7). These data indicate that DAZL is post-transcriptionally suppressed in a 3'-UTR-dependent manner in follicular oocytes.

Role of DAZL suppression in female reproduction

To investigate the role of 3'-UTR-dependent DAZL suppression in female reproduction,

I crossed BAC transgenic females with WT males when female mice reached 6 weeks old. Each pair was kept in a breeding cage until female mice became 30 weeks old, and the number of pups delivered during this period was counted. I found that BAC transgenic females were fertile regardless of the presence or absence of the *Dazl* 3'-UTR (Fig. 8A). The number of total pups delivered by *Dazl3F* females (39.8 ± 5.5 , $n=5$) was slightly lower compared with that by control females (53.1 ± 9.1 , $n=7$). Interestingly, *Dazl 3F; Flp* females produced less than half the number of pups compared to control and *Dazl3F* females (18.6 ± 11.3 , $n=5$). Thus, these results suggest that DAZL overexpression results in litter size reduction. We next analyzed the number of deliveries and the number of pups in each delivery. The number of pups in each delivery was fewer in mutants than WT females but much clear difference was observed in *Dazl 3F; Flp* mice (Fig. 8B). On the other hand, the number of deliveries was not significantly different among genotypes (Fig. 8C). In addition, there were no biases in sex ratio of delivered pups (Fig.8D). These results suggest that the reduced female fecundity was due to defects during follicular development, fertilization, or zygote development after fertilization, but not the shortened reproductive lifespan.

Excess DAZL is deleterious for pre-implantation development

To determine the cause of the litter size reduction in the DAZL overexpressing females, I examined the development of oocytes, fertilization, and pre-implantation development. Histological analysis revealed that DAZL overexpressing ovaries did not have significantly different numbers of primordial, primary, secondary or antral follicles compared with WT ovaries (Fig. 9A and B). I next asked whether ovulation normally occurs by counting the number of ovulated one-cell embryos. However, the number was not significantly different among the genotypes (Fig. 9C). These data suggest that folliculogenesis and subsequent ovulation proceeds normally even in DAZL overexpressing females. Thus, to examine whether these ovulated eggs developed normally, I measured the proportion of blastocysts by flushing E3.5 embryos from oviducts. I cultured the collected embryos for a further two days and then counted the embryos to avoid the lower number only due to the different timing for fertilization (Fig. 10A). I found that only 56.1% of embryos derived from *Dazl 3F; Flp* females developed into blastocysts, whereas more than 97.3 and 97.1% embryos derived from control and *Dazl 3F* females became blastocysts, respectively. The development of the remaining 43.9% of *Dazl 3F; Flp* embryos stopped at the 1-cell to morula stages. These observations were reproduced in 1-cell embryo culture experiments, in which development was strongly disrupted in embryos from *Dazl 3F; Flp* females (Fig. 10B).

Statistical analysis revealed that development was arrested during 1- to 4-cell and 8-cell to blastocyst stages in embryos from *Dazl3F; Flp* mother because number of survived embryos were significantly reduced compared to number of 1 cell embryos (Fig. 10C). Besides, the spindle morphology was normal in *Dazl3F; Flp* oocytes (Fig. 11). These results indicate that the reduction of pups in *Dazl 3F; Flp* females was due to defective pre-implantation development. As strong DAZL expression was observed in *Dazl 3F; Flp* until the MII oocyte stage but decreased in 1-cell embryos and was no longer detectable in 2-cell embryos (Fig. 12A, B and C), it is likely that the stronger expression of DAZL until MII oocytes causes the defect in pre-implantation development.

Effect of DAZL overexpression on its target mRNAs

As *Dazl* is implicated in translational promotion in mice, excess DAZL expression in *Dazl 3F; Flp* oocytes may abnormally induces protein expression of its target genes and may make deleterious effects for pre-implantation development. To test this possibility, I examined the mRNA and protein expression of a well-known DAZL target gene *Tex19.1* in MII oocytes [26]. On the contrary to my speculation, the expression levels of *Tex19.1* is reduced and the TEX19.1 protein expression did not show significant change in *Dazl 3F; Flp* oocytes (Fig. 13A and B). From this result, I speculated that the excess

DAZL may abnormally suppress its target RNAs because DAZL also work as a component of stress granules, cytoplasmic RNP granules involved in translational suppression or mRNA storage in the testis [27]. Thus, I investigated the mRNA expression of the other putative DAZL targets shown in previous study [20,28]. However, there were no significant expression changes among the genotype (Fig. 13C). Although more analysis is required, it is unlikely that excess TEX19.1 protein production which shown here is responsible for pre-implantation developmental defects.

5. Discussion

In this study, I demonstrated that DAZL expression is post-transcriptionally suppressed in a 3'-UTR-dependent manner in postnatal oocytes. Although DAZL has been thought to function in postnatal oocytes, our data suggest that DAZL is not required for postnatal oocyte development. As support for this idea, analysis of conditional *Dazl* knockout mice revealed that DAZL is dispensable for postnatal oocyte development. Furthermore, excess DAZL expression results in litter size reduction. These data indicate that post-transcriptional suppression of *Dazl* plays a crucial role in normal female reproduction.

It was previously reported that DAZL was expressed in growing oocytes [16], but a later study stated that DAZL was not detectable in the postnatal ovary [22]. Therefore, it has been unclear whether DAZL plays a role in follicular oocytes. Our results answered this question; DAZL expression is suppressed in follicular oocytes and is dispensable for oogenesis after birth. Interestingly, this suppression coincides with the formation of primordial follicles. As *Dazl* mRNA was continuously expressed in oocytes regardless of developmental stages, it is likely that post-transcriptional gene regulatory mechanisms shift between cystic oocytes and follicular oocytes. Importantly, DAZL suppression requires its 3'-UTR, suggesting the presence of some mechanisms

regulating DAZL expression via recognizing the *Dazl* 3'-UTR sequence in postnatal oocytes. In many developmental processes, post-transcription is regulated by microRNAs and RNA-binding proteins [29]. However, it was reported that the function of microRNA is globally suppressed in oocytes and early embryonic development [30]. Thus, it is possible that *Dazl* expression is regulated by some RNA-binding proteins (RBPs). One possible candidate RBP for DAZL suppression is CPEB1, a mammalian ortholog of *Xenopus* CPEB. CPEB acts as both a translational activator and suppressor of its target mRNAs depending on its phosphorylation state [31,32]. CPEB1 is expressed in postnatal oocytes and promotes the translation of *Dazl* in MII oocytes[20], thus it may also suppress *Dazl* in follicular oocytes. Further expression and functional analyses, including those of the phosphorylation state of CPEB1 are required to address this question.

Our oocyte-specific *Dazl* KO females exhibited no ovarian developmental defect and the MII oocytes had no spindle abnormalities. Furthermore, the *Dazl* cKO females produced normal numbers of pups. These observations were inconsistent with Chen and colleague's results that DAZL depletion in MII oocytes results in defective spindle formation in meiosis II [20]. One possible explanation for this contradiction is the method of gene depletion. I used the Cre-loxP system for *Dazl* cKO *in vivo*, whereas

Chen et al. used morpholino knock-down in MII oocytes. A recent zebrafish report found that approximately 80% of phenotypes induced by morpholino do not correlate with mutant phenotypes induced by ZFN, TALEN or CRISPER/Cas9; therefore, the above-mentioned knock-down phenotype may result from indirect effects [33]. Alternatively, it is possible that some system that compensates for DAZL function works in *Dazl*-cKO MII oocytes because a previous study reported that the activation of a compensation system rescued deleterious mutations, which was not observed after translational or transcriptional knockdown [34]. Further analysis is required to evaluate the contribution of RNA-binding proteins for the progression of meiosis II.

Introducing the BAC transgenic allele in the *Dazl*^{+/+} background reduced litter size even in the presence of the 3'-UTR (Fig. 8). As a previous study reported that *Dazl*^{+/-} females produced more pups than *Dazl*^{+/+} females [22], the slight reduction in litter size by our *Dazl* 3F mice may be attributed to the dosage effect of the *Dazl* gene. However, our histological and embryo culture experiments did not reveal any abnormalities in *Dazl* 3F mice. In addition, I was unable to observe obvious differences in resorption after implantation (data was not shown). One possible explanation is that insertion of the BAC transgene influences female reproduction.

Our results suggest that the suppression of *Dazl* translation in follicular oocytes

is required for producing the proper number of progenies. However, why excess DAZL expression causes defective pre-implantation development remains unclear. As DAZL has been implicated in the positive regulation of translation [14,35,36], it is possible that the observed defect may be due to abnormal translational promotion. However, our RT-qPCR and western blotting analyses failed to support the idea. Alternatively, it is also possible that excess DAZL abnormally suppresses its target RNAs because DAZL works as a component of stress granules, cytoplasmic RNP granules involved in translational suppression or mRNA storage, in the testis [27,37]. This might explain the *Tex19.1* reduction in in *Dazl 3F; Flp* oocytes. Thus, downregulation of DAZL may be required for the promotion rather than suppression of some target translation. In any cases, further analysis is required for downstream event which caused pre-implantation defects in *Dazl3F; Flp*.

Chapter II: Analysis of pre-granulosa cell progenitor differentiation in primordial follicle formation

6. Introduction

Primordial follicle (PF) formation is the first important step of folliculogenesis. During fetal development, female germ cells proliferate with incomplete cytokinesis and constitute germline cysts, in which oocytes are connected each other via intercellular bridges (Fig. 14) [38,39]. From prenatal embryonic stage, germ cells start to separate each other and are finally enclosed by pre-granulosa cells, resulting in the formation of PFs around birth (Fig. 14) [40,41]. Afterward, some PFs start to grow and/or die while the others retain their dormant state, which regulates female reproductive life span [23,42]. As follicles develop, the pre-granulosa cells become cuboidal granulosa cells in the primary follicle and proliferate into multilayers in the secondary and antral follicles. If serious defects occurred in either oocytes or granulosa cells during the PF formation, female may become infertile.

To accomplish PF formation, reciprocal interactions between oocytes and granulosa cells must be required (Fig. 15). It is reported that RAC1 facilitates the nuclear import of STAT3 to activate the expression of *Nobox* in oocytes [43]. Up-regulated transcriptional factor NOBOX may further activate transcriptions of *Jag1*,

Gdf9 and *Bmp15*, which promotes pre-granulosa cell development, germline cysts breakdown, and PF formation [43]. Other than STAT3-dependent pathway, KIT and JNK signaling are involved in this step [44,45]. In addition, FIGLA, a germ cell-specific transcription factor regulating the expression of oocyte-specific genes, has been implicated in PF formation [46,47].

In ovarian development, all granulosa cell lineages originate from GATA4+ cells (blue cell in Fig. 16). Some of them directly differentiate into FOXL2+ cells (magenta in Fig. 16) in early embryonic stage, which become medullary follicle and contribute to the follicle development in young adulthood (not focused on this study). The other cells that localize to cortical region marked by *Lgr5* (green in Fig. 16) contribute to the primordial follicle formations, whereas a part of *Lgr5*+ cells differentiate into FOXL2+ during embryonic stage as a medullary follicle. The other *Lgr5*+ cells that contribute to primordial follicle formation finally differentiate into FOXL2+ cell (focused on this study). Therefore, it has been shown that *Lgr5*-positive cells are the major source of pre-granulosa cells.

LGR5 is known to enhance the WNT/ β -catenin signaling pathway, which may be pivotal for ovarian pre-granulosa cell differentiation and various morphogenetic processes [48,49]. *Lgr5*-positive cells (Fig. 14 shown as green cells) emerge from E13.5

and are distributed in the cortical region of ovary and ovarian surface epithelium in the late embryonic stage [50]. Around birth, *Lgr5*-positive cells locating in the cortical area differentiate into pre-granulosa cells marked by FOXL2 expression (Fig. 14 shown as magenta cells), which enclose single oocyte to form PF [50,51,52]. FOXL2 is a transcription factor crucially required for granulosa cell differentiation [53,54,55,56,57]. In the FOXL2 positive pre-granulosa cells, the NOTCH2 signaling pathway is activated by binding with oocyte-derived ligand protein JAG1 [47,58]. The activation of the NOTCH2 signaling pathway up-regulates downstream transcription factors, which are necessary for germ cell cyst breakdown and PF formation [59].

To accomplish PF formation, differentiation of *Lgr5*-positive cells to *Foxl2*-positive pre-granulosa cells is one of fundamental event. However, it is still unclear what is the difference between *Lgr5*-positive progenitor and pre-granulose cells at molecular level and how germ cells contribute to the differentiation of pre-granulosa cells. To address these questions, I decided to perform transcriptome analysis of differentiating granulosa cells in a different time point along developmental timeline. I also analyzed transcriptomes of *Lgr5*-positive cells derived from two distinct mutant ovaries; *Nanos3*-KO lacking germ cells and *Figla*-KO exhibiting abnormal PF formation.

My transcriptome analyses revealed that the perinatal period from E17.5 to P1 is a critical period for pre-granulosa cell differentiation, in which mutual interaction with germ cells are required. I also found that cell-autonomous program may exist for the initial development and maintenance of pre-granulosa progenitors. These results help the deep understanding of gene regulatory network in differentiating pre-granulosa cell during PF formation.

7. Result

Isolation of *Lgr5*-positive pre-granulosa progenitors

To investigate gene expression profile of pre-granulosa cells (hereafter we refer pre-G cells) during PF formation, it is required to isolate pre-G progenitors from perinatal ovaries. Recent study reported that *Lgr5* was expressed in pre-G progenitors (Fig. 17A)[51,60]. Thus, I took advantage of *Lgr5-GFP-Ires-CreERT2* (*Lgr5-GFP*) mice to identify pre-G progenitors [61]. However, *Lgr5* is also expressed in ovarian epithelial (OE) cells. To distinguish pre-G progenitor and epithelial cells, I developed a method to isolate only *Lgr5*-GFP-positive pre-G progenitor by using Mito tracker, an orange fluorescent dye, which labels mitochondria in living cells. By culturing perinatal ovaries from *Lgr5-GFP* mice with Mito tracker for a short time, I could label only OE cells as the dye does not penetrate inside of ovary (Fig. 17B). Then, *Lgr5*-GFP single-positive cells and *Lgr5*-GFP/Mito tracker double-positive cells were separately isolated by fluorescence-activated cell sorter (FACS) (Fig. 17C). I confirmed successful isolation of each population by direct fluorescence observation (Fig. 17D) and RT-qPCR using specific marker genes for germ cells (*Mvh*) and pre-granulosa cells (*Foxl2*) (Fig. 17E). *Lgr5*-GFP single positive cells exhibited stronger *Foxl2* expression whereas both *Lgr5*-GFP single and *Lgr5*-GFP/Mitotracker double positive cells showed weaker

expression of *Mvh*, respectively (Fig. 17E). These results indicate that the method I developed works effectively for the isolation of pre-G progenitors.

Gene expression profile of pre-G progenitors during PF formation

I collected *Lgr5*-GFP single-positive cells from E17.5, P1, and P3 ovaries by FACS sorting (green square shown in Fig. 18A). Density plot analysis showed that signal intensities of *Lgr5*-GFP single-positive cells was gradually decreased as ovarian development proceeded (Fig. 18A). These observations are consistent with previous reports showing that *Lgr5*-positive cells differentiate to FOXL2-positive pre-G cells [50,51]. As previously reported, oocytes that were connected each other and surrounded by *Lgr5*-positive cells at E17.5 (we refer this structure as germ line cyst) were mostly separated each other and developed to PFs at P3 (Upper panel in Fig. 18A). I found that each oocyte was surrounded by *Lgr5*-weak positive cells at P3 ovaries (Upper panel in Fig. 18A). These data suggest that *Lgr5*-GFP single-positive cells collected from E17.5, P1 and P3 correspond to the pre-G lineage. I also collected *Lgr5*-GFP/Mitotracker double-positive cells (OE cells) from P1 ovaries for the comparison.

To examine gene expression changes in pre-G lineages involved in PF formation, I performed RNA-seq analyses for triplicated each sample. The clustering

analysis indicated that individual *Lgr5*-GFP single-positive samples (pre-G lineages) derived from each time point were closely associated except one P1 and P3 samples, and OE samples were clearly separated as an outgroup (Fig. 18B). To gain more insight into cell-type and developmental difference, I performed principal component analysis (PCA). I found that pre-G lineages and OE samples were separated in PC1 axis (Fig. 18C), indicating that PC1 represents cell-type difference. Furthermore, pre-G lineages aligned with PC2 axis (Fig. 18C), indicating that PC2 represents developmental stages.

Importantly, the distance between pre-G lineages were greatly separated between E17.5 to P1 in PC2 axis (Fig. 18C). Differential gene expression analysis revealed that 537 and 363 genes were up- and down-regulated, respectively between E17.5 to P1 (adjusted p-value < 0.01) (Fig. 19A blue dots, Table 1), whereas 39 and 46 genes were up- and -down-regulated, respectively between P1 to P3 (adjusted p-value < 0.01) (Fig. 19B blue dots, Table 2). Furthermore, the differentially expressed genes (DEGs) between E17.5 to P1 representing more than 2-fold changes (489 and 319 of up- and down- regulated genes, respectively, Table1) included *Foxl2* as up-regulated and *Lgr5* as down-regulated genes (Fig. 19A and B red dots, Fig. 19C). These data suggest that the time period between E17.5 to P1 is crucial in pre-granulosa cell differentiation.

To explore molecular or cellular events during PF formation, enrichment analysis of the DEGs was performed (Fig. 19D and E). I found that terms related to extracellular matrix and cell adhesion (extracellular matrix organization, cell-cell adhesion, cell-substrate adhesion, and laminin interactions and positive regulation of cell migration related genes) were included in the top of the list of the up-regulated DEGs (Fig. 19D, Table 3). As pre-granulosa cells become to attach to oocytes, genes involved in these terms may play important roles during PF formation. I also found that genes involved in signal transduction (transmembrane receptor protein tyrosine kinase signaling pathway including *Igf1r*, Notch signaling related factors *Notch1*, *Notch2*, *Nrarp*, *Hey1*, *Heyl* and TGF- β signaling mediator, *Smad3*) and a putative transcription factor, *Dmrt1*, were up-regulated. As some of these genes were reported to play roles in PF formation or folliculogenesis [62,63,64,65,66,67] (Fig.19D), our RNA-seq data provide reasonable candidate genes involved in PF formation.

On the other hands, I found that results of enrichment analyses for the down-regulated genes between E17.5 to P1 contain “regulation of response to external signal” and “negative regulation of cell differentiation and proliferation” (Fig. 19E, Table 4). These results are consistent with the fact that *Lgr5*-positive progenitor cells do not actively proliferate [51]. Furthermore, down-regulated genes enrolled in GO term

“endocardial cushion development” include factors involving TGF- β signaling pathway (*Bmp2*, *Fst*, *Id2*, *Id3*, *Nog*, *Acvr1c*). One of TGF- β signaling antagonist, FST (Follistatin) is known to be expressed in both granulosa cell and germ cell at different timing. Previous study showed FST expressed in germ cells prevented germ cell cyst breakdown by suppressing somatic cell Notch signaling expression [37]. In addition, BMP2 enhances *Fst* expression in the downstream of WNT4 together with FOXL2 to suppress coelomic vessel formation, a feature of testis [68]. It is possible that these TGF- β signaling related genes may be involved in the maintenance of ovarian morphology. Besides, genes involved in the regulation of Wnt signaling pathway (*Lgr5*, *Nog*, *Snai2*, *Wnt2b*, *Gprc5b*, *Cthrc1*, *Daam2*, *Scyl2*, *Caprin2* and *Shisa6*) were highly expressed in pre-G cells at E17.5. As one of pre-G cell marker, LGR5, facilitates Wnt/ β -catenin signaling and RSPO1/WNT4/ β -catenin signals act at multiple critical steps in bipotential gonad formation, such as granulosa cell differentiation and ovarian cortex formation in fetal ovaries [69,70,71], Wnt signaling may have a role in pre-G progenitor cells..

To gain further insights into gene regulatory network during PF formation, I extracted transcription factors (TFs) from up- and down- regulated DEGs. Up-regulated DEGs contains *Smad3*, *Foxl2*, *Mycl*, *Dmrta1*, *Hey1*, *Arnt2*, *Klf13* and *Heyl*, among

which *Smad3*, *Foxl2*, *Dmrt1* are involved in folliculogenesis (Fig.20) [55,66,67]. Besides, TFs in down-regulated DEGs were *Nr0b1*, *Bhlhe41*, *Snai2*, *Pbx3*, *Sp5*, *Zfp52*, *Id2*, *Rfx5*, *Id3*, *Tcf12*, *Sox11* and *Zfp503* (Fig. 21). Notably, *Nr0b1* and *Snai2* are known to be important for male fertility, implying that down regulation of male differentiation gene occurred during PF formation [72,73,74]. Taken together, the transcriptome analyses identified the global gene expression changes putatively involved in differentiation and maintenance of pre-G lineages.

Crosstalk between germ cell and pre-G lineages is required for pre-granulosa cell differentiation

Interaction between germ cells and granulosa cells is required for PF formation. However, it is largely unknown how germ cells contribute to the pre-G differentiation during PF formation. To address this question, I examined the differentiation of pre-G lineages in two types of germ cell defective mutants, *Nanos3*-KO and *Figla*-KO. *Nanos3*-KO causes complete germ cell loss in embryonic gonads before E13.5 [75], whereas *Figla*-KO causes germ cell death within few days after birth due to the defective cyst breakdown [46].

First, I investigated *Nanos3*-KO ovaries to ask whether pre-granulosa cell

progenitors exist even in the absence of germ cells. Interestingly, *Lgr5*-positive cells were observed in both OE cells and cortical region of the ovary even in *Nanos3*-KO ovaries like the intact ovary at E16.5, indicating that the appearance of *Lgr5*-positive cells is independent of germ cells (Fig. 22A). Consistently, *Lgr5*-positive cells were observed normally in *Figla*-KO ovaries. Next, I asked whether pre-G differentiation is affected in these mutants after birth. Strong *Lgr5* expression was restricted in ovarian epithelial cells in P1 ovaries and most of *Lgr5*-positive pre-G progenitors already started to differentiate to FOXL2-positive cells after P4 in the control. On the other hand, *Lgr5*-strong-positive cells were retained in cortical region in both *Nanos3*-KO at 1W and *Figla*-KO at P4 (Fig. 22A and B). Though *Lgr5*-positive pre-G cells in *Figla*-KO differentiated into FOXL2-positive cells by 7 days after birth (1W in Fig. 22B), those cells were retained longer in the *Nanos3*-KO (Fig. 22A right panel) although they also finally differentiated to FOXL2-positive cells by 2W (Fig. 22A). These results suggest that pre-G cell differentiation was delayed in both mutants. In addition, the timing of pre-G cell differentiation is influenced not only by the presence of germ cells but also by the developmental progression of oocytes. Figure 22C summarized the results. My data suggest that proper pre-G cell development requires crosstalk with germ cells. Furthermore, as pre-G progenitors finally differentiate into

FOXL2 positive cells even in the absence of germ cells, it is likely that both germ cell-dependent and -independent mechanisms for pre-granulosa cell differentiation exist in the ovary.

Classification of pre-granulosa cell differentiation related gene as germ cell-dependent and -independent candidates

From the investigation of germ cell defective mutants, I expected that the appearance of *Lgr5*-positive pre-G progenitor is independent of germ cells but its differentiation timing is largely dependent not only on presence of germ cells but also on their differentiation because *Lgr5*-GFP expression was prolonged even in *Figla* knockout ovaries. To explore genes possibly influenced by the germ cells during PF formation, I performed transcriptome analysis of pre-G lineage in *Nanos3*-KO and *Figla*-KO at P3 and compared with those from control ovaries. In the PCA analysis, PC1 represents developmental stages of pre-G cells (Fig. 23A). Interestingly, *Figla*- and *Nanos3*-KO data were plotted close to those of control at E17.5, which was consistent with the prolonged expression of *Lgr5*-GFP in *Figla*- and *Nanos3*-KO ovaries shown in Fig. 22. These data indicate that *Lgr5*-positive cells in both mutants retained undifferentiated states. Besides, *Nanos3*-KO appeared to retain more undifferentiated state than *Figla*

KO as *Nanos3*-KO data were plotted more right side along PC1 (Fig. 23A).

Based on these results, I hypothesized that genes increasing from E17.5 to P1 in the wildtype and decreasing in the germ cell defective mutants contain the genes involving differentiation of PF. As mutant pre-G cells retain more immature state similar to those in E17.5 wildtype (Fig23A), transcriptome data from mutants were compared to those from P1 wildtype to extract genes affected by germ cell defects. The strategy for the extraction of candidate genes was summarized in Figure 23B. I compared the DEG obtained from the comparison between P1 vs E17.5 of the control embryos (① in Fig. 23B) to DEGs obtained from the comparison between P3 *Figla*- or *Nanos3*-KO vs P1 control (② and ③ in Fig. 23B, Table 5 and 6). Venn diagram in Fig. 23B right side and 24A showed the overlaps between genes up-regulated in P1 in wildtype (I in Fig. 23B) and down-regulated genes in P3 germ cell defective mutants (down regulated genes in ② and ③ in Fig. 23B). The overlapped 266 genes were the genes whose expression was up-regulated from E17.5 to P3 in wildtype but their expression was not increased in germ cell defective mutant. I classified the 266 genes as germ cell-dependent genes (III in Fig. 23B). On the other hands, non-overlapped 117 genes were classified as germ cell-independent genes because their expression was not influenced in germ cell defective mutants (IV in Fig. 23B). To explore the molecular or

cellular events associated with germ cell-dependent and -independent pathway, I performed enrichment analysis for the extracted DEGs (Fig. 24B and C, Table 7 and 8). The terms enriched in germ cell-dependent genes contained extracellular matrix organization, regulation of cell adhesion, and cell-cell adhesion, regulation of epithelial cell proliferation, and cell division (Fig. 24B), suggesting that germ cell development affects cell adhesion, motility, and proliferation in pre-G progenitors for PF formation. In addition, these 266 genes contained important genes for follicle formation (*Notch* related genes, *Dmrt1*, and *Smad3*).

On the other hands, enrichment analysis for germ cell-independent genes contained terms related to negative regulation of apoptosis (“regulation of mitochondrial outer membrane permeabilization involved in negative regulation of apoptotic signaling pathway” and “apoptotic signaling pathway”), suggesting that survival of pre-G progenitor is regulated by a germ cell-independent manner (Fig. 24C). Moreover, terms related to cell-cell adhesion, cell-matrix adhesion and focal adhesion were also enriched. Thus, adhesive properties between germ cells and pre-G progenitor may be controlled by both germ cell-dependent and -independent pathways.

I also classified TFs shown in Fig. 20 based on the germ cell dependency. I found that *Heyl*, *Arnt2*, *Hey1*, *Mycl*, *Smad3*, *Dmrt1* were classified as germ

cell-dependent and *Klf13* were classified as germ cell-independent factors (Fig. 25). However, *Klf13* expression level in P3 control is strongly higher than that of germ cell defective mutant, suggesting that *Klf13* is up-regulated in a germ cell dependent pathway after P1 stage. Taken together, these results suggest that germ cell have crucial role in gene regulatory network of differentiating pre-G cells.

Classification of pre-granulosa progenitor related gene as germ cell-dependent or independent candidates

Conversely, I hypothesized that genes down-regulated in the normal PF development but retained higher expression in the germ cell defective mutants play important roles in pre-G progenitors. I expected that these genes must be repressed after birth mainly depending on germ cell status, as germ cell defective mutants maintained *Lgr5*-positive pre-G cells longer than wildtype. Venn diagram in Fig. 23B right side and Fig. 26A showed the overlap between genes down-regulated in the control P1 (II in Fig. 23B) and up-regulated genes in germ cell defective mutants (up regulated genes in ② and ③ in Fig. 23B). The overlapped 133 genes were regarded as reliable germ cell-dependent genes (V in Fig. 23B). On the other hands, non-overlapped 111 genes were regarded as germ cell-independent genes (VI in Fig. 23B).

Enrichment analysis for germ cell-dependent genes contained terms for “response to hormone”, “regulation of hormone levels”, “hormone-mediated signaling pathway”, suggesting that hormonal regulation mediated by oocytes are involved in retaining the feature of pre-G progenitors (Fig. 26B, Table 9). In addition, I found that genes involved in Wnt signaling pathway (*Bmp2*, *Lgr5*, *Grk5*, *Tiam1*, *Gprc5b*, *Cthrc1*, *Daam2*, *Cela1*, *Scyl2*, *Shisa6*) were included in this category. Therefore, Wnt signaling pathway genes including *Lgr5* are regulated in a germ cell-dependent manner, which is consistent with the fact that *Lgr5* expression was maintained in the germ cell defective mutants but not in the wild-type (1W in Fig. 22A and P4 in Fig. 22B). Furthermore, consistent with the negative regulation of cell proliferation in *Lgr5*-positive cells, Cyclin Dependent Kinase Inhibitor 1C (*Cdkn1c*), a cell proliferation inhibitor, was enriched in *Lgr5*-positive cells.

Meanwhile, enrichment analysis for 111 germ cell-independent candidates included “alpha-amino acid metabolic processes” and “vitamin metabolic process” (Fig. 26C, Table 10). It suggests that genes involved in the metabolism process required for survival of the cells could be expressed in a germ cell-independent manner. Besides, germ cell-independent candidates contain *Fst*, one of TGF- β antagonist and putative candidate gene involved in pre-G progenitor maintenance.

Moreover, TFs shown in Fig. 21 were classified based on the germ-cell dependency. *Nr0b1*, *Bhlhe41*, *Sp5*, *Id2*, *Zfp503* were categorized as germ cell-dependent and *Snai2*, *Pbx3*, *Rfx5*, *Tcf12*, *Sox11* were germ cell-independent factors. However, some of germ cell-independent TFs showed higher expression levels in both mutants than that of P3 control, implying that these genes expression were affected by germ cell (Fig. 27). These results suggest not only germ cell-dependent but also germ cell-independent pathways contribute to gene regulatory network in pre-G progenitor.

Pre-G differentiation genes influenced by germ cells in the embryonic stage

In addition to overlapped genes III and V in Fig.23B as germ cell-dependent candidates, genes which enclosed in red and blue line of Fig. 28A and B are also germ cell-dependent candidates, but only in the embryonic stage, because those gene expressions were only influenced by *Nanos3*-KO but not in *Figla*-KO ovaries. The up-regulated 96 genes contain female-type sex-differentiation genes such as *Bmp4*, *Esr2*, *Foxl2* and *Nupr1*, MAPK cascade and positive regulation of ERK1/ERK2 cascade, *Igf1r* and *Notch2*, implying that these pathways were regulated in a germ cell-dependent mechanism in the embryonic stage (Fig. 28C, Table 11).

On the other hands, 65 down regulated genes were up-regulated only in

Nanos3-KO (Fig. 28B). Enrichment analysis for 65 genes showed metabolism related terms (“Biosynthesis of amino acids”, “small molecule biosynthetic process”, “Metabolism of carbohydrates”) (Fig.28D and Table 12). It suggests that germ cells may provide some cue to influence metabolic status of *Lgr5*-positive cells.

8. Discussion

Although PF formation is a fundamental event for folliculogenesis, gene expression changes associating with PF formation is poorly understood. Utilizing *Lgr5*-EGFP mice with Mito tracker, I succeeded to develop a method to isolate granulosa cell precursors during PF formation. As far as I know, this is the first report on transcriptome analyses of differentiating pre-G lineage. By combining with data obtained from germ cell defective mutants, I also demonstrated a significant contribution of germ cells in regulating PF formation.

The most significant changes I noticed during PF formation was down-regulation of Wnt and TGF- β signaling related genes, and up-regulation of Notch and PI3K signaling pathway genes and TFs known to be involved in folliculogenesis (*Dmrt1*, *Smad3*) (Fig. 29). In addition, previous studies suggested that Wnt signaling inhibits FSH target genes and steroid production associated with maturation and differentiation of rat ovarian follicles [76], while FSH is also implicated in promoting cyst breakdown and PF formation in mouse organ culture study [77], implying that Wnt signaling related genes in my data may have a role in retaining pre-G cells by suppressing FSH related pathways. Therefore, I expect that Wnt signaling related factors are major regulators required for protecting germ line cyst from the cyst

breakdown. Though Wnt signaling factors were classified as germ cell-dependent, I think that germ line cyst may be retained via both internal and external signals because *Lgr5* positive cells were emerged in germ cell less mutants.

Other than PF formation promoting genes, the up-regulated genes include important genes for follicle development such as *Smad3* and *Igf1r*. IGF1R recruits the Ras/MAPK and phosphoinositide 3-kinase/protein kinase B (PI3K/AKT) pathways [78] and also is known to have the cross-talk with the EGFR pathway [79]. As factors included in PI3K and EGFR pathway were contained in my list, it is possible that these signaling pathways also have roles in PF formation in the downstream of IGF1R. Besides, the number of germ cell-dependent genes was approximately twice in up-regulated gene during PF formation than that of germ cell-independent ones, supporting the idea that differentiation of pre-G is strongly affected by the interaction with germ cells.

To investigate transcriptional regulatory network in pre-G progenitor differentiation, I extracted TFs from up- and down-regulated DEGs in wildtype which contains well known factor for PF formation and folliculogenesis (Notch signaling-related genes, *Dmrta1*, *Foxl2*, *Smad3*). Other than these factors, I found TFs, *Arnt2* and *Mycl* as up-regulated genes and *Id2*, *Id3*, *Nr0bi*, *Sp5* and *Pbx3* as

down-regulate genes. Among them, *Mycl* and *Sp5* knockout mice are known to be viable and fertile though the detailed function in the ovary is unknown. DNA-binding protein inhibitors, *Id2* and *Id3*, are targets of TGF- β signaling [80], suggesting that TGF- β signaling works in pre-G progenitor cells. In addition, down regulation of *Nr0b1* is shown to be important for male gonad development, suggesting that this male pathway related regulator may be suppressed during female somatic cell differentiation. According to the Mouse Genome Informatics (MGI, <http://www.informatics.jax.org/>) data, *Pbx3* heterozygous mutant shows ovarian defect. I expect that *Pbx3* might involve in the appearance or the maintenance of pre-G progenitor cells to allow functional ovary development in a germ cell-independent pathway.

In early embryonic ovaries, GATA4 positive cells are precursors for all granulosa cell lineages and differentiate to FOXL2 and *Lgr5*-positive cells which become localized in medullary and cortical region, respectively (Fig. 29) [49]. Some *Lgr5*-FOXL2-double positive cells exist at the medullar region during embryonic stage, indicating that parts of FOXL2-positive cells are derived from *Lgr5*-positive cells as shown previously [50,51]. I found that *Lgr5*-positive pre-G progenitors in cortical region emerged even in the absence of the germ cells. Therefore, I speculate that *Lgr5*-positive cells can be separated into two cell groups based on their developmental

fates; one can differentiate to FOXL2-positive cells in the embryonic stage, which is germ cell-independent, while others maintain *Lgr-5* expression until PF formation and finally differentiate to FOXL2-positive cell after birth, which process must be germ cell-dependent. My transcriptome analyses using mutant ovaries identified possible candidate genes involved in each process. I indicated that Wnt signaling may involve in pre-G progenitor in a germ cell-dependent pathway, but it is still largely unknown how Wnt signaling works besides the fact that WNT4 have a role in maintaining E-cadherin junctions between oocytes inside cyst [45]. Although I mainly focused on *Lgr5*-positive cells, LGR5 function during PF formation is still unknown, because *Lgr5*-KO causes neonatal lethality [81]. For further analysis, I like to identify pre-G progenitor-specific genes to use as markers and to create specific Cre-expressing mouse lines. As candidates, I extracted 55 genes including *Lgr5* among 171 down regulated genes by removing contaminating germ cell genes and genes showing lower expression level (Table 13). I expect that those contain genes not only useful as the pre-G marker but also have important roles in the maintenance of pre-G progenitor because these genes expression is decreased during PF formation.

In conclusion, my transcriptome data unveiled up- and down-regulated genes during PF formation. Furthermore, these genes were classified into germ cell-dependent

and -independent candidates, which will help further analyses to uncover gene regulatory networks between somatic cells and germ cells. As defective formation of PFs cause germ cell death or multiple oocyte follicles, my data will provide useful resources for revealing the cause of female infertility.

9. Material and Methods of Chapter I

Ethics Statement

All mouse experiments were approved by the Animal Experimentation Committee at the National Institute of Genetics (approval number 30-5) and Yokohama National University (approval number 2017-09) and conducted under the Regulations for Animal Experiments at the National Institute of Genetics, Research Organization of Information and Systems and the guideline at Yokohama National University.

Mice

Mice were housed in a specific-pathogen-free animal care facility at the National Institute of Genetics (NIG). All experiments were approved by the NIG Institutional Animal Care and Use Committee and the animal experimental committee at Yokohama National University. The genetic background of mice used in this study was C57BL/6N (Clea Japan), except in the DAZL expression analysis and conditional *Dazl* knockout mice (mixed genetic background of ICR and C57BL/6N). The BAC-carrying transgenic mouse line was generated in a previous study [25]. The BAC transgenic mice were backcrossed with C57BL/6N at least 3 times. *Dazl* flox mice were generated from an ES cell line produced by the Knock Out Mouse Project (KOMP, *Dazl*^{tm2a (KOMP) Wtsi}).

Reverse transcription-quantitative polymerase chain reaction (RT-qPCR)

Total RNAs were isolated from whole gonads of wild-type and BAC transgenic mice at each stage by RNeasy Mini Kit (Qiagen). One hundred ng (1W to 5W) and 40 ng (E12.5 to P0) of total RNA were used for cDNA synthesis using Prime Script RT Reagent Kits with gDNA Erase according to the manufacturer's protocol (Takara). Real time PCR was performed with KAPA SYBR FAST qPCR kits using a thermal cycle dice real time system (Takara). The obtained data was normalized by *Mvh* or *Hprt*.

The following primers were used for PCR amplification:

Dazl

Forward: 5'-CACGCCTCAGTGA CTGGCGAC-3'

Reverse: 5'-CGAAGCATA CAGACAGTGGTC-3'

Mvh

Forward: 5'-GTTGAAGTATCTGGACATGATGCAC-3'

Reverse: 5'-CGAGTTGGTGCTACAATAATACTC-3'

G3pdh

Forward: 5'-ACCACAGTCCATGCCATCAC-3'

Reverse: 5'-TCCACCACCCTGTTGCTGTA-3'

FLAG tagged *Dazl*

Forward: 5'-CACGCCTCAGTGACTCGGCGAC-3'

Reverse: 5'-CACCGTCATGGTCTTGTAGTC-3'

Dazl cKO

Forward: 5'-GACTTACATGCAGCCTCCAACCATG-3'

Reverse: 5'-AACAGGCAGCTGATATCCAGTGATG-3'

Tex19.1

Forward: 5'-AAAATGGGCCACCCACATCTC-3'

Forward: 5'-CCACTGGCCCTTGGACCAGAC-3'

Tpx2

Forward: 5'-CATCAAAGATGAGGAAGAGGA-3'

Forward: 5'-GGGTATCAAAGGAGAACGG-3'

Cdc20

Forward: 5'-TACAGTCAGAAAGCCACGC-3'

Forward: 5'-AGATTCAGGTAGTAGTCATTCCG-3'

Bub1b

Forward: 5'-TTACAACCTCTTGACAATCGTG-3'

Forward: 5'-GTCGTGGATTCTGTTTCGT-3'

Suz12

Forward: 5'-AACTATTGCTGTTAAGGAGACG-3'

Forward: 5'-CTGGCTTCTGTCTGTTGTC-3'

Arid1a

Forward: 5'-TCCCAGCAAACCTGCCTATTC-3'

Forward: 5'-CATATCTTCTTGCCCTCCCTTAC-3'

Hprt

Forward: 5'-TCGAAGTGTTGGATACAGGCCAG-3'

Forward: 5'-TCAACTTGCGCTCATCTTAGGC-3'

Western blotting

Ovaries were lysed in RIPA buffer (50 mM Tris-HCl (pH8.0), 150 mM NaCl, 0.5% Sodium deoxycholate, 0.1% Sodium dodecyl sulfate, 1% NP-40) and sonicated. After removing the debris by centrifugation, lysates were dissolved in 2xSDS sample buffer, and heated. MII oocytes and 1-cell zygotes were lysed in 10 μ l 2xSDS sample buffer. Each sample was applied to gels for SDS-PAGE and transferred to nitrocellulose membranes. The membranes were blocked in 5% skim-milk in TBST (50mM Tris-HCl (pH7.5), 150mM NaCl, 0.1% Tween-20) for 1 hour at room temperature (RT). Membranes were incubated with primary antibodies (Abcam, rabbit anti-DAZL

antibody, 1:2000 for ovarian sample or 1:500 for MII, 1-cell and 2-cell zygote / Abcam, rabbit anti-DDX4 antibody, 1:1000/Santa Cruz, mouse anti- β actin, 1:2000/Sigma, anti-FLAG antibody, 1:2000/ Given from Jeremy Wang, rabbit anti-TEX19.1, 1:500) diluted in 3% skim-milk in TBST or Can Get Signal immunoreaction Enhancer Solution (TOYOBO) overnight at 4°C. After washing the membranes with TBST, membranes were incubated with anti-rabbit HRP-conjugated secondary antibody (Cell signaling, 1:5000) and anti-mouse HRP-conjugated secondary antibody (Cell signaling, 1:5000) in TBST or Can Get Signal immunoreaction Enhancer Solution, respectively, at RT for 90 min. The signals were detected by Super Signal West Femto Maximum Sensitivity Substrate (Thermo Scientific) and AE-9300H EZ-CAPTURE MG (ATTO). Western blotting results were quantified by Gel Analysis with ImageJ software.

Immunostaining for paraffin embedded samples

Ovaries were fixed in 4% PFA (paraformaldehyde) at 4°C overnight and embedded in paraffin wax. Each sample was sliced at 6- μ m thickness and placed on glass slides. After removing the paraffin wax and autoclaving in antigen unmasking solution/high pH (Vector Laboratories), glass slides were washed in PBST (PBS, 0.1% Tween-20) and pre-incubated in 3% skim milk in PBST blocking solution at RT for 1 hour. The slides

were reacted with primary antibodies (Anti-DAZL antibody, Abcam, 1:200 / Anti-FOXL2 antibody, Abcam, 1:200/ Anti-FLAG antibody, SIGMA, 1:10000) at 4°C overnight. Then, slides were washed with PBST and incubated with second antibodies (Alexa 488 Donkey anti-Rabbit, Life technologies, 1:1000 /Alexa 594 Donkey anti-Mouse, Life technologies, 1:1000/Alexa 594 Donkey anti-Goat, Life technologies, 1:1000 / Cy5 Donkey anti-goat, Rockland, 1:1000) at RT for 60 min. DNA was counter-stained with DAPI, and fluorescent images were obtained using confocal microscopy FV1200 (Olympus).

Immunostaining for frozen samples

Ovaries were fixed with 4% PFA (paraformaldehyde) at 4°C overnight, which was then graded to 30% sucrose, and ovaries were then embedded in O.C.T compound (Sakura Fine tek). Each sample was sliced at 6-µm thickness. After removing the O.C.T compound, slides were incubated with 3% skim milk in PBST (PBS, 0.1% Tween-20) for 1 hour. Primary antibody reactions were performed with the following dilutions (Anti-DAZL antibody, Abcam, 1:200 / Anti-FOXL2 antibody, Abcam, 1:200) at 4°C overnight. After washing with PBST, secondary antibody reaction was performed with the following dilutions (Alexa 488 Donkey anti-Rabbit, Life technologies, 1:400 /Alexa

594 Donkey anti-Goat, Life technologies, 1:400) at RT for 90 min. Slides then were counter-stained by DAPI at RT for 15 min. Fluorescent images were obtained by confocal microscopy FV1200 (Olympus).

Immunostaining of MII oocytes

MIII oocytes were fixed with MeOH at -20°C for 3 minutes, washed with PBS-TX (0.1% TritonX, PBS), and were then incubated with blocking solution (3% BSA, 0.1% TritonX, PBS) at 4 °C for 3 hours. Primary antibody reactions were performed with the following dilutions (Anti- α -tubulin antibody, Sigma, 1:1000) at 4°C overnight. After washing with PBS-TX, secondary antibody reaction was performed with the following dilutions (Alexa 488 Donkey anti-Rabbit, Life technologies, 1:1000) and DAPI at RT for 60 min. Then, oocytes were washed with PBS-TX. Fluorescent images were obtained using confocal microscopy FV1200 (Olympus).

Histological analysis

Histological analysis was carried out by PAS (Periodic acid-Schiff) staining according to the standard protocol. Briefly, ovaries were fixed in Bouin solution, embedded in paraffin wax, and sliced at 6- μ m thickness. The sections were submerged in xylene,

100%, 90%, 70% ethanol, and distilled water at RT, and stained with PAS solution.

Ovarian images were obtained with an inverted microscope BX 51 and 61(Olympus).

Follicle stages were counted on every 5 sections.

Litter size investigation

Dazl^{+/+}, *Dazl* 3*F*, and *Dazl* 3*F*;*Flp* females at 6 weeks old were crossed with C57BL/6N

males, and kept together until female mice reached 30 weeks old. The number of pups

and deliveries was recorded. Pups were removed after counting the number and sex.

Females that killed their pups were excluded from the analysis.

Collection of MII oocytes, 1-cell, 2-cell embryos

To obtain MII, 1-cell and 2-cell oocytes for western blotting, female mice were injected

with PMSG (ASKA Pharmaceutical). Forty-eight hours after PMSG injection, mice

were stimulated with hCG (ASKA Pharmaceutical) for 14 h and MII oocytes were

collected. To obtain western blotting samples of 1-cell and 2-cell embryos, each female

was crossed with a WT male after hCG injection. Eggs with obvious abnormalities were

removed from experiments.

Ovulation number and survival rate analysis

One-cell embryos for investigation of ovulation number and pre-implantation development investigation were obtained from the ampulla of pregnant females at E0.5. Obtained 1 cell embryos were cultured in KSOM medium (Ark resource) and checked survival rate at each stage. Blastocysts for examining progression of early embryonic development were obtained by flushing oviducts at E3.5. Collected blastocysts were cultured for two days in KSOM medium because some of embryos delayed its development depends on fertilization timing.

Statistical analysis

Significance was assessed by the Student's t-test for differences between two samples. For quantitative analyses among multiple samples, significance was assessed using one-way ANOVA followed by Tukey HSD (Honest Significant Difference) test. Asterisks in figures indicate significance: * $P < 0.05$, ** $P < 0.005$.

10. Material and Methods of Chapter II]

Mice

Mice were housed in a specific-pathogen-free animal care facility at the National Institute of Genetics (NIG). All experiments were approved by the NIG Institutional Animal Care. *Lgr5*-GFP mouse line was kindly provided from Dr. T. Sato's group in Keio University. *Nanos3*-KO mouse line was established in our lab [75]. *Figla*-KO mouse line was established in our laboratory by using CRIPR/Cas9 and the phenotypes were confirmed to be similar to those of previously reported *Figla*-KO mice [46].

Immunostaining for ovaries

Ovaries were fixed with 4% PFA (paraformaldehyde) at 4°C overnight, which was then graded to 30% sucrose, and ovaries were then embedded in O.C.T compound (Sakura Fine tek). Each sample was sliced at 6- μ m thickness. After removing O.C.T compound, slides were autoclaved with Target Retrieval Solution (TRS) (Dako) to antigen retrieval and cooling. Then slides were pre-incubated in 3% skim milk in PBST blocking solution at RT for 1 hour. Primary antibody reaction was performed with the following dilutions (Anti-GFP antibody, Aves Labs, 1:400 / Anti-MVH antibody, abcam, 1:200/ Anti-FOXL2 antibody, abcam, 1:200) at 4°C overnight. After washing with PBST,

secondary antibody reaction was performed with the following dilutions (Alexa 594 Donkey anti-Rabbit, Life technologies, 1:1000/ Alexa 488 Donkey anti-chick, Jackson ImmunoResearch, 1:1000/ Cy5 Donkey anti-Goat, Rockland, 1:1000) at RT for 60 min. After washing with PBST, Slides were counter-stained by DAPI at RT for 15 min. Fluorescent images were obtained by confocal microscopy FV1200 (Olympus).

Mitotracker treatment and whole mount observation of Mitotracker treated ovary

Ovaries were treated with Mito Tracker Orange (ThermoFisher) which was diluted in culture medium to a final concentration of 1 μ M for 5min and washed them with PBS 5min three times. Whole mount investigation of treated ovary was performed by multi-photon microscope, Zeiss LSM7MP (Zeiss).

Reverse transcription-quantitative polymerase chain reaction (RT-qPCR)

Total RNAs were isolated from sorted *Lgr5*-EGFP or *Lgr5*-EGFP/ Mitotracker positive cells prepared from *Lgr5*-EGFP ovaries at P1 by RNeasy Mini Kit (Qiagen). Total RNAs were used for cDNA synthesis using Prime Script RT Reagent Kits with gDNA Erase according to the manufacturer's protocol (Takara). Real-time PCR was performed with KAPA SYBR FAST qPCR kits using a thermal cycle dice real time system

(Takara). The obtained data was normalized by Hprt.

The following primers were used for PCR amplification:

Hprt

Forward: 5' – TCGAAGTGTTGGATACAGGCCAG–3'

Forward: 5' – TCAACTTGCGCTCATCTTAGGC–3'

Mvh

Forward: 5' –GTTGAAGTATCTGGACATGATGCAC–3'

Reverse: 5' –CGAGTTGGTGCTACAATAATACTC–3'

K8

Forward: 5' – TGGAAGGACTGACCGACGAGAT –3'

Reverse: 5' – GGCACGAACTTCAGCGATGATG –3'

Foxl2

Forward: 5' – GCCTCAACGAGTGCTTCATCAAGGT –3'

Reverse: 5' – AGTTGTTGAGGAACCCCGATTGCAG–3'

Oocyte labeling and RNA-seq sample collection

Genotyping was performed for each sample before dissection. Gonads used for RNA-seq analyses were treated by Mito Tracker Orange (ThermoFisher) for 5min to

stain most outer layer of the gonads. Next, gonads were treated by collagenase for 10 min at 37°C and followed by trypsin treatment for 10 min at 37°C. Then, same amount of FBS containing medium were added for each sample to stop enzyme reaction. After pipetting to disperse the gonads and dispersed cells were collected by centrifugation. These cells were sorted by Desktop cell sorter (JSAN). After removing supernatant, samples were stored at -80°C until enough samples for RNA-seq were collected.

Preparation of RNA for RNAseq

Total RNA was extracted from sorted somatic cells by using RNeasy Micro kit (Qiagen). Then, amplification of total RNA was performed by Target Amp 1-Round aRNA Amplification Kit103 (epicentre). These amplified samples were utilized for making library of RNA-seq using KAPA Stranded mRNA-Seq Kit Illumina platform (KAPA) and barcoded with DNA adapters using KAPA single-indexed adaptor kit (KAPA). I used AMPure XP (Beckman coulter) to cleanup synthesized library. Quality check of library was performed by using Agilent DNA1000 Kit (Agilent). The libraries were sequenced pair end 100 on an illumine Hiseq2500 (illumina).

Bioinformatic Analysis of RNA-Seq

For pre-processing, quality control (QC) of raw paired end reads was performed in 3step to trim/remove poor quality sequences or technical sequences like adapters. In step1, reads were trimmed poly-A/T tails and filter out sequence shorter than 36 nt by PRINSEQ-lite (v0.20.4) with parameters "-out_format 3 -trim_tail_right 5 -ns_max_p 20 -min_len 36"[82]. In Step2, removing adapters and other Illumina-specific sequences from the reads by step1, and, for performing a sliding-window based trimming of low quality bases from each read were performed by using TrimmomaticPE (trimmomatic v0.38) with parameters "-threads 14 -phred33 ILLUMINACLIP:TruSeq3-PE-2.fa:2:30:10:1:TRUE LEADING:3 TRAILING:3 SLIDINGWINDOW:4:15 MINLEN:36"[83]. In Step3, process same as step1 was performed to trim the remaining poly-A/T tails and filtered out sequences shorter than 36 nt. Before each of the above steps, QC of reads was performed using FastQC (v0.11.7) (<http://www.bioinformatics.babraham.ac.uk/projects/fastqc>). A fasta file contains adapter sequences (TruSeq3-PE-2.fa) were downloaded from trimmomatic/adapters page of github (<https://github.com/timflutre/trimmomatic/tree/master/adapters>). After QC, Reads were mapped to the mouse reference genome (mm9) by using HISAT2 (v2.1.0) with parameters "-p 4 -q --dta --no-discordant --no-mixed" [84]. By this mapping, properly

paired reads were output to sam format file. Uniquely mapped reads were selected and the sam format file were converted into bam format file using SAMtools (version 1.7) "view" command with parameters "-@ 6 -q 4 -b" [85]. The obtained bam files were sorted by genomic coordinates using the SAMtools "sort" command. Detection of differentially expressed genes and statistical analysis were performed by using the R Bioconductor/DESeq2 package (www.bioconductor.org) [86]. Principal component analysis was performed using plot PCA function in DESeq2. Heatmap of sample to sample distance were represented by RColorBrewer and pheatmap for data I obtained. DEGs were cut off by criteria \log_2 (fold change) > 1 or <-1 and adjusted p value < 0.01. Mouse TFs information was obtained from AnimalTFDB [87]. TFs in DEGs were cut off by criteria base mean >1000. Venn diagram was made by using BioVenn [88]. Enrichment analysis was performed by Metascape (<http://metascape.org>) [89].

11. Table Legends (only attached in electric file)

Table 1. DEGs from E17.5 to P1 stage of pre-G progenitor cells

This table contains genes which represent $\text{padj} < 0.01$ in RNA seq analysis between P1 vs E17.5 pre-G progenitors. DEGs which represent fold change > 1 or < -1 were shown in red and blue highlight.

Table 2. DEGs from P1 to P3 stage of pre-G progenitor cells

This table contains genes which represent $\text{padj} < 0.01$ in RNA seq analysis between P3 vs P1 pre-G progenitors. DEGs which represent fold change > 1 or < -1 were shown in red and blue highlight.

Table 3. Enrichment analysis for up-regulated DEGs from E17.5 to P1

The result of enrichment analysis by metascape for up-regulated DEGs from E17.5 to P1

Table 4. Enrichment analysis for down-regulated DEGs from E17.5 to P1

The result of enrichment analysis by metascape for down-regulated DEGs from P1 to P3

Table 5. DEGs between *Figla*-KO vs P1 control pre-G progenitor cells

This table contains genes which represent $\text{padj} < 0.01$ in RNA seq analysis between *Figla*-KO vs P1 pre-G progenitors. DEGs which represent fold change >1 or <-1 were shown in red and blue highlight.

Table 6. DEGs between *Nanos3*-KO vs P1 control pre-G progenitor cells

This table contains genes which represent $\text{padj} < 0.01$ in RNA seq analysis between *Nanos3*-KO vs P1 pre-G progenitors. DEGs which represent fold change >1 or <-1 were shown in red and blue highlight.

Table 7. Enrichment analysis for up-regulated DEGs classified as germ cell-dependent

The result of enrichment analysis by metascape for germ cell-dependently up-regulated DEGs.

Table 8. Enrichment analysis for up-regulated DEGs classified as germ cell-independent

The result of enrichment analysis by metascape for germ cell-independently up-regulated DEGs.

Table 9. Enrichment analysis for down-regulated DEGs classified as germ cell-dependent

The result of enrichment analysis by metascape for germ cell-dependently down-regulated DEGs.

Table 10. Enrichment analysis for down-regulated DEGs classified as germ cell-independent

The result of enrichment analysis by metascape for germ cell-independently down-regulated DEGs.

Table 11. Enrichment analysis for up-regulated DEGs classified as germ cell-dependent in early stage

The result of enrichment analysis by metascape for up-regulated DEGs merged with down-regulated genes in *Nanos3*-KO.

Table 12. Enrichment analysis for down-regulated DEGs classified as germ cell-dependent in early stage

The result of enrichment analysis by metascape for down-regulated DEGs merged with up-regulated genes in *Nanos3*-KO.

Table 13. Candidate gene having a role in pre-G progenitor

Down-regulated DEGs which showed lower expression in oocytes and higher expression in pre-G progenitor (baseMean >1000) were listed as candidate gene having a role in pre-G progenitor.

12. References

1. Thomson TC, Fitzpatrick KE, Johnson J (2010) Intrinsic and extrinsic mechanisms of oocyte loss. *Mol Hum Reprod* 16: 916-927.
2. Weill L, Belloc E, Bava FA, Mendez R (2012) Translational control by changes in poly(A) tail length: recycling mRNAs. *Nat Struct Mol Biol* 19: 577-585.
3. Kang MK, Han SJ (2011) Post-transcriptional and post-translational regulation during mouse oocyte maturation. *BMB Rep* 44: 147-157.
4. Groisman I, Huang YS, Mendez R, Cao Q, Theurkauf W, et al. (2000) CPEB, maskin, and cyclin B1 mRNA at the mitotic apparatus: implications for local translational control of cell division. *Cell* 103: 435-447.
5. Stutz A, Conne B, Huarte J, Gubler P, Volkel V, et al. (1998) Masking, unmasking, and regulated polyadenylation cooperate in the translational control of a dormant mRNA in mouse oocytes. *Genes Dev* 12: 2535-2548.
6. Racki WJ, Richter JD (2006) CPEB controls oocyte growth and follicle development in the mouse. *Development* 133: 4527-4537.
7. Guzeloglu-Kayisli O, Lalioti MD, Aydinler F, Sasson I, Ilbay O, et al. (2012) Embryonic poly(A)-binding protein (EPAB) is required for oocyte maturation and female fertility in mice. *Biochem J* 446: 47-58.
8. Tay J, Richter JD (2001) Germ cell differentiation and synaptonemal complex formation are disrupted in CPEB knockout mice. *Dev Cell* 1: 201-213.
9. Mak W, Fang C, Holden T, Dratver MB, Lin H (2016) An Important Role of Pumilio 1 in Regulating the Development of the Mammalian Female Germline. *Biol Reprod* 94: 134.
10. Medvedev S, Pan H, Schultz RM (2011) Absence of MSY2 in mouse oocytes perturbs oocyte growth and maturation, RNA stability, and the transcriptome. *Biol Reprod* 85: 575-583.
11. Yu J, Hecht NB, Schultz RM (2002) RNA-binding properties and translation repression in vitro by germ cell-specific MSY2 protein. *Biol Reprod* 67: 1093-1098.
12. Fu XF, Cheng SF, Wang LQ, Yin S, De Felici M, et al. (2015) DAZ Family Proteins, Key Players for Germ Cell Development. *Int J Biol Sci* 11: 1226-1235.
13. Venables JP, Ruggiu M, Cooke HJ (2001) The RNA-binding specificity of the mouse Dazl protein. *Nucleic Acids Res* 29: 2479-2483.
14. Reynolds N, Collier B, Maratou K, Bingham V, Speed RM, et al. (2005) Dazl binds in vivo to specific transcripts and can regulate the pre-meiotic translation of Mvh in germ cells. *Hum Mol Genet* 14: 3899-3909.
15. Jenkins HT, Malkova B, Edwards TA (2011) Kinked beta-strands mediate high-affinity

- recognition of mRNA targets by the germ-cell regulator DAZL. *Proc Natl Acad Sci U S A* 108: 18266-18271.
16. Ruggiu M, Speed R, Taggart M, McKay SJ, Kilanowski F, et al. (1997) The mouse *Dazl* gene encodes a cytoplasmic protein essential for gametogenesis. *Nature* 389: 73-77.
 17. Saunders PT, Turner JM, Ruggiu M, Taggart M, Burgoyne PS, et al. (2003) Absence of *mDazl* produces a final block on germ cell development at meiosis. *Reproduction* 126: 589-597.
 18. Gill ME, Hu YC, Lin Y, Page DC (2011) Licensing of gametogenesis, dependent on RNA binding protein DAZL, as a gateway to sexual differentiation of fetal germ cells. *Proc Natl Acad Sci U S A* 108: 7443-7448.
 19. Lin Y, Gill ME, Koubova J, Page DC (2008) Germ cell-intrinsic and -extrinsic factors govern meiotic initiation in mouse embryos. *Science* 322: 1685-1687.
 20. Chen J, Melton C, Suh N, Oh JS, Horner K, et al. (2011) Genome-wide analysis of translation reveals a critical role for deleted in azoospermia-like (*Dazl*) at the oocyte-to-zygote transition. *Genes Dev* 25: 755-766.
 21. Koubova J, Hu YC, Bhattacharyya T, Soh YQ, Gill ME, et al. (2014) Retinoic acid activates two pathways required for meiosis in mice. *PLoS Genet* 10: e1004541.
 22. McNeilly JR, Watson EA, White YA, Murray AA, Spears N, et al. (2011) Decreased oocyte DAZL expression in mice results in increased litter size by modulating follicle-stimulating hormone-induced follicular growth. *Biol Reprod* 85: 584-593.
 23. Pepling ME, Spradling AC (2001) Mouse ovarian germ cell cysts undergo programmed breakdown to form primordial follicles. *Dev Biol* 234: 339-351.
 24. Lan ZJ, Xu X, Cooney AJ (2004) Differential oocyte-specific expression of Cre recombinase activity in GDF-9-iCre, Zp3cre, and Msx2Cre transgenic mice. *Biol Reprod* 71: 1469-1474.
 25. Kato Y, Katsuki T, Kokubo H, Masuda A, Saga Y (2016) *Dazl* is a target RNA suppressed by mammalian NANOS2 in sexually differentiating male germ cells. *Nat Commun* 7: 11272.
 26. Zeng M, Lu Y, Liao X, Li D, Sun H, et al. (2009) DAZL binds to 3'UTR of *Tex19.1* mRNAs and regulates *Tex19.1* expression. *Mol Biol Rep* 36: 2399-2403.
 27. Kim B, Cooke HJ, Rhee K (2012) DAZL is essential for stress granule formation implicated in germ cell survival upon heat stress. *Development* 139: 568-578.
 28. Chen HH, Welling M, Bloch DB, Munoz J, Mientjes E, et al. (2014) DAZL limits pluripotency, differentiation, and apoptosis in developing primordial germ cells. *Stem Cell Reports* 3: 892-904.
 29. Loffreda A, Rigamonti A, Barabino SM, Lenzken SC (2015) RNA-Binding Proteins in the

- Regulation of miRNA Activity: A Focus on Neuronal Functions. *Biomolecules* 5: 2363-2387.
30. Suh N, Baehner L, Moltzahn F, Melton C, Shenoy A, et al. (2010) MicroRNA function is globally suppressed in mouse oocytes and early embryos. *Curr Biol* 20: 271-277.
 31. Radford HE, Meijer HA, de Moor CH (2008) Translational control by cytoplasmic polyadenylation in *Xenopus* oocytes. *Biochim Biophys Acta* 1779: 217-229.
 32. Mendez R, Hake LE, Andresson T, Littlepage LE, Ruderman JV, et al. (2000) Phosphorylation of CPE binding factor by Eg2 regulates translation of *c-mos* mRNA. *Nature* 404: 302-307.
 33. Kok FO, Shin M, Ni CW, Gupta A, Grosse AS, et al. (2015) Reverse genetic screening reveals poor correlation between morpholino-induced and mutant phenotypes in zebrafish. *Dev Cell* 32: 97-108.
 34. Rossi A, Kontarakis Z, Gerri C, Nolte H, Holper S, et al. (2015) Genetic compensation induced by deleterious mutations but not gene knockdowns. *Nature* 524: 230-233.
 35. Collier B, Gorgoni B, Loveridge C, Cooke HJ, Gray NK (2005) The DAZL family proteins are PABP-binding proteins that regulate translation in germ cells. *EMBO J* 24: 2656-2666.
 36. Reynolds N, Collier B, Bingham V, Gray NK, Cooke HJ (2007) Translation of the synaptonemal complex component Sycp3 is enhanced in vivo by the germ cell specific regulator Dazl. *RNA* 13: 974-981.
 37. Kedersha N, Anderson P (2002) Stress granules: sites of mRNA triage that regulate mRNA stability and translatability. *Biochem Soc Trans* 30: 963-969.
 38. Pepling ME, Spradling AC (1998) Female mouse germ cells form synchronously dividing cysts. *Development* 125: 3323-3328.
 39. Peters H (1970) Migration of gonocytes into the mammalian gonad and their differentiation. *Philos Trans R Soc Lond B Biol Sci* 259: 91-101.
 40. Borum K (1961) Oogenesis in the mouse. A study of the meiotic prophase. *Exp Cell Res* 24: 495-507.
 41. Menke DB, Koubova J, Page DC (2003) Sexual differentiation of germ cells in XX mouse gonads occurs in an anterior-to-posterior wave. *Dev Biol* 262: 303-312.
 42. Matzuk MM, Burns KH, Viveiros MM, Eppig JJ (2002) Intercellular communication in the mammalian ovary: oocytes carry the conversation. *Science* 296: 2178-2180.
 43. Zhao L, Du X, Huang K, Zhang T, Teng Z, et al. (2016) Rac1 modulates the formation of primordial follicles by facilitating STAT3-directed Jagged1, GDF9 and BMP15 transcription in mice. *Sci Rep* 6: 23972.
 44. Jones RL, Pepling ME (2013) KIT signaling regulates primordial follicle formation in the

- neonatal mouse ovary. *Dev Biol* 382: 186-197.
45. Niu W, Wang Y, Wang Z, Xin Q, Feng L, et al. (2016) JNK signaling regulates E-cadherin junctions in germline cysts and determines primordial follicle formation in mice. *Development* 143: 1778-1787.
 46. Soyal SM, Amleh A, Dean J (2000) FIGalpha, a germ cell-specific transcription factor required for ovarian follicle formation. *Development* 127: 4645-4654.
 47. Liang L, Soyal SM, Dean J (1997) FIGalpha, a germ cell specific transcription factor involved in the coordinate expression of the zona pellucida genes. *Development* 124: 4939-4947.
 48. Carmon KS, Lin Q, Gong X, Thomas A, Liu Q (2012) LGR5 interacts and cointernalizes with Wnt receptors to modulate Wnt/beta-catenin signaling. *Mol Cell Biol* 32: 2054-2064.
 49. Gustin SE, Hogg K, Stringer JM, Rastetter RH, Pelosi E, et al. (2016) WNT/beta-catenin and p27/FOXL2 differentially regulate supporting cell proliferation in the developing ovary. *Dev Biol* 412: 250-260.
 50. Rastetter RH, Bernard P, Palmer JS, Chassot AA, Chen H, et al. (2014) Marker genes identify three somatic cell types in the fetal mouse ovary. *Dev Biol* 394: 242-252.
 51. Ng A, Tan S, Singh G, Rizk P, Swathi Y, et al. (2014) Lgr5 marks stem/progenitor cells in ovary and tubal epithelia. *Nat Cell Biol* 16: 745-757.
 52. Capel B (2014) Ovarian epithelium regeneration by Lgr5(+) cells. *Nat Cell Biol* 16: 743-744.
 53. Uhlenhaut NH, Jakob S, Anlag K, Eisenberger T, Sekido R, et al. (2009) Somatic sex reprogramming of adult ovaries to testes by FOXL2 ablation. *Cell* 139: 1130-1142.
 54. Schmidt D, Ovitt CE, Anlag K, Fehsenfeld S, Gredsted L, et al. (2004) The murine winged-helix transcription factor Foxl2 is required for granulosa cell differentiation and ovary maintenance. *Development* 131: 933-942.
 55. Ottolenghi C, Omari S, Garcia-Ortiz JE, Uda M, Crisponi L, et al. (2005) Foxl2 is required for commitment to ovary differentiation. *Hum Mol Genet* 14: 2053-2062.
 56. Uda M, Ottolenghi C, Crisponi L, Garcia JE, Deiana M, et al. (2004) Foxl2 disruption causes mouse ovarian failure by pervasive blockage of follicle development. *Hum Mol Genet* 13: 1171-1181.
 57. Wang C, Zhou B, Xia G (2017) Mechanisms controlling germline cyst breakdown and primordial follicle formation. *Cell Mol Life Sci* 74: 2547-2566.
 58. Xu J, Gridley T (2013) Notch2 is required in somatic cells for breakdown of ovarian germ-cell nests and formation of primordial follicles. *BMC Biol* 11: 13.
 59. Trombly DJ, Woodruff TK, Mayo KE (2009) Suppression of Notch signaling in the

- neonatal mouse ovary decreases primordial follicle formation. *Endocrinology* 150: 1014-1024.
60. Mork L, Maatouk DM, McMahon JA, Guo JJ, Zhang P, et al. (2012) Temporal differences in granulosa cell specification in the ovary reflect distinct follicle fates in mice. *Biol Reprod* 86: 37.
 61. Barker N, van Es JH, Kuipers J, Kujala P, van den Born M, et al. (2007) Identification of stem cells in small intestine and colon by marker gene *Lgr5*. *Nature* 449: 1003-1007.
 62. Baumgarten SC, Armouti M, Ko C, Stocco C (2017) IGF1R Expression in Ovarian Granulosa Cells Is Essential for Steroidogenesis, Follicle Survival, and Fertility in Female Mice. *Endocrinology* 158: 2309-2318.
 63. Terauchi KJ, Shigeta Y, Iguchi T, Sato T (2016) Role of Notch signaling in granulosa cell proliferation and polyovular follicle induction during folliculogenesis in mouse ovary. *Cell Tissue Res* 365: 197-208.
 64. Guo M, Zhang H, Bian F, Li G, Mu X, et al. (2012) P4 down-regulates *Jagged2* and *Notch1* expression during primordial folliculogenesis. *Front Biosci (Elite Ed)* 4: 2631-2644.
 65. Tomic D, Brodie SG, Deng C, Hickey RJ, Babus JK, et al. (2002) *Smad 3* may regulate follicular growth in the mouse ovary. *Biol Reprod* 66: 917-923.
 66. Tomic D, Miller KP, Kenny HA, Woodruff TK, Hoyer P, et al. (2004) Ovarian follicle development requires *Smad3*. *Mol Endocrinol* 18: 2224-2240.
 67. Balciuniene J, Bardwell VJ, Zarkower D (2006) Mice mutant in the DM domain gene *Dmrt4* are viable and fertile but have polyovular follicles. *Mol Cell Biol* 26: 8984-8991.
 68. Kashimada K, Pelosi E, Chen H, Schlessinger D, Wilhelm D, et al. (2011) *FOXL2* and *BMP2* act cooperatively to regulate *follistatin* gene expression during ovarian development. *Endocrinology* 152: 272-280.
 69. Glinka A, Dolde C, Kirsch N, Huang YL, Kazanskaya O, et al. (2011) *LGR4* and *LGR5* are R-spondin receptors mediating *Wnt/beta-catenin* and *Wnt/PCP* signalling. *EMBO Rep* 12: 1055-1061.
 70. Koo BK, Clevers H (2014) Stem cells marked by the R-spondin receptor *LGR5*. *Gastroenterology* 147: 289-302.
 71. Schuijers J, Clevers H (2012) Adult mammalian stem cells: the role of *Wnt*, *Lgr5* and R-spondins. *EMBO J* 31: 2685-2696.
 72. Yu RN, Ito M, Saunders TL, Camper SA, Jameson JL (1998) Role of *Ahch* in gonadal development and gametogenesis. *Nat Genet* 20: 353-357.
 73. Bouma GJ, Albrecht KH, Washburn LL, Recknagel AK, Churchill GA, et al. (2005)

- Gonadal sex reversal in mutant Dax1 XY mice: a failure to upregulate Sox9 in pre-Sertoli cells. *Development* 132: 3045-3054.
74. Perez-Losada J, Sanchez-Martin M, Rodriguez-Garcia A, Sanchez ML, Orfao A, et al. (2002) Zinc-finger transcription factor Slug contributes to the function of the stem cell factor c-kit signaling pathway. *Blood* 100: 1274-1286.
 75. Tsuda M, Sasaoka Y, Kiso M, Abe K, Haraguchi S, et al. (2003) Conserved role of nanos proteins in germ cell development. *Science* 301: 1239-1241.
 76. Stapp AD, Gomez BI, Gifford CA, Hallford DM, Hernandez Gifford JA (2014) Canonical WNT signaling inhibits follicle stimulating hormone mediated steroidogenesis in primary cultures of rat granulosa cells. *PLoS One* 9: e86432.
 77. Lei L, Jin S, Mayo KE, Woodruff TK (2010) The interactions between the stimulatory effect of follicle-stimulating hormone and the inhibitory effect of estrogen on mouse primordial folliculogenesis. *Biol Reprod* 82: 13-22.
 78. Tao Y, Pinzi V, Bourhis J, Deutsch E (2007) Mechanisms of disease: signaling of the insulin-like growth factor 1 receptor pathway--therapeutic perspectives in cancer. *Nat Clin Pract Oncol* 4: 591-602.
 79. van der Veecken J, Oliveira S, Schiffelers RM, Storm G, van Bergen En Henegouwen PM, et al. (2009) Crosstalk between epidermal growth factor receptor- and insulin-like growth factor-1 receptor signaling: implications for cancer therapy. *Curr Cancer Drug Targets* 9: 748-760.
 80. Kowanetz M, Valcourt U, Bergstrom R, Heldin CH, Moustakas A (2004) Id2 and Id3 define the potency of cell proliferation and differentiation responses to transforming growth factor beta and bone morphogenetic protein. *Mol Cell Biol* 24: 4241-4254.
 81. Morita H, Mazerbourg S, Bouley DM, Luo CW, Kawamura K, et al. (2004) Neonatal lethality of LGR5 null mice is associated with ankyloglossia and gastrointestinal distension. *Mol Cell Biol* 24: 9736-9743.
 82. Schmieder R, Edwards R (2011) Quality control and preprocessing of metagenomic datasets. *Bioinformatics* 27: 863-864.
 83. Bolger AM, Lohse M, Usadel B (2014) Trimmomatic: a flexible trimmer for Illumina sequence data. *Bioinformatics* 30: 2114-2120.
 84. Kim D, Langmead B, Salzberg SL (2015) HISAT: a fast spliced aligner with low memory requirements. *Nat Methods* 12: 357-360.
 85. Li H, Handsaker B, Wysoker A, Fennell T, Ruan J, et al. (2009) The Sequence Alignment/Map format and SAMtools. *Bioinformatics* 25: 2078-2079.
 86. Love MI, Huber W, Anders S (2014) Moderated estimation of fold change and dispersion for RNA-seq data with DESeq2. *Genome Biol* 15: 550.

87. Hu H, Miao YR, Jia LH, Yu QY, Zhang Q, et al. (2018) AnimalTFDB 3.0: a comprehensive resource for annotation and prediction of animal transcription factors. *Nucleic Acids Res.*
88. Hulsen T, de Vlieg J, Alkema W (2008) BioVenn - a web application for the comparison and visualization of biological lists using area-proportional Venn diagrams. *BMC Genomics* 9: 488.
89. Tripathi S, Pohl MO, Zhou Y, Rodriguez-Frandsen A, Wang G, et al. (2015) Meta- and Orthogonal Integration of Influenza "OMICs" Data Defines a Role for UBR4 in Virus Budding. *Cell Host Microbe* 18: 723-735.

13. Acknowledgement

Firstly, I am deeply grateful to Dr. Yumiko Saga and Dr. Yuzuru Kato for supervising entire my research. Their suggestion helped me in all the time of research and writing of this thesis. Besides, discussions with committee members, Dr. T. Hirata, Dr. Y. Sakai, Dr. H. Sawa and Dr. K. Saito have been insightful to precede my study. Advice and comments given by all Saga lab members has been a great help for progressing my research. I thank Dr. T. Chinen, Dr. S. Yamamoto and Dr. D. Kitagawa for helping with the immunostaining of MII spindle, Ms. A. Masuda and Mr. T. Naka for helping some of experiments in Chapter I and Danelle Wright for editing this manuscript. I appreciate for Mr. M. Muraoka for programing and its support in second part.

In addition, first part is supported by Grant-in-Aid for JSPS Research Fellow. RNA-seq analysis in Chapter II was supported by Platform for Advanced Genome Science (PAGS).

Last, I would like to thank my family, friends and fish in Shizuoka prefecture for supporting my quality of life.

Figure 1

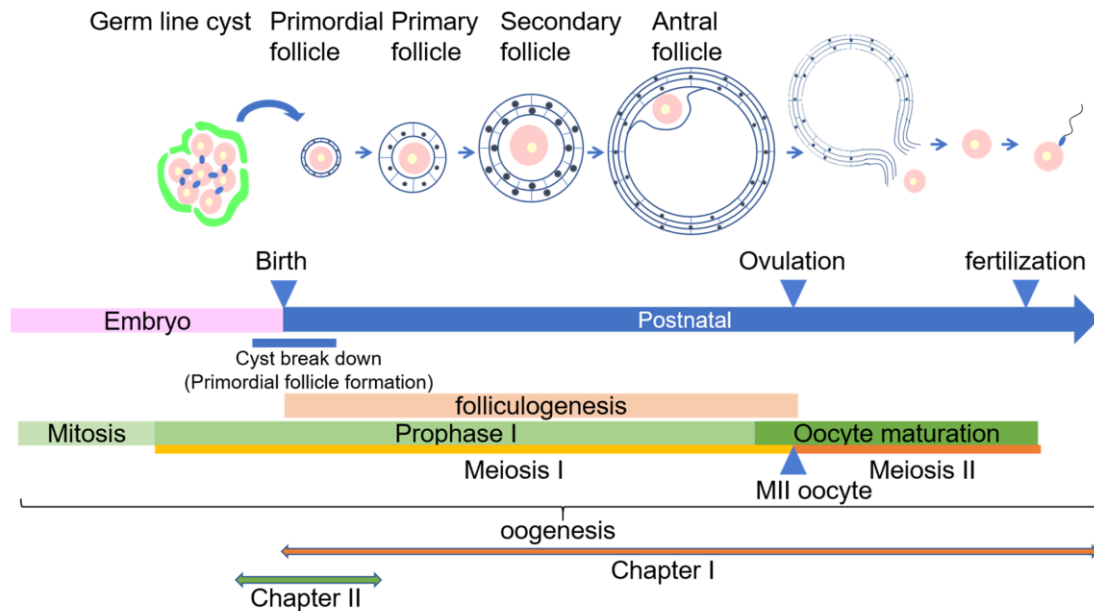


Figure 1. Schematic presentation of oogenesis timeline in mice

Mammalian oogenesis consists of two genetically distinct events, meiosis and folliculogenesis. Female germ cells enter meiosis around E13.5 and arrest at prophase-I until puberty. Following completion of meiosis-I just before ovulation, oocytes enter meiosis-II and arrest for the second time. Fertilization triggers restart and completion of meiosis-II. Folliculogenesis is initiated by cyst breakdown followed by primordial follicle formation in neonatal ovaries, by which oocytes are enclosed by pre-granulosa cells. Activated follicles develop to primary, secondary, antral follicle with growth of oocytes and proliferation of granulosa cells and finally are ovulated. In this study, I focused on DAZL function in postnatal stage in Chapter I (shown in orange two-way arrow) and pre-granulosa cell differentiation around birth in Chapter II (shown in green two-way arrow).

Figure 2

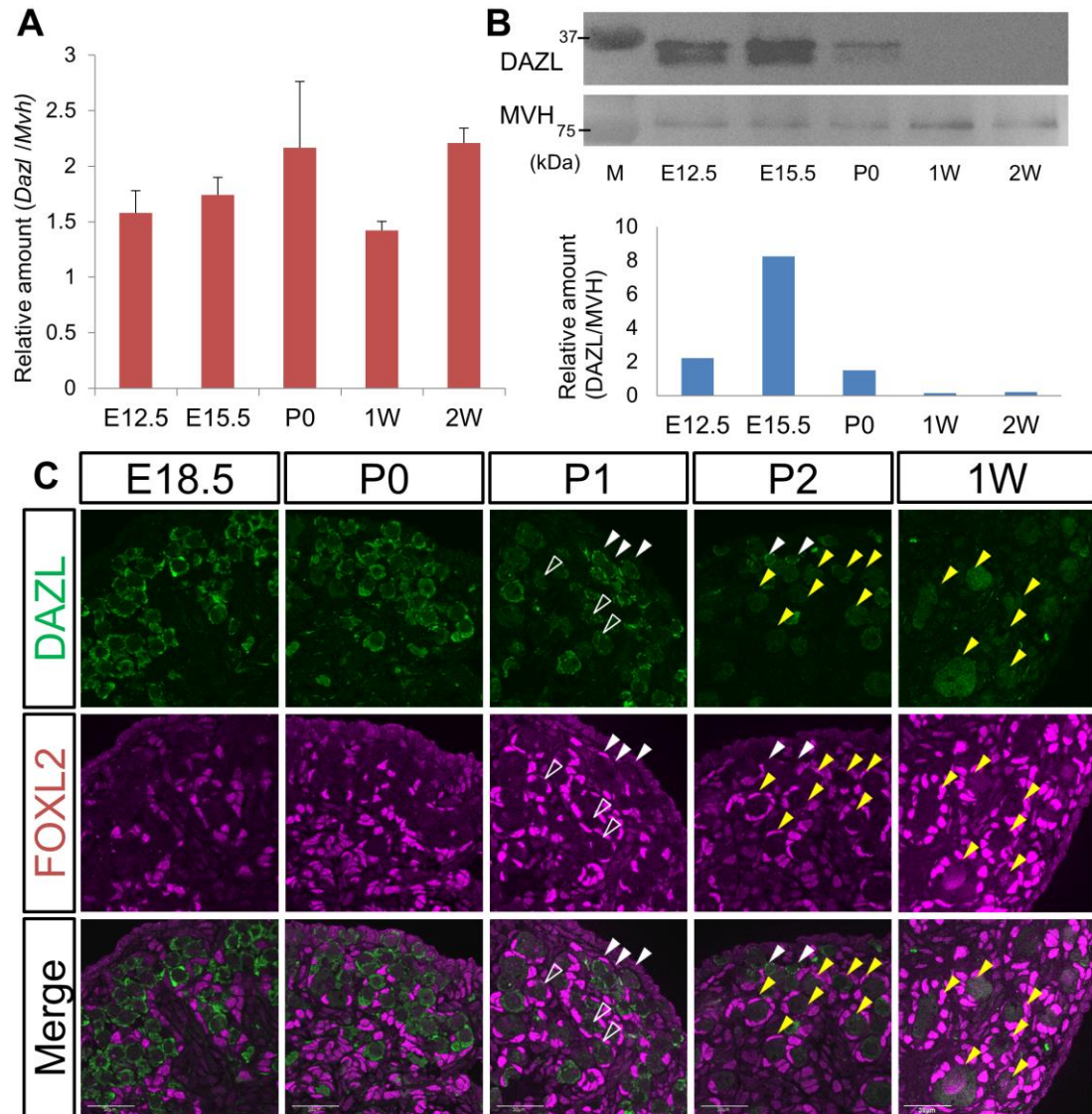


Figure 2. DAZL expression is suppressed in postnatal oocytes

(A) RT-qPCR analysis for *Dazl* in wild-type (WT) female gonads at E12.5 (n=4), E15.5 (n=3), P0 (n=3), 1 week (1W) (n=3), and 2 weeks (2W) (n=3). *Mvh* (also known as *Ddx4*) was used as a normalizer because this gene is continuously expressed in germ cells from E12.5 to secondary follicles. The vertical axis represents relative expression level of *Dazl* to *Mvh*. Error bars represent S.D. (B) Western blotting analysis for DAZL from E12.5 to 2W ovaries. Two bands representing DAZL were detected. As the molecular weight of DAZL is estimated to be 33KDa, the lower band corresponds with this. However, both bands disappear in *Dazl* knockout ovaries, indicating that both two bands are DAZL signals. Quantification of western data is shown below. The vertical axis represents relative DAZL expression level normalized by MVH. (C) Immunofluorescence analysis for DAZL (green) and FOXL2 (magenta) from E18.5 to P2, and 1W ovaries. White arrowheads indicate cystic oocytes, and yellow arrowheads indicate primordial follicles. Open arrowheads indicate oocytes showing weaker DAZL expression. Scale bar, 30 μ m.

Figure 3

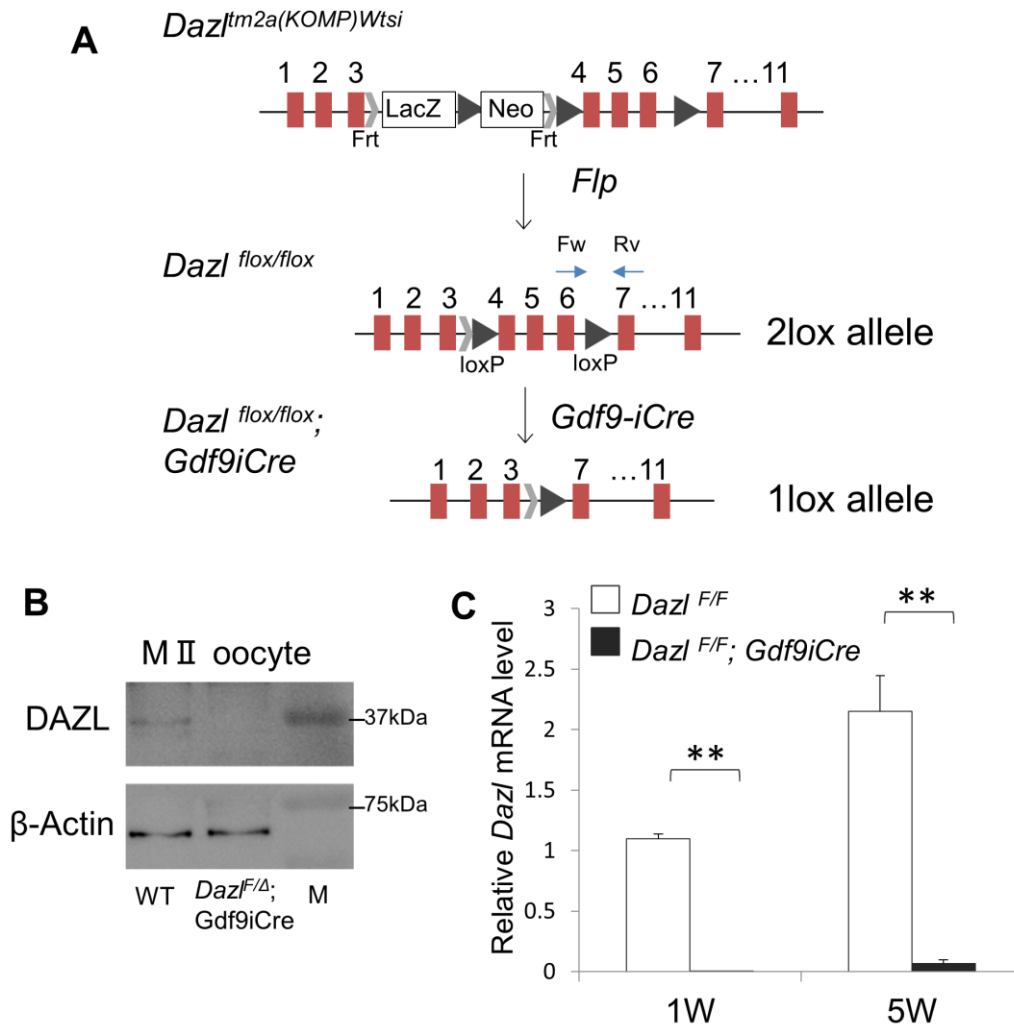


Figure 3. *Dazl* expression is effectively eliminated in postnatal oocytes

(A) A schematic diagram of the generation of conditional *Dazl* knockout mice. *Dazl* flox/flox females were crossed with *Dazl* flox/flox; *Gdf9-iCre* male mice to obtain *Dazl* flox/flox; *Gdf9-iCre* (conditional *Dazl* knockout) females. Blue arrows indicate the position of primers used for RT-qPCR in (C). (B) Western blotting analysis for WT and *Dazl* cKO MII oocytes (C) RT-qPCR analysis for *Dazl* in 1 and 5W ovaries using a primer set that amplifies only the WT allele (lower graph, n=3). Error bars represent S.D. Significance level of changes are indicated (two-tailed student's t-test; ** P < 0.005).

Figure 4

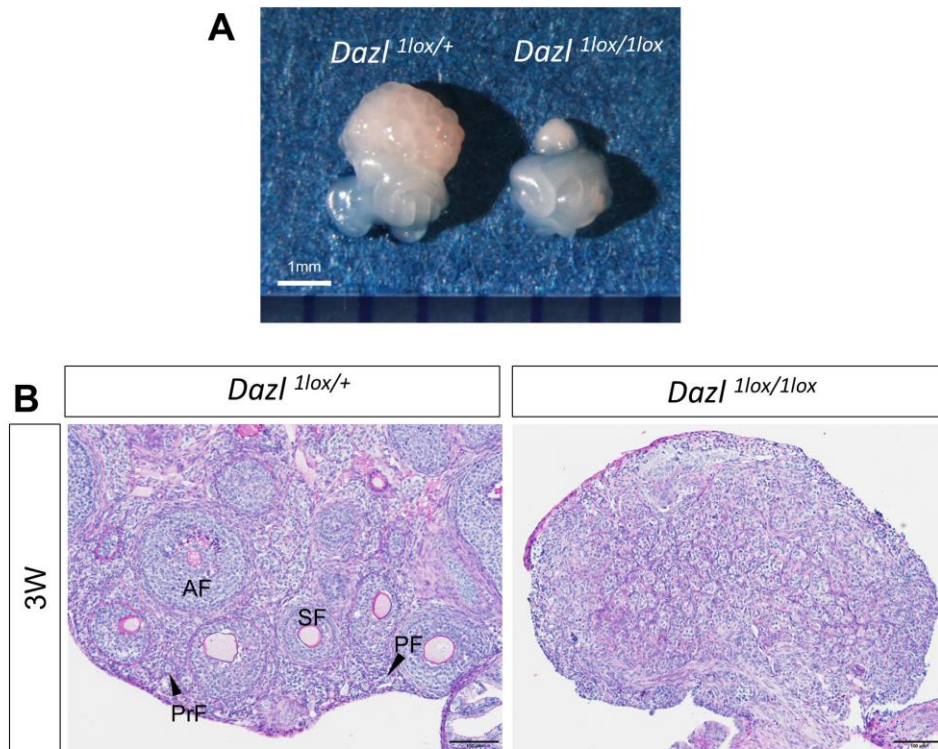


Figure 4. 1lox allele reproduce *Dazl* KO phenotype

(A) A photograph of *Dazl*^{1lox/+} and *Dazl*^{1lox/1lox} 3W ovaries. Scale bar, 1 mm.

(B) Periodic acid-Schiff (PAS) staining of *Dazl*^{1lox/+} and *Dazl*^{1lox/1lox} 3W ovaries. Note that homozygous mutants contain no oocytes, reminiscent of the previous *Dazl* knockout ovary. PF, primordial follicle; PrF, primary follicle; SF, secondary follicle; and AF, antral follicle. Scale bars, 100 μm.

Figure 5

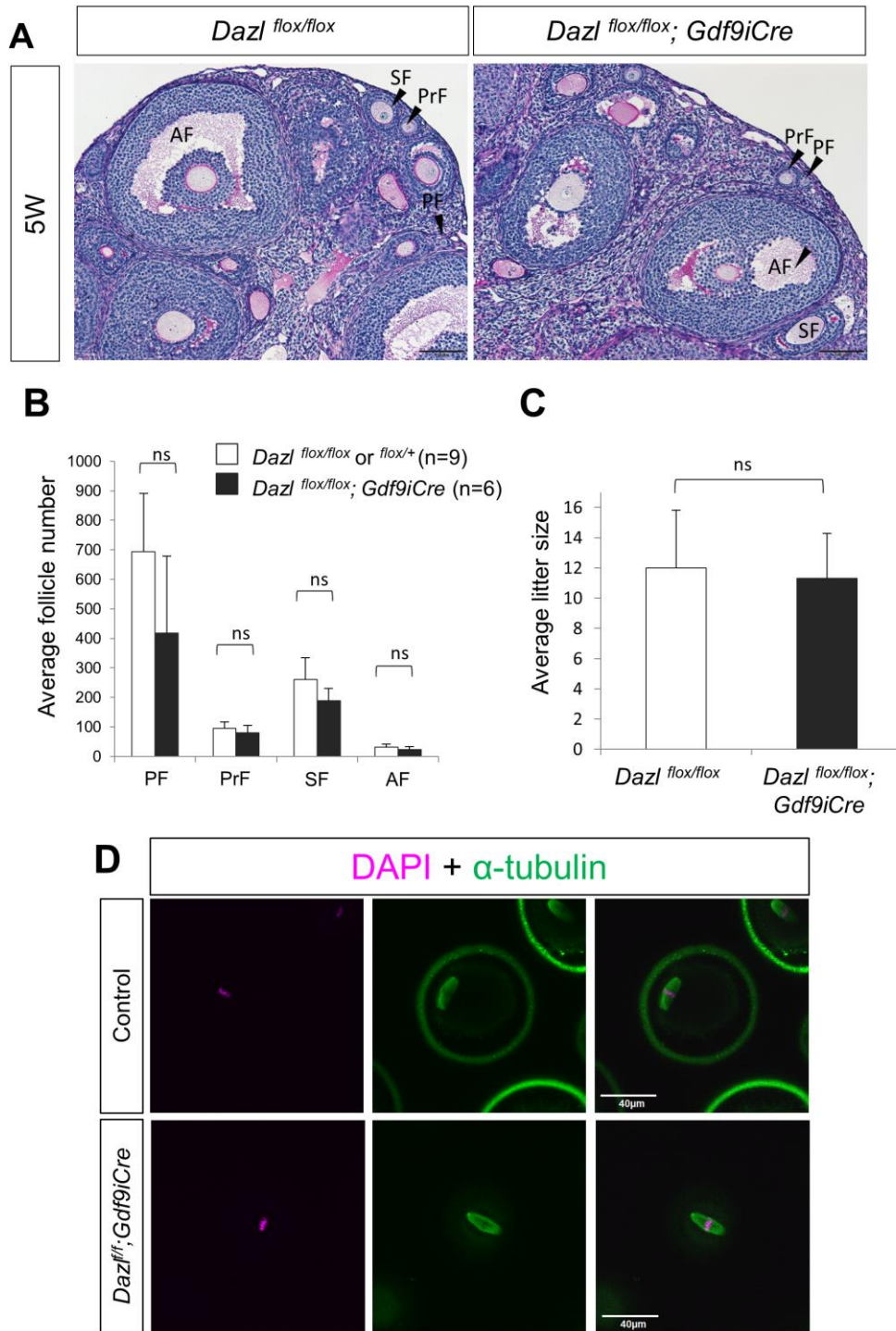


Figure 5. Postnatal oocyte-specific *Dazl* knock-out mice do not exhibit any defects

(A) PAS staining of control (left) and cKO (right) ovaries at 5W after birth. PF, primordial follicle; PrF, primary follicle; SF, secondary follicle; and AF, antral follicle. Scale bars, 100 μ m (B) Follicle counting analysis of control (white bar, n=9) and *Dazl* cKO (black bar, n=6) ovaries at 5 weeks after birth. Error bars represents S.D. ns, no significant difference between control and *Dazl* cKO ovaries (two-tailed student's t-test). (C) Average litter size of control (n=3) and *Dazl* cKO females (n=5). Error bars represent S.D. ns, same as in (B). (D) Immunostaining of MII oocytes of control (n=85) and *Dazl*^{fl/fl}; *Gdf9iCre* (n=34), *Dazl* 3F (n=45) using an antibody against for α -tubulin (green). DNA was counterstained with DAPI (magenta). Scale bar, 40 μ m.

Figure 6

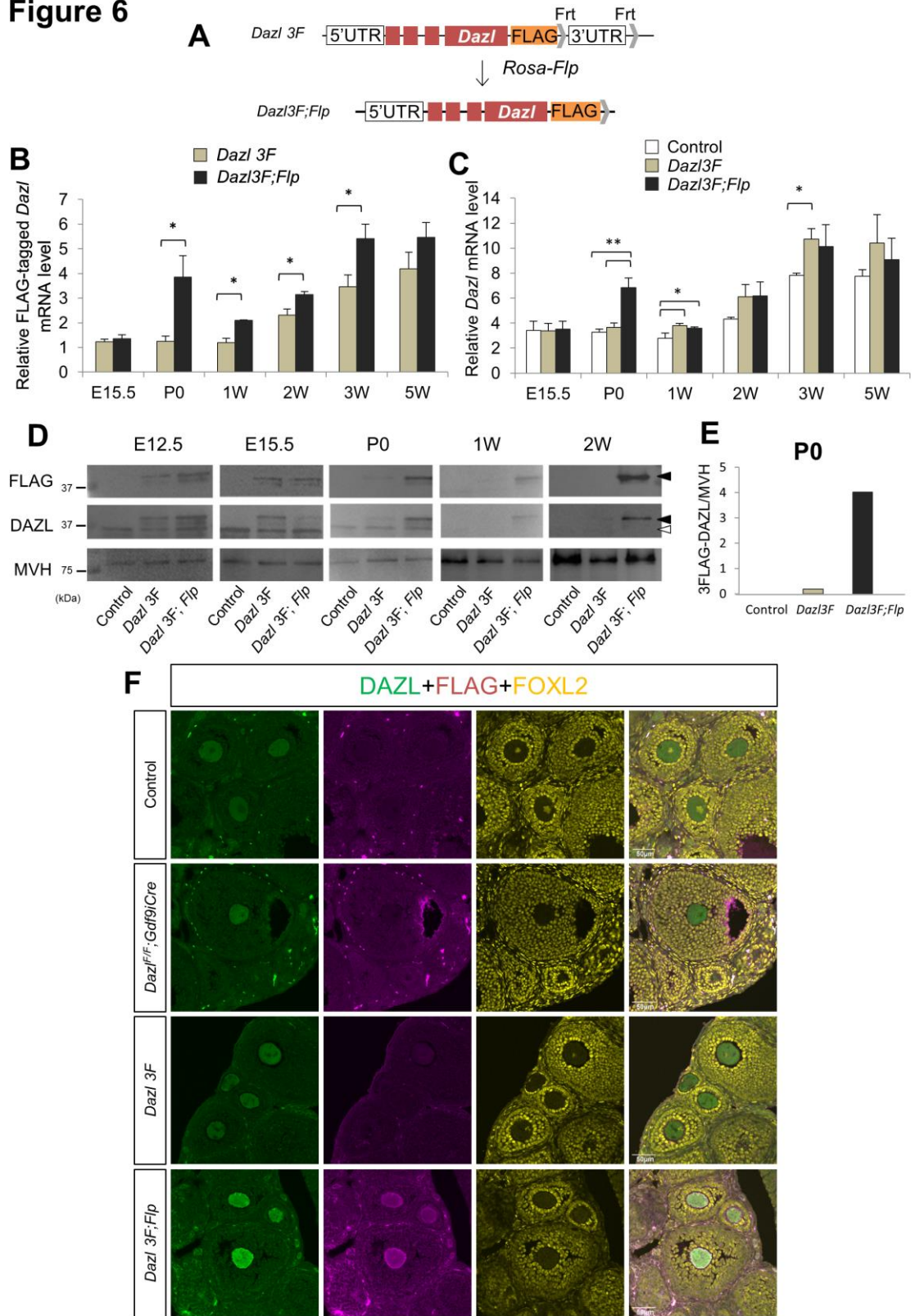


Figure 6. 3'-UTR-dependent suppression of DAZL in follicular oocytes

(A) Schematic diagram of the bacterial artificial chromosome (BAC)-carrying transgenic mouse line. The *Dazl*'s 3'-UTR was removed by crossing with Rosa-Flp hetero male mice. (B) RT-qPCR for 3Flag-*Dazl* using ovary extracts from E15.5 to 5 weeks (n=3, except for *Dazl* 3F; *Flp* at E15.5, n=4). The vertical axis represents the relative mRNA expression level of 3Flag-*Dazl* normalized by *Mvh*. Significance level of changes are indicated (two-tailed student's t-test; *p < 0.05). (C) RT-qPCR for total (endogenous and 3Flag) *Dazl* from E15.5 (control, n=8; *Dazl* 3F, n=3; *Dazl* 3F; *Flp*, n=4), P0 (n=3), 1W (n=4; 3; 3), 2W (n=3; 3; 4), and 5W (n=3) ovaries. The vertical axis represents relative mRNA expression level of total *Dazl* normalized by *Mvh*. Significance level of changes are indicated (two-tailed student's t-test; **P<0.005, *P<0.05). (D) Western blotting analysis of FLAG (top) and endogenous DAZL (middle). MVH was used as a control. Filled and open arrowheads indicate FLAG- and endogenous DAZL, respectively. (E) Relative quantification of FLAG-DAZL between control (white bar), *Dazl* 3F (gray bar), and *Dazl* 3F; *Flp* (black bar) in P0 ovary. The vertical axis represents the normalized values of FLAG-DAZL by MVH. (F) Immunostaining of 3W ovary from control, *Dazl* cKO, *Dazl* 3F and *Dazl* 3F; *Flp* using antibodies against for DAZL (green), FLAG (magenta), and FOXL2 (yellow). Scale bars, 50 μ m.

Figure 7

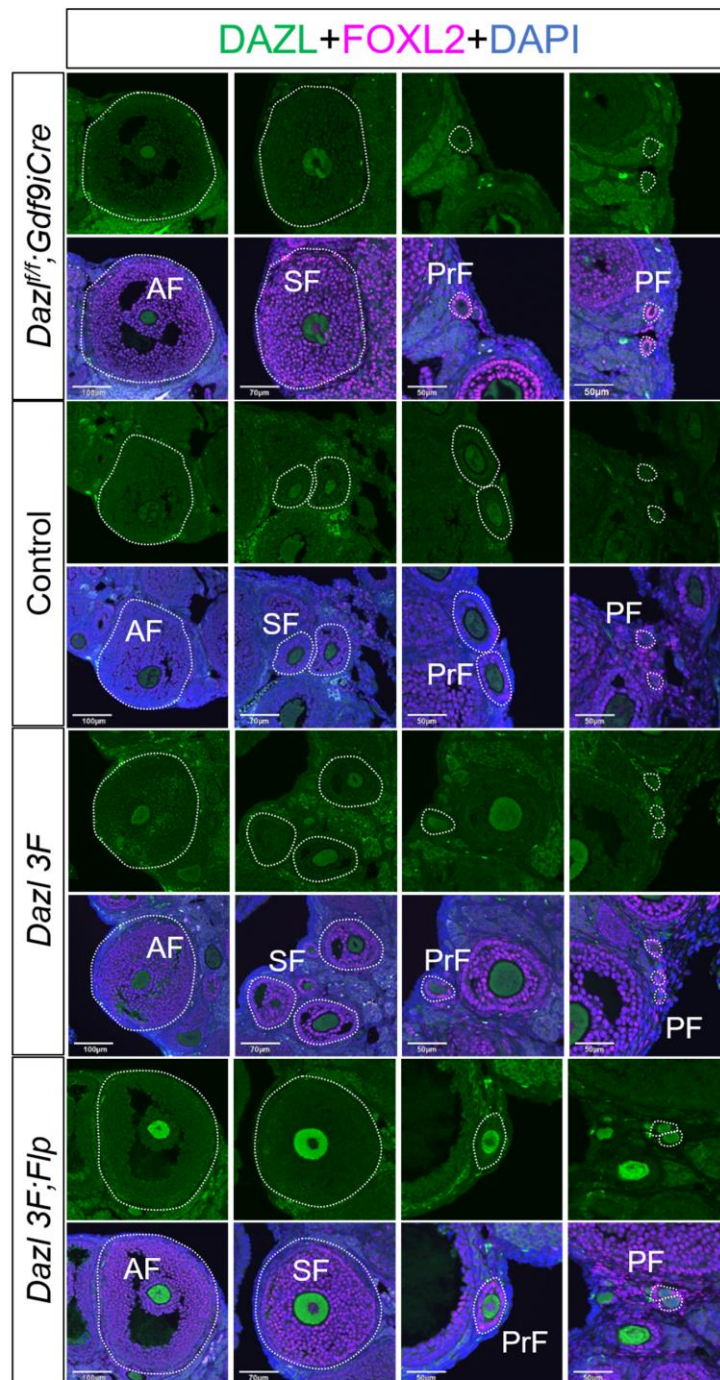


Figure 7. DAZL expression is retained in all stage of follicular oocyte in *Dazl 3F; Flp* mice

Immunostaining of 5W ovaries of control, *Dazl^{fl/fl}; Gdf9iCre*, *Dazl 3F* and *Dazl 3F; Flp* mice. Antibodies against for DAZL (green) and FOXL2 (magenta) were used, and DNA was counterstained with DAPI. PF, primordial follicle; PrF, primary follicle; SF, secondary follicle; and AF, antral follicle. Scale bar, 50 μ m.

Figure 8

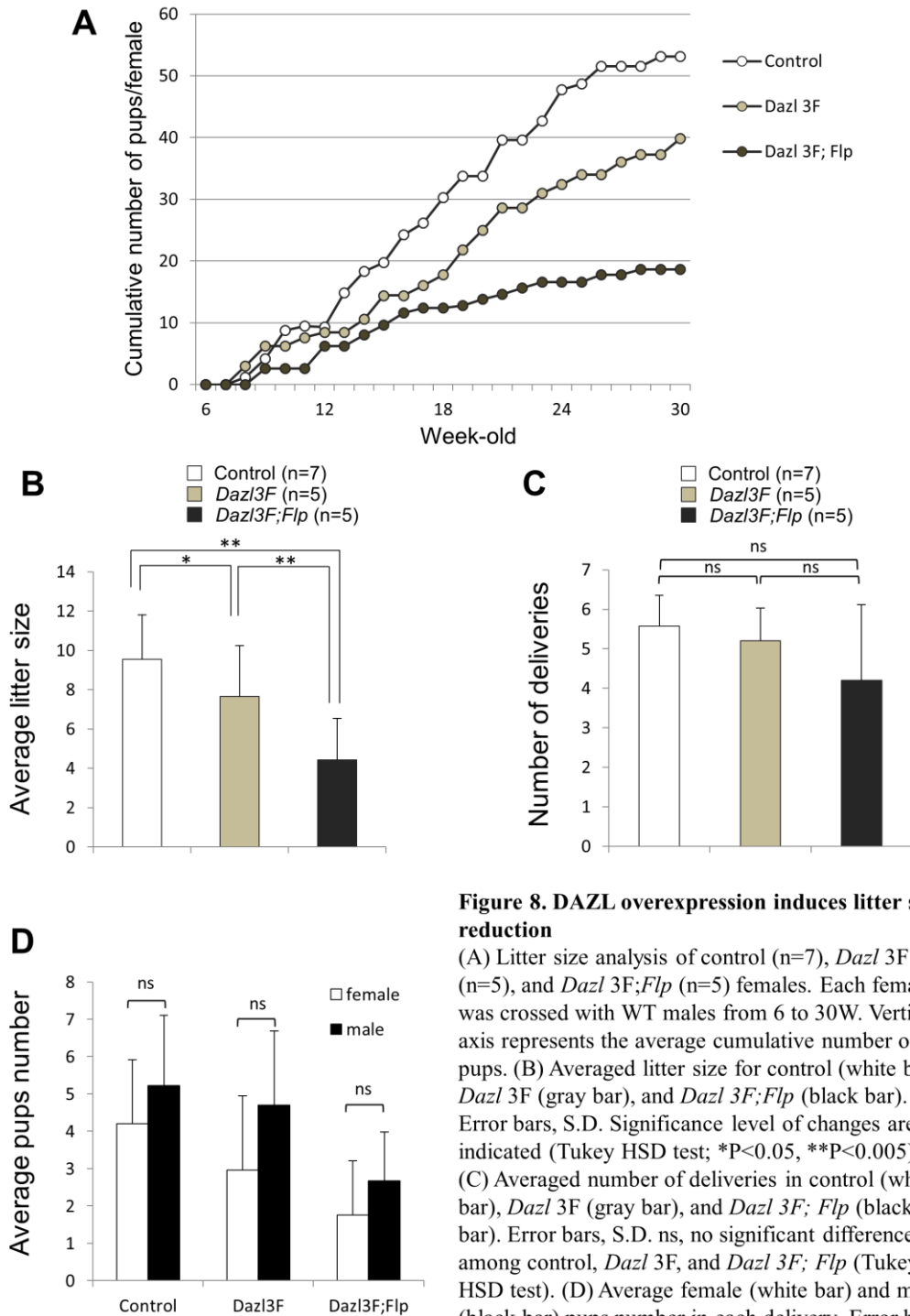


Figure 8. DAZL overexpression induces litter size reduction

(A) Litter size analysis of control (n=7), *Dazl 3F* (n=5), and *Dazl 3F;Flp* (n=5) females. Each female was crossed with WT males from 6 to 30W. Vertical axis represents the average cumulative number of pups. (B) Averaged litter size for control (white bar), *Dazl 3F* (gray bar), and *Dazl 3F; Flp* (black bar). Error bars, S.D. Significance level of changes are indicated (Tukey HSD test; *P<0.05, **P<0.005). (C) Averaged number of deliveries in control (white bar), *Dazl 3F* (gray bar), and *Dazl 3F; Flp* (black bar). Error bars, S.D. ns, no significant differences among control, *Dazl 3F*, and *Dazl 3F; Flp* (Tukey HSD test). (D) Average female (white bar) and male (black bar) pups number in each delivery. Error bars, S.D. ns, no significant differences between male and female in control, *Dazl 3F*, and *Dazl 3F; Flp* (Student's t-test).

Figure 9

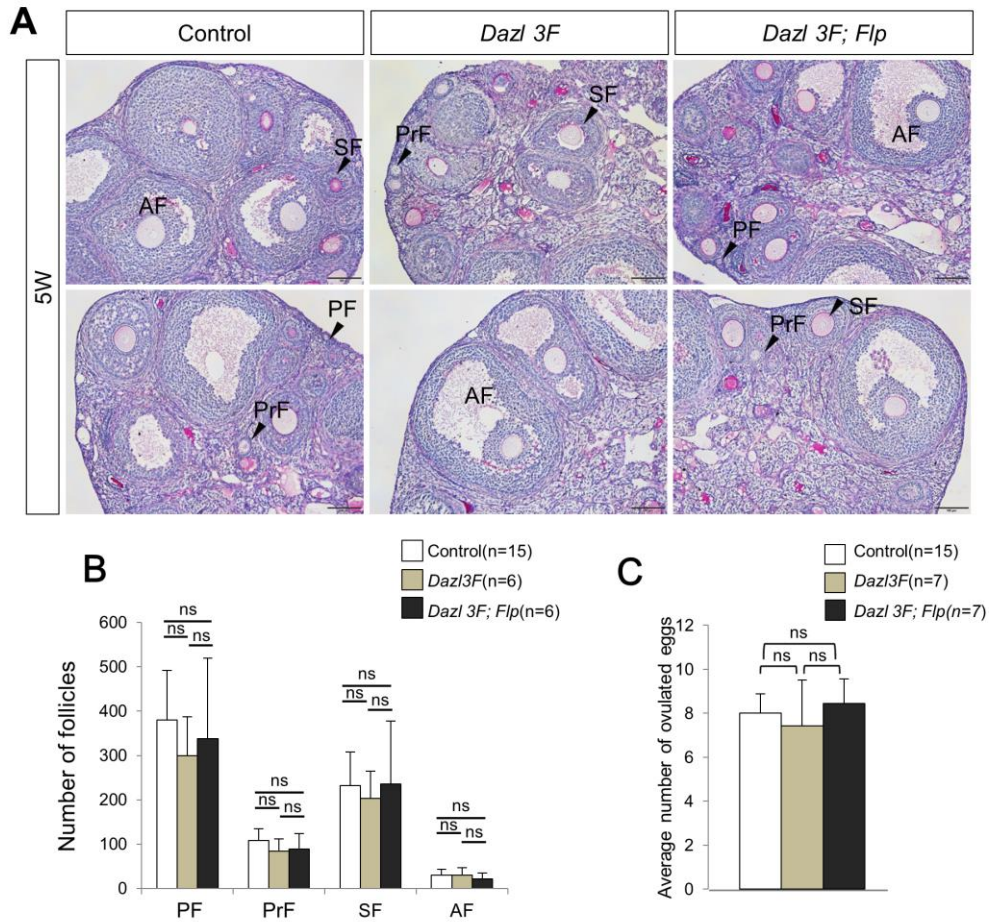
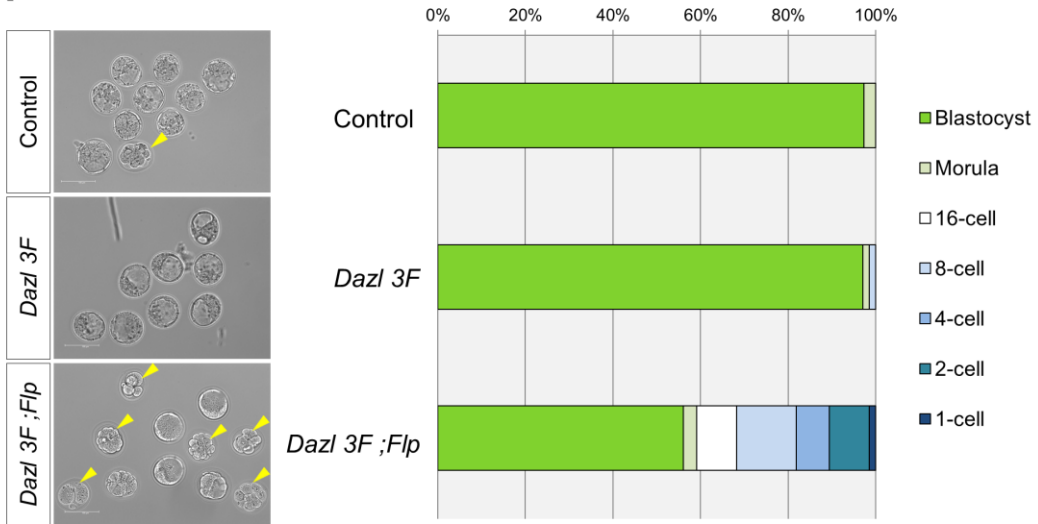


Figure 9. Excess DAZL expression didn't cause defects folliculogenesis and ovulation of oocytes.

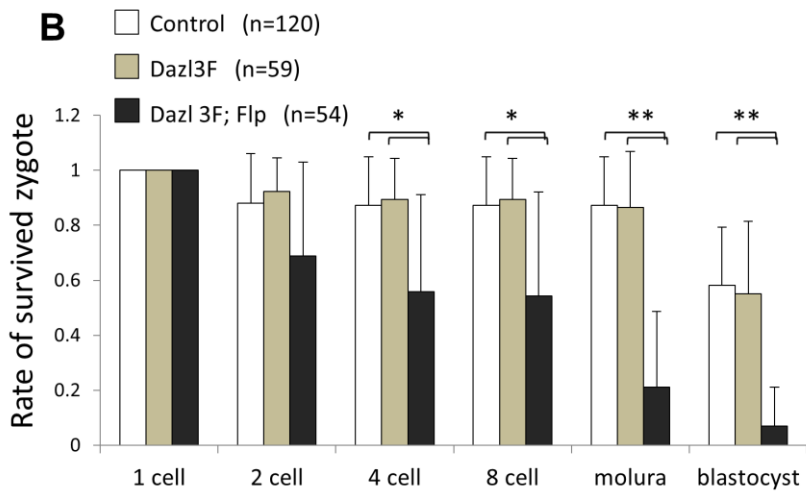
(A) PAS staining of control, *Dazl 3F*, and *Dazl 3F; Flp* ovaries at 5 weeks after birth. PF, primordial follicle; PrF, primary follicle; SF, secondary follicle; and AF, antral follicle. Scale bars, 100 μ m. (B) Follicle counting analysis for control (n=15), *Dazl 3F* (n=6), and *Dazl 3F; Flp* (n=6) using ovarian sections at 5 weeks after birth. Error bars represent S.D. ns, no significant difference among control, *Dazl 3F*, and *Dazl 3F; Flp*. (C) The average number of ovulated eggs from control (n=15), *Dazl 3F* (n=7), and *Dazl 3F; Flp* (n=7) females. Error bars, S.D. ns, no significant difference among control, *Dazl 3F*, and *Dazl 3F; Flp* (Tukey HSD test).

Figure 10

A



B



C

P value of Dazl 3F; Flp from 1cell zygote to blastocyst

	1cell	2cell	4cell	8cell	Molura	Blastocyst
1cell	-	0.2046919	0.026038	0.0193553	0.000045	0.0000026
2cell	0.2046919	-	0.9342966	0.896228	0.034777	0.0028901
4cell	0.026038	0.9342966	-	0.9999966	0.2522386	0.034777
8cell	0.0193553	0.896228	0.9999966	-	0.3067357	0.0460896
Molura	0.000045	0.034777	0.2522386	0.3067357	-	0.9342966
Blastocyst	0.0000026	0.0028901	0.034777	0.0460896	0.9342966	-

Figure 10. Defective pre-implantation development is a cause of the litter size reduction.

(A) Analysis of pre-implantation development in BAC transgenic females. (Left) E3.5 embryos from control, *Dazl* 3F, and *Dazl* 3F; *Flp* females. Yellow arrowheads indicate abnormal embryos. Scale bars, 100 μ m. (Right) Proportion of embryos that developed to each stage up to blastocysts. Embryos collected from pregnant females at E3.5 were counted. Delayed embryos were cultured for an additional two days and ones that reached the blastocyst stage were added. Control (n=75), *Dazl* 3F (n=69) and *Dazl* 3F; *Flp* (n=56). (B) Survival rates of preimplantation embryos. One-cell stage zygotes (n=total number of embryos examined, number of used mothers) were collected from control (n=120, 15), *Dazl* 3F (n=59, 7) and *Dazl* 3F; *Flp* (n=54, 7) mothers. The proportion of surviving zygotes at each stage was calculated as follows: the number of surviving zygotes out of the number of 1-cell zygotes in each experiment (mother). Error bars, S.D. Significance level of changes are indicated (Tukey HSD; **P<0.005, *P<0.05). (C) Statistical analysis of surviving zygotes compared to 1-cell zygotes with two cell zygote to blastocysts in *Dazl* 3F; *Flp* (n=54). The p-value for the average number of zygotes in each stage was calculated using Tukey HSD. P<0.05 is written in red.

Figure 11

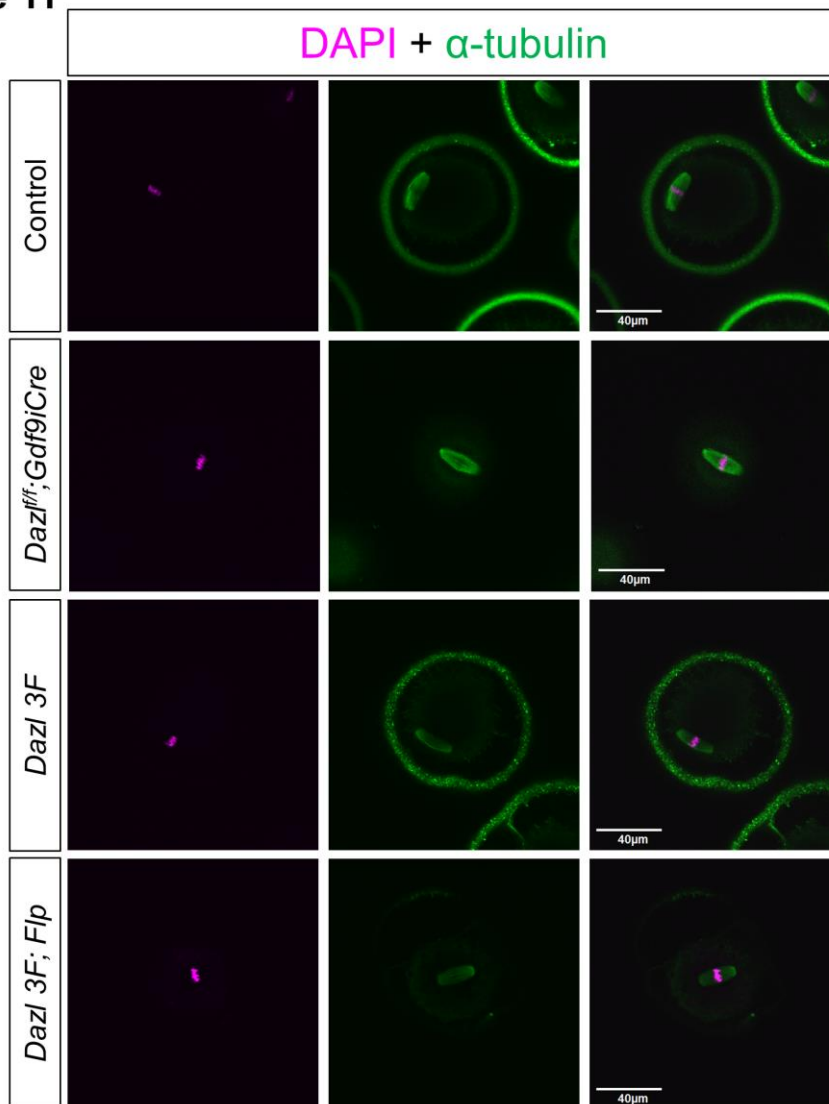


Figure 11. MII spindle is normally formed in all genotypes.

Immunostaining of MII oocytes of control (n=85), *Dazl^{fl/fl}; Gdf9iCre* (n=34), *Dazl 3F* (n=45) and *Dazl 3F; Flp* (n=37) MII oocytes using an antibody against for α -tubulin (green). DNA was counterstained with DAPI (magenta). Scale bar, 40 μ m.

Figure 12

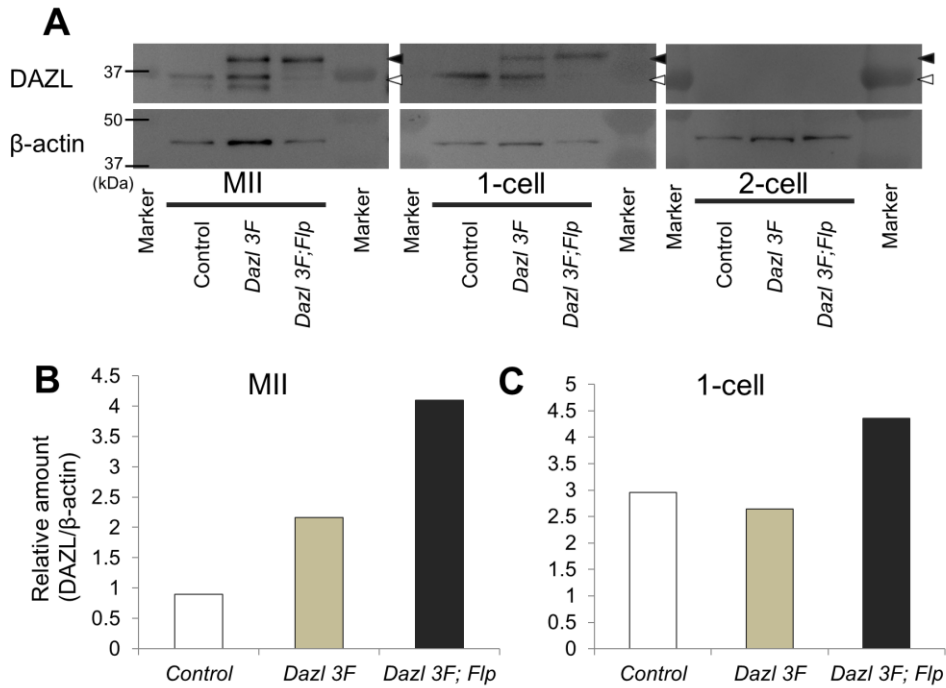


Figure 12. DAZL expression in preimplantation embryos

(A) Western blotting analysis of MII oocytes and 1- and 2-cell embryos. Both FLAG and endogenous DAZL were detected using the anti-DAZL antibody. Anti- β actin antibody was used as a loading control. Note that both FLAG and endogenous DAZL were not detectable in 2-cell embryos. Filled and open arrowheads indicate FLAG- and endogenous DAZL, respectively. (B,C) Quantification of western blotting results for MII and 1-cell samples. The vertical axis represents relative DAZL expression level normalized by β actin.

Figure 13

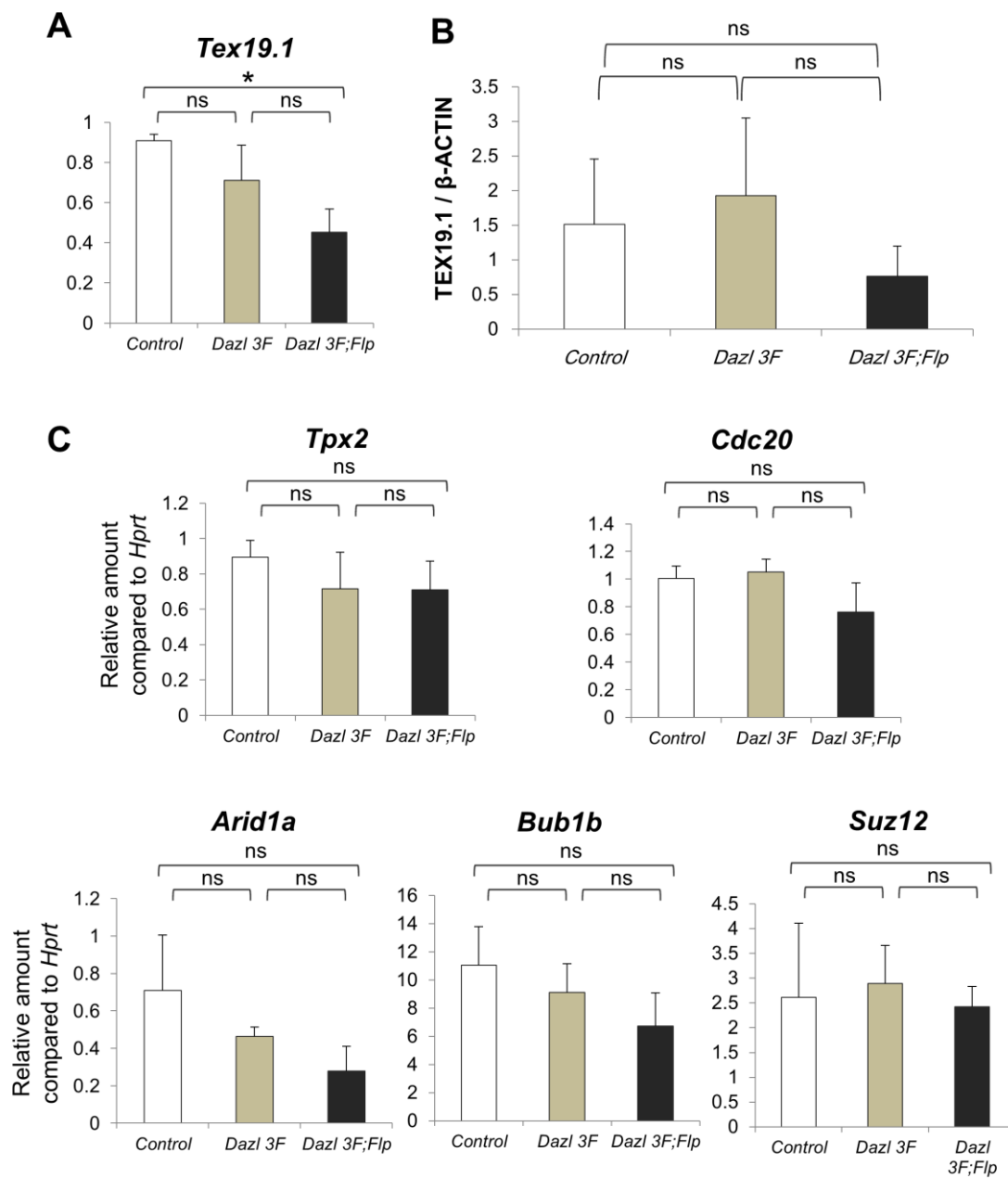


Figure 13. Expression level of Putative Dazl target gene M II oocytes in *Dazl 3F; Flp*

(A) RT-qPCR for *Tex19.1* using M II oocyte from control (n=3), *Dazl 3F* (n=3), and *Dazl 3F; Flp* (n=3). Vertical axis represents relative mRNA expression level normalized by *Hprt*. Significance level of changes are indicated (Tukey HSD; *p < 0.05). (B) Quantification of western blotting results of TEX19.1 for MII oocyte from control, *Dazl 3F*, and *Dazl 3F; Flp* samples. The vertical axis represents relative DAZL expression level normalized by β -ACTIN. Error bars, S.D. ns, no significant differences. Significance level of changes are indicated (Tukey HSD test; *P<0.05). (C) RT-qPCR for putative *Dazl* target genes using M II oocyte from control (n=3), *Dazl 3F* (n=3), and *Dazl 3F; Flp* (n=3). Vertical axis represents relative mRNA expression level normalized by *Hprt*. Error bars, S.D. ns, no significant differences.

Chapter II

Figure 14

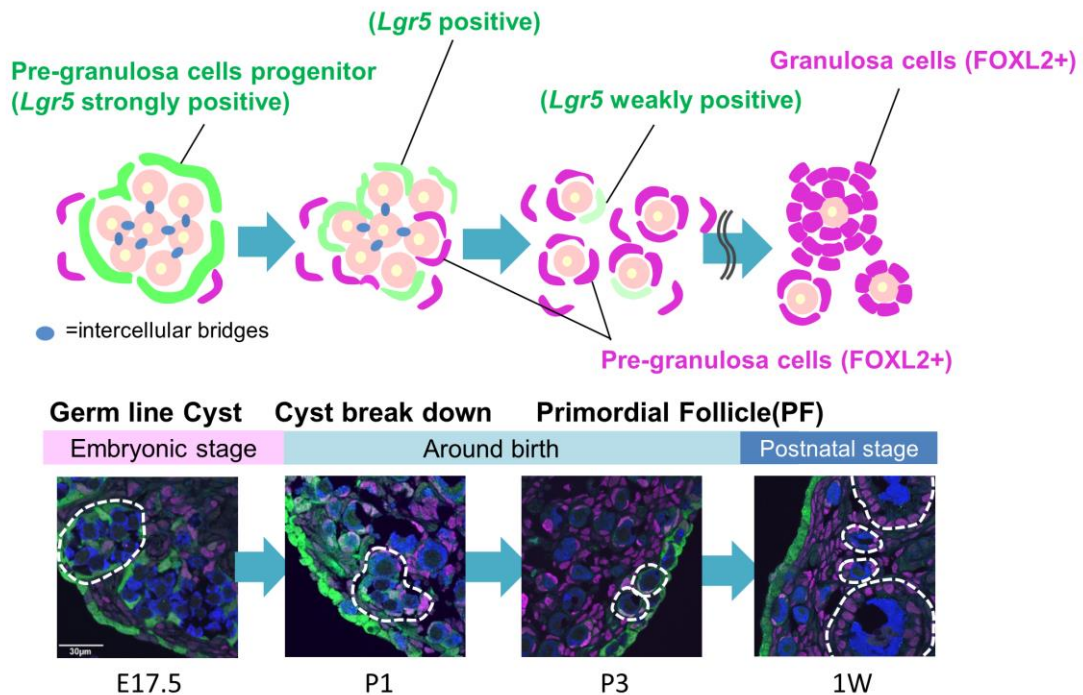


Figure 14. Process of primordial follicle (PF) formation

In the late embryonic stage (E17.5), germ cells (pink in upper scheme and blue in lower pictures) are connected each other via intercellular bridges (blue oval shown in upper scheme) and compose germ line cyst which were enclosed by pre-granulosa cell progenitor (*Lgr5*-positive cells shown in green in upper and lower panels). Around birth (P1 and P3), pre-granulosa cell progenitors start to differentiate into pre-granulosa cells (FOXL2-positive cells shown in magenta in upper and lower panels). Pre-granulosa cells invade between oocytes and separate them to make primordial follicle. In the postnatal development (1W), some of follicles begin follicle growth concomitant with morphological changes of pre-granulosa cells to cuboidal shape. Thereafter, oocytes become bigger and bigger with increase the number of granulosa cells to grow up mature oocytes. Dashed lines shown in lower pictures indicate germ line cyst in E17.5 and P1, and indicate each follicle in P3 and 1W. Immunostaining for each stage is performed by using antibodies against for GFP (green), MVH (blue), and FOXL2 (magenta).

Figure 15

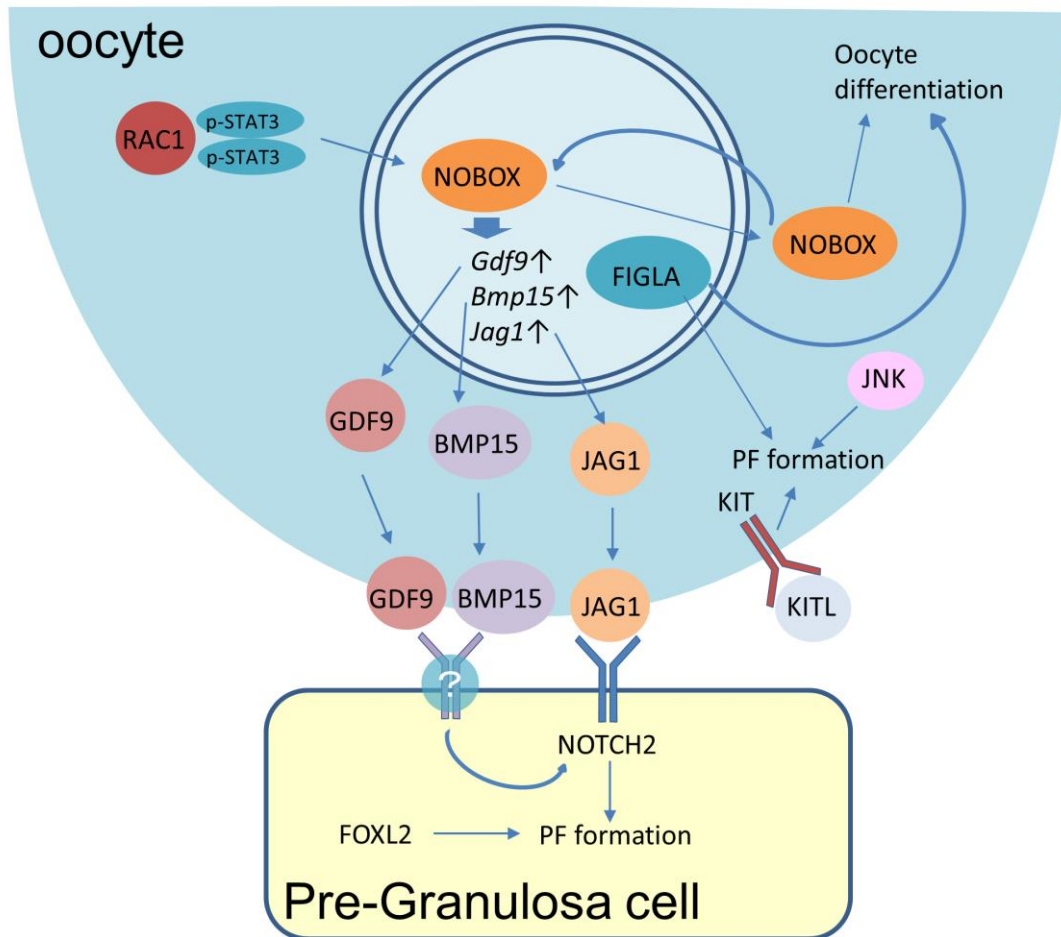


Figure 15. Known molecular network during primordial follicle formation

In oocyte, STAT3 translocated to the nucleus by RAC1 promotes transcription of *Jag1*, *GDF9*, *BMP15* and *Nobox*. The transcriptional factor *Nobox* have a key role in follicular development of oocyte. In addition, GDF9 and BMP15 bind to the receptor in pre granulosa cells and activate mTORC1, which facilitates *Notch2* translation in pre-granulosa cell. JAG1 binds to NOTCH2 to activate Notch signaling pathway. Activated NOTCH2 promotes germline cell cysts breakdown and primordial follicle formation. Other than STAT3-mediated pathway, KIT and JNK signaling pathways and transcription factor FIGLA are known to involve in PF formation. Furthermore, in pre-granulosa cell, FOXL2 have a crucial role in follicular cell development.

Figure 16

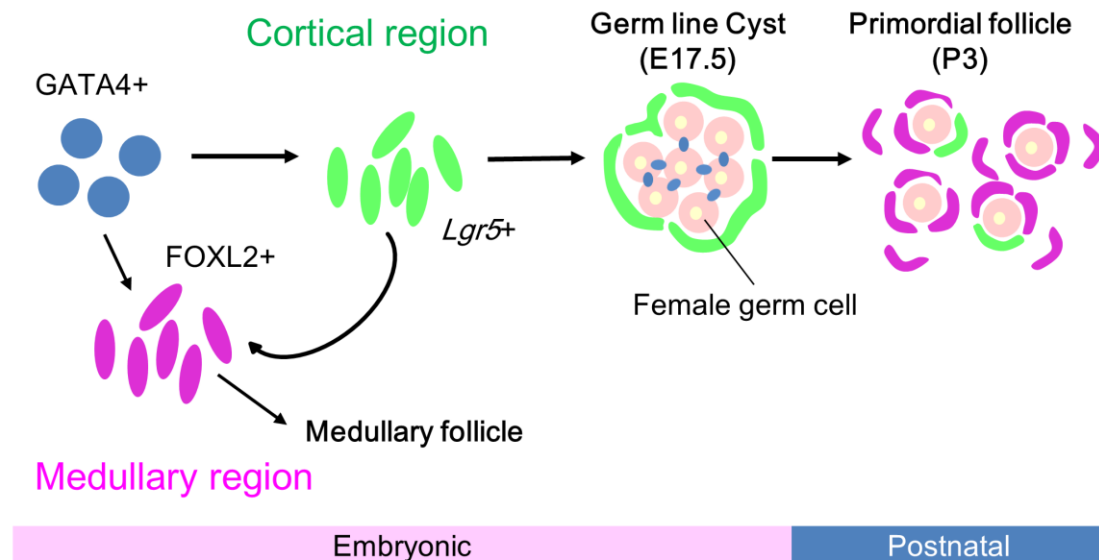


Figure 16. Lineage of granulosa cell

All pre-G lineage originates from GATA4+ cells (blue cell). Some of them directly differentiate into FOXL2+ cell (magenta) in early embryonic stage, which become medullary follicle and contribute to the fertility in young adulthood (not focused on this study). The other cells localized to cortical region marked by *Lgr5*+ cells (green) contribute to the fertility the rest of the reproductive life. A part of *Lgr5*+ cells differentiate into FOXL2+ during embryonic stage as a medullary follicle. Other *Lgr5*+ cells retained around birth which may contribute to primordial follicle formation and finally differentiate into FOXL2+ cell (focused on this study).

Figure 17

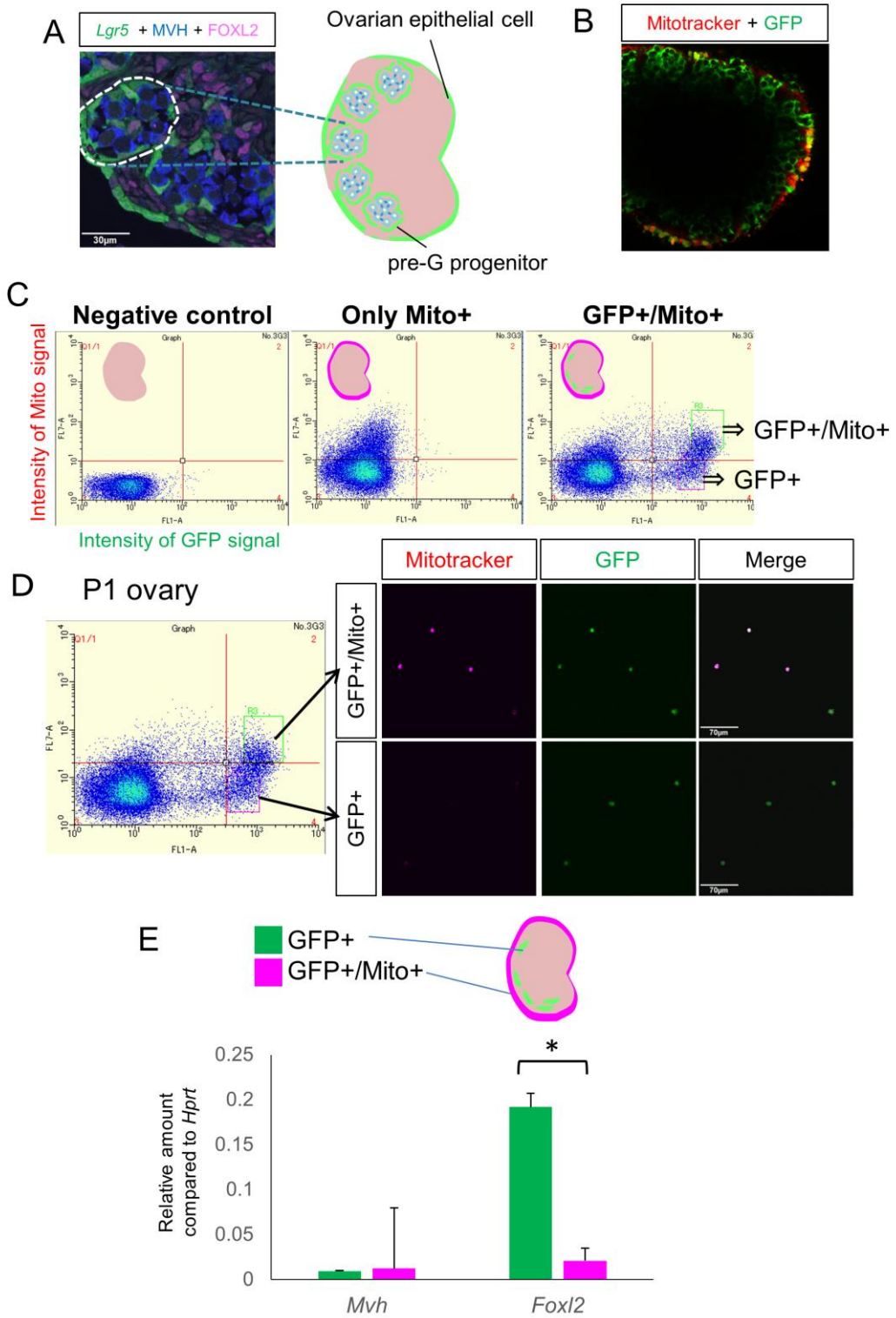


Figure 17. Development of a method to isolate pre-granulosa cell progenitors

(A) Immunostaining analysis of E17.5 *Lgr5*-EGFP mouse ovary to GFP (green), MVH (blue) and FOXL2 (magenta). *Lgr5* expression was observed in OE cells and pre-G progenitors. **(B)** A representative image taken by multi photon microscopy for Mitotracker (red) and GFP (green) of whole mount P1 *Lgr5*-EGFP ovary. **(C)** Dot plots of ovarian cells from P1 control, Mitotracker-treated ovaries (Mito +), and *Lgr5*-EGFP ovaries treated with Mitotracker (GFP +/ Mito +). X and Y axes represent GFP and Mitotracker intensity, respectively. Green square represent as R3 contains GFP +/Mito + and pink square represent as R4 contains GFP+ cells. **(D and E)** Evaluation of GFP positive cells. **(D)** Fluorescent images of isolated GFP +/ Mito + (Upper panel) and GFP+ (Lower panel) cells observed by fluorescent microscopy. Magenta signals represent Mitotracker and Green signals represent GFP signal. **(E)** RT-qPCR analysis for *Mvh* and *Foxl2* for *Lgr5*-single positive cells (green bar) and Mitotracker/*Lgr5*-double positive cells (magenta bar). The vertical axis represents relative expression level of *Mvh* and *Foxl2* to *Hprt*.

Figure 18

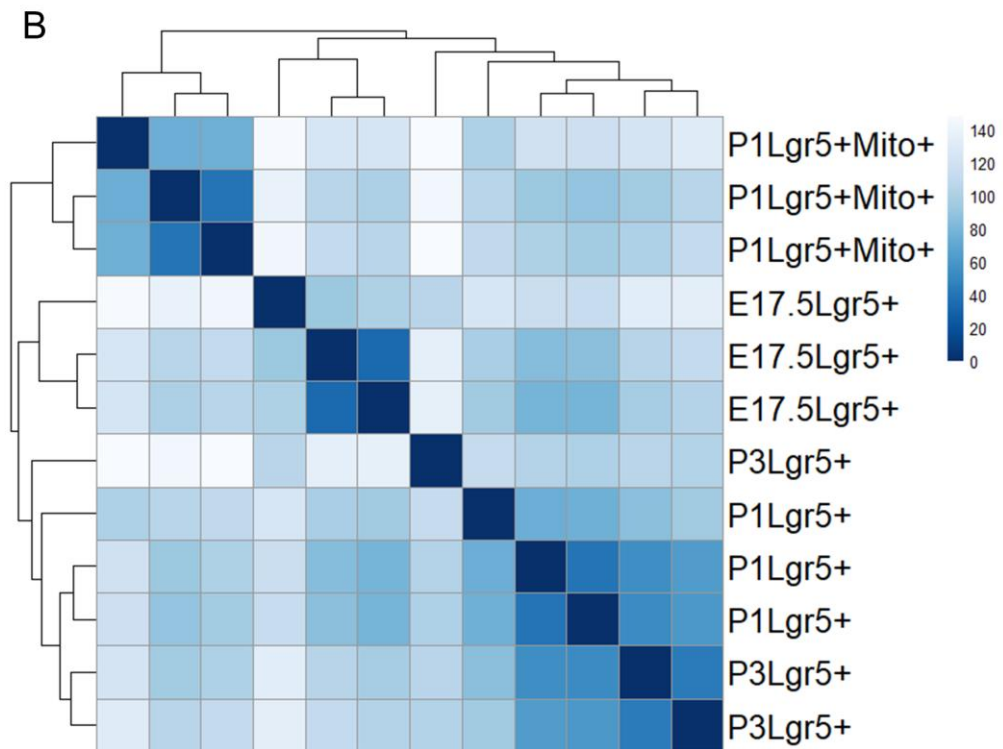
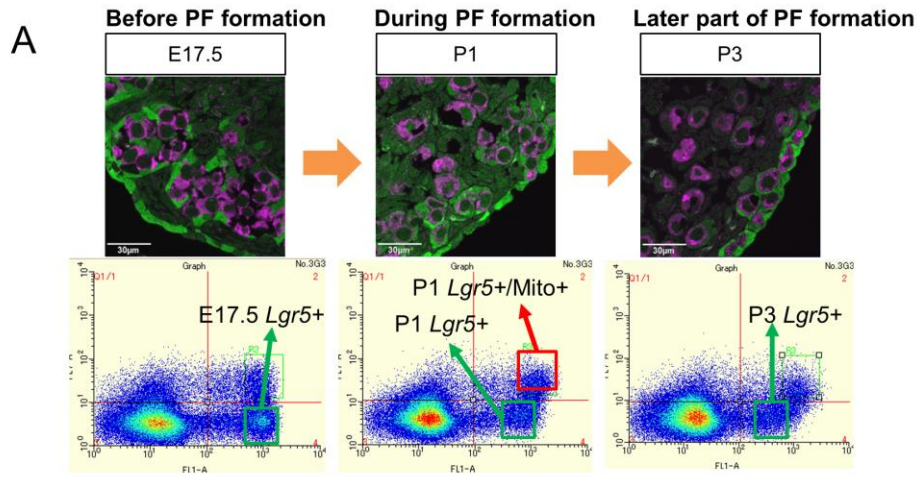


Figure 18 continued

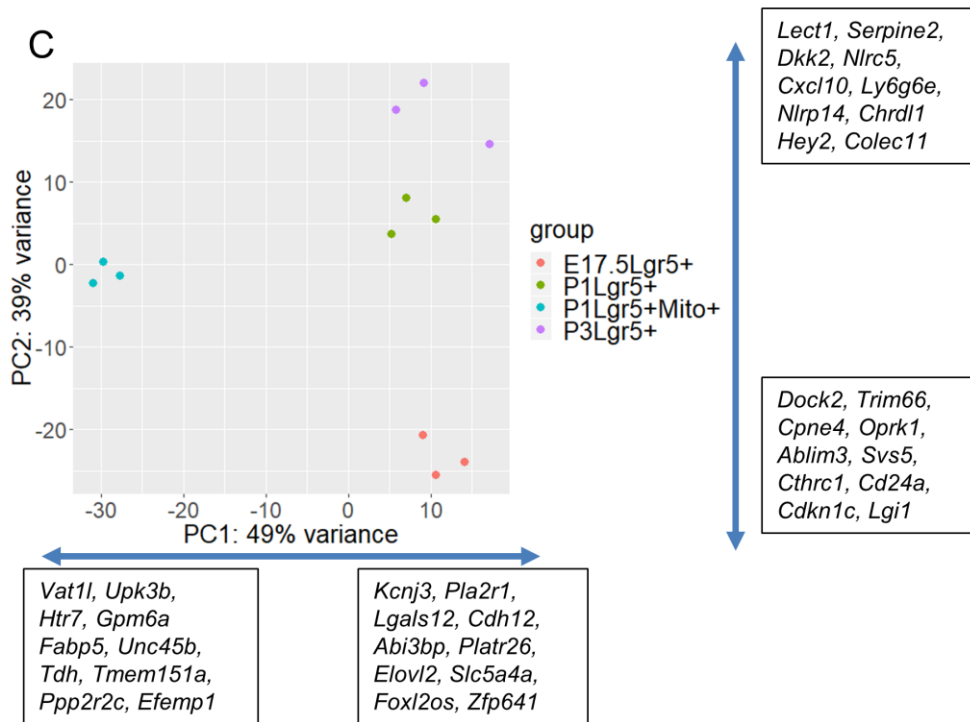


Figure 18. Transcriptome analysis for pre-granulosa cell progenitor during primordial follicle formation

(A) Cells used for transcriptome analysis were collected from E17.5 (left panel), P1 (middle panel) and P3 (right panel) ovaries. GFP+/ Mito + and GFP+ cells were collected from red and green squires, respectively. Upper panels show immunostaining images of E17.5, P1 and P3 ovaries using antibodies against for GFP (green), MVH (blue), and FOXL2 (magenta). (B) A heat map of sample to sample distance matrix represents overview of similarity. Darker color shows higher similarity and light color shows lower similarity. (C) Principal Component Analysis (PCA) of pre-G during PF formation for the first two axes. X and Y axes represent PC1 and PC2, respectively. Each replicate is plotted as an individual data point of E17.5 (red dot), P1(green dot), P3(purple) *Lgr5*-single positive cells and P1 *Lgr5*/ Mitotracker double positive cells(blue). Percentage of variance for PC1 and PC2 is 49 and 39%, respectively. The top 10 variable gene for PC1 and PC2 in each direction is represented in black Square.

Figure 19

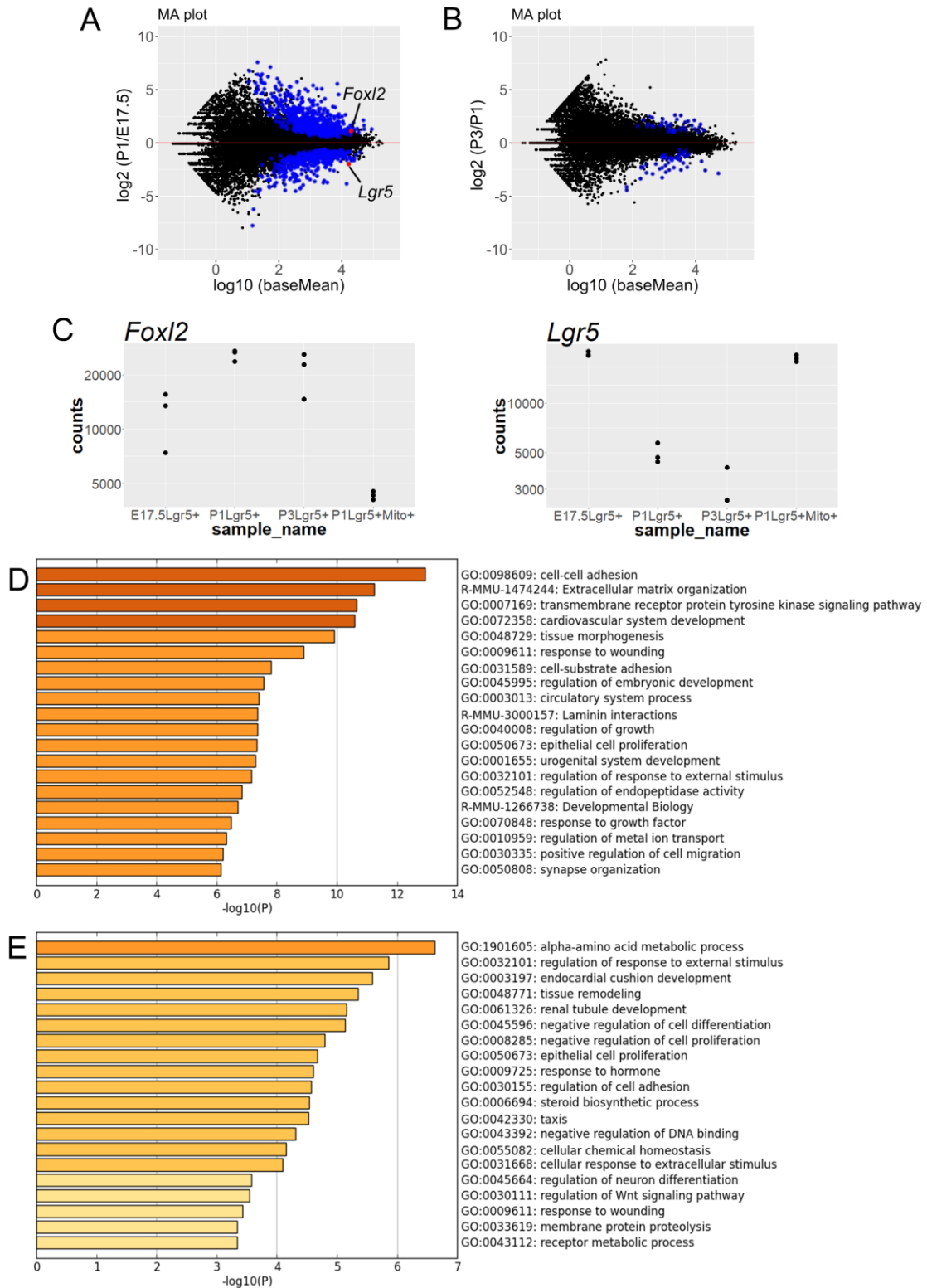


Figure 19. Enrichment analysis for up- and down- regulated DEGs

(A) MA plot of P1 vs E17.5 comparison. All genes used for analysis are shown in black dots. Blue dots represent genes passing significance threshold ($\text{padj} < 0.01$). Red dots represent *Foxl2* and *Lgr5*. (B) MA plot of P1 vs P3 comparison. All genes used for analysis are shown in black dots. Blue dots represent genes passing significance threshold ($\text{padj} < 0.01$). (C) Dot plot show the expression level of *Foxl2* and *Lgr5* obtained from RNA-seq data of each sample. (D) Enrichment analysis for DEGs which represent padj is less than 0.01 and 2-fold up-regulation in P1 as E17.5 comparison. Horizontal axis represent $-\log_{10}$ (p-value). (E) Enrichment analysis for DEGs which represent padj is less than 0.01 and 2-fold down-regulation in P1 as E17.5 comparison Horizontal axis of bar graph represent $-\log_{10}$ (p-value).

Figure 20

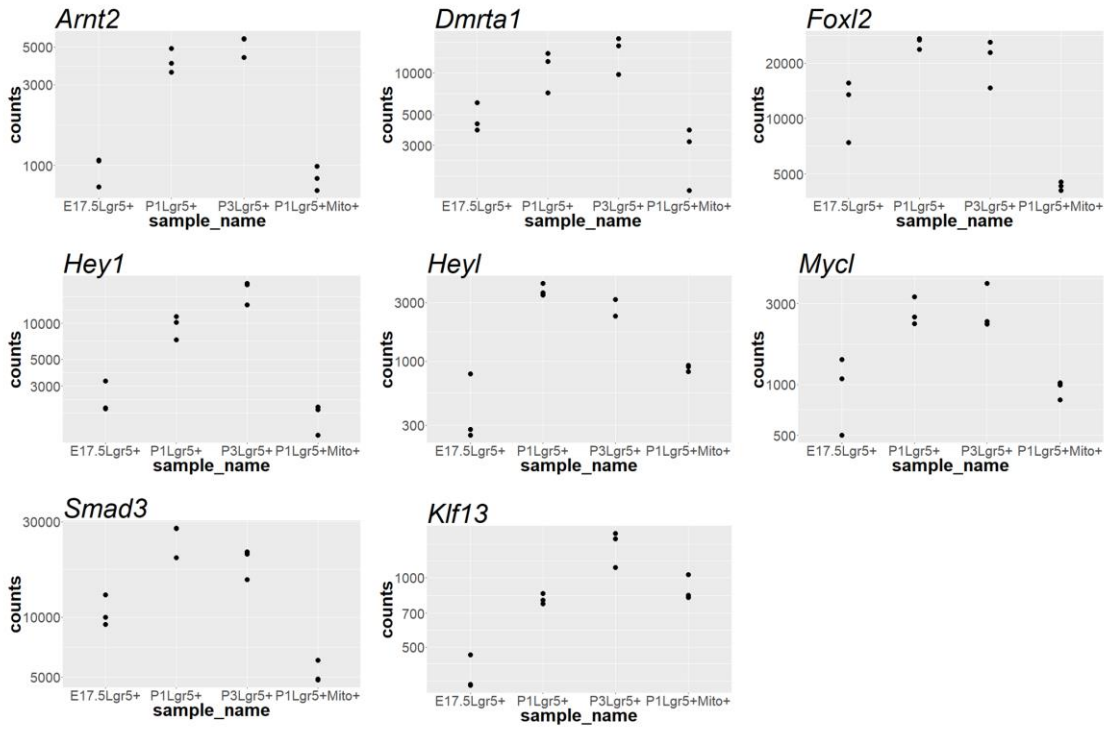


Figure 20. TFs in up-regulated DEGs

Dot plot show the expression level of TFs in up-regulated DEGs between E17.5 to P1 which represent baseMean >1000.

Figure 21

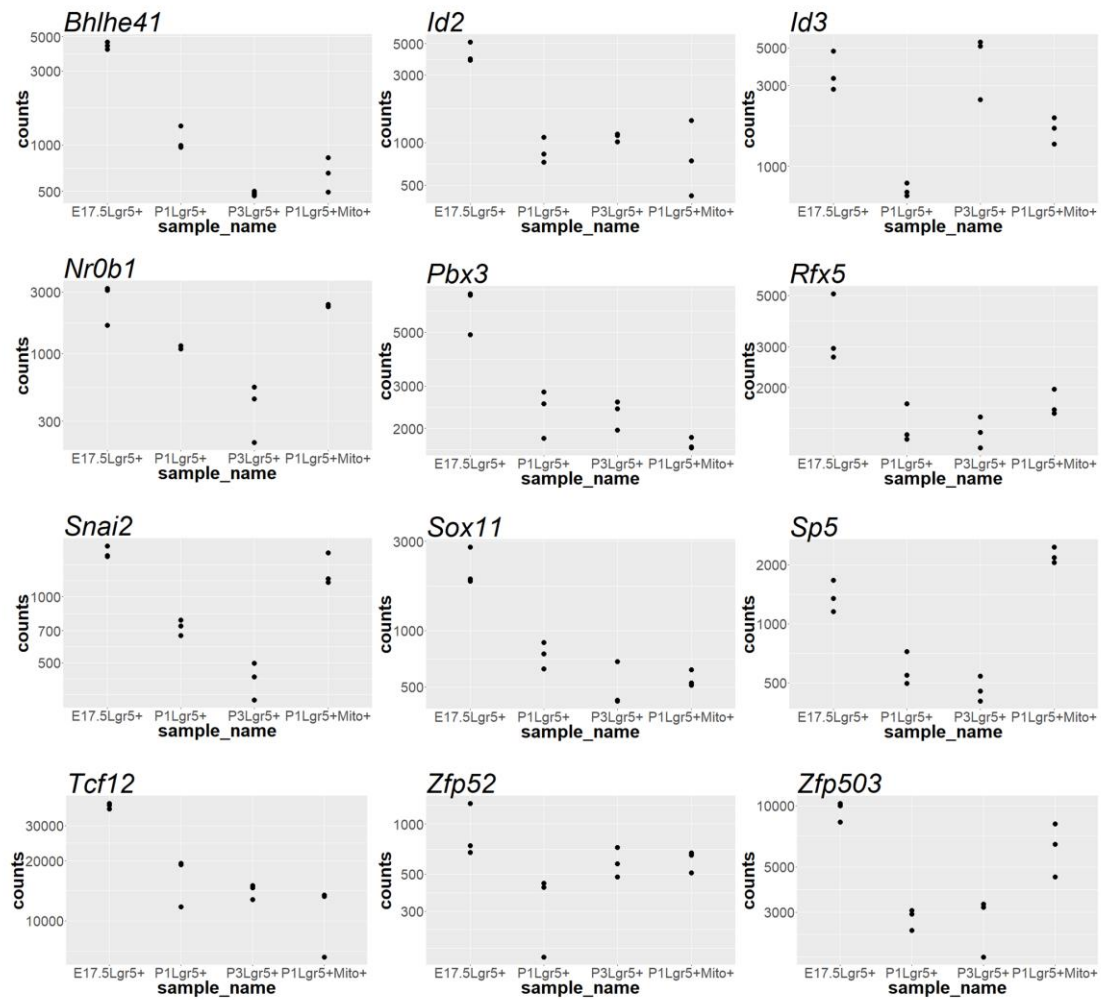


Figure 21. TFs in down-regulated DEGs

Dot plot show the expression level of TFs in down-regulated DEGs between E17.5 to P1 which represent baseMean >1000.

Figure 22

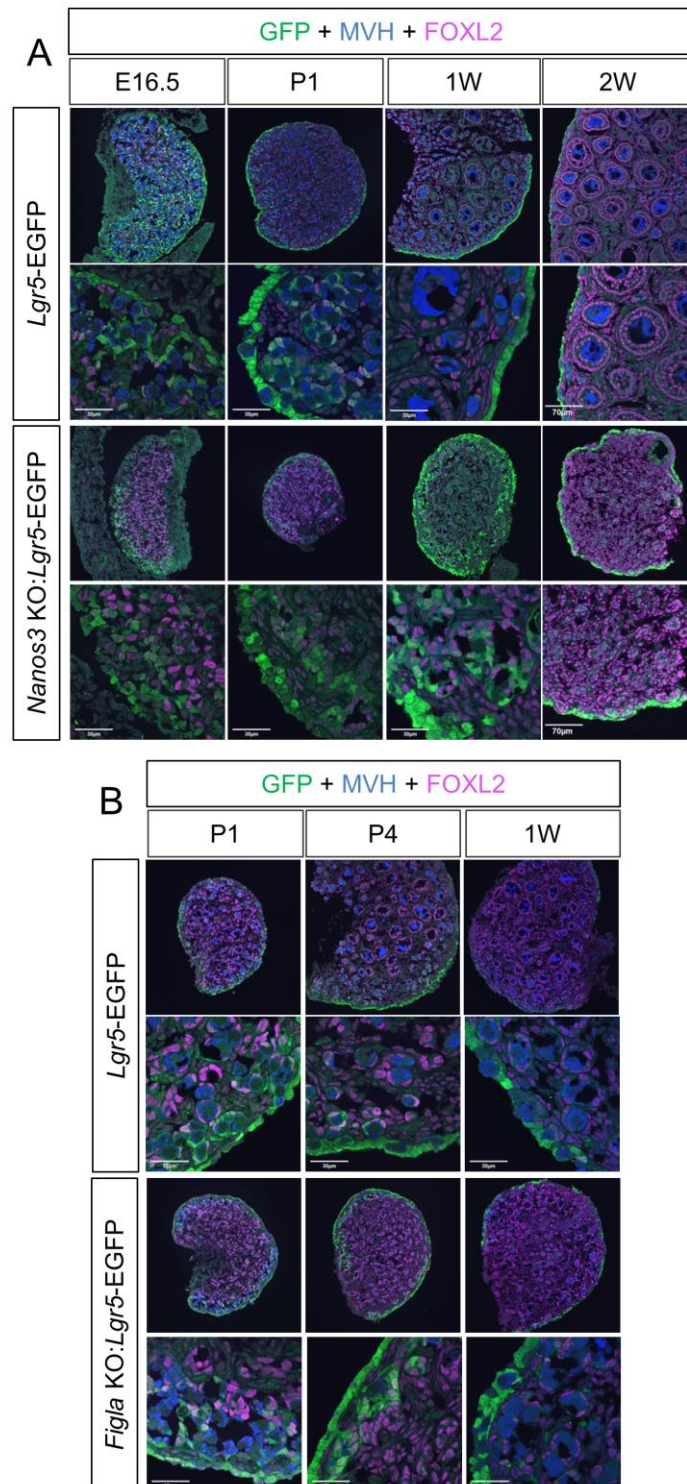
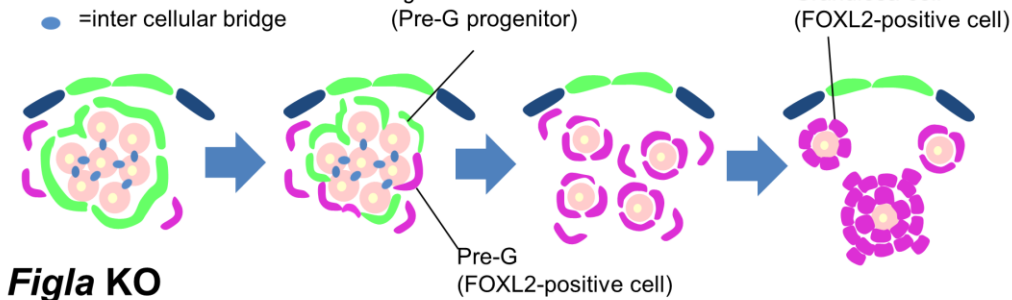


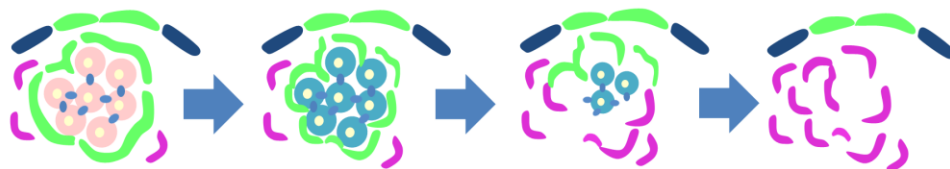
Figure 22 continued

C

Control



Figla KO



Pre-G cell differentiation was delayed even in the PF formation defective mutant.

Nanos3 KO

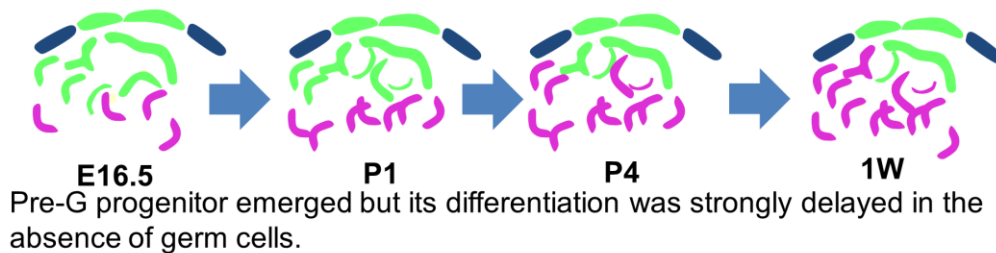
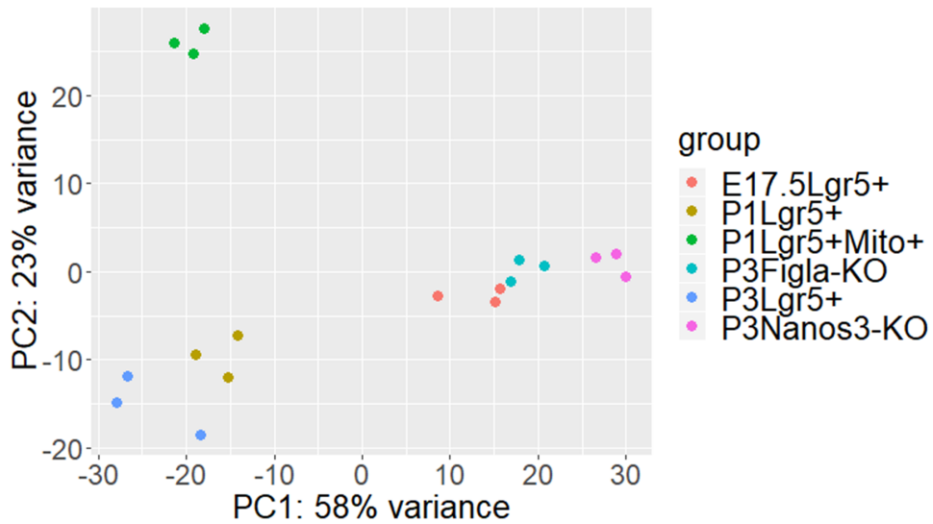


Figure 22. Germ cell-defects delay pre-G differentiation

(A) Immunohistochemical analysis of control and *Nanos3*-KO ovaries at E16.5, P1, 1W and 2W using antibodies against for GFP (green), MVH (blue), and FOXL2 (magenta). Scale bars, 30 μ m in E16.5 to 1W and 70 μ m in 2W. (B) Immunohistochemical analysis of control and *Figla*-KO ovaries at P1, P4 and 1W using antibodies against for GFP (green), MVH (blue), and FOXL2 (magenta). Scale bars, 30 μ m. (C) Schematic summary of *Figla*- and *Nanos3*- KO phenotypes. In the control, pre-G progenitor (shown in green) closely attached to germ line cyst around E16.5 and gradually invade between germ cells with differentiation into pre-G cells (shown in magenta) in P1. Most of pre-G progenitor differentiate into pre-G in P4 and started to follicle growth after that like 1W. As *Figla*-KO ovary causes defect around birth, there are no apparent defects in embryonic stage compared to control but its differentiation was strongly delayed. Different from control, P4 *Figla*-KO ovary still contains pre-G progenitor inner side of the ovary, yet these retained pre-G is finally differentiate into *Foxl2* positive cells. In the case of germ cell less mutant, *Nanos3*-KO, pre-G cells were emerged in embryonic stage but its differentiation was strongly delayed more than *Figla*-KO like 1W.

Figure 23

A



B

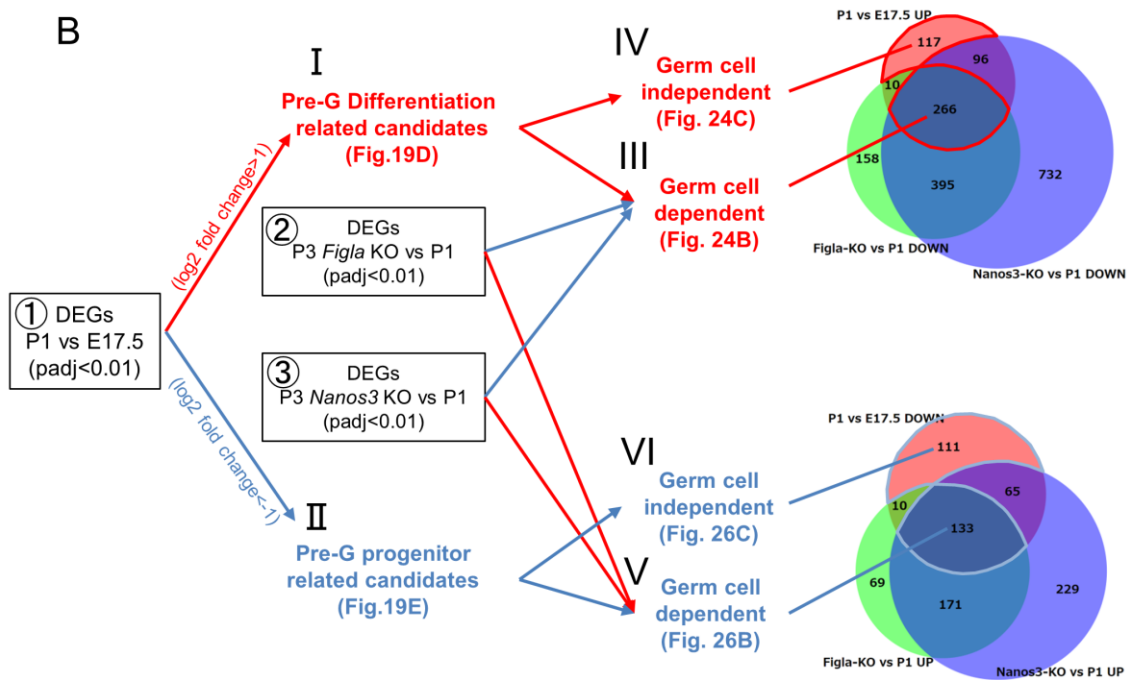


Figure 23. Transcriptome analysis of germ cell defective mutants.

(A) PCA of pre-G from control and germ cell defective mutants for the first two axes. X and Y axes represent PC1 and PC2, respectively. Each replicate is plotted as an individual data point of E17.5 (red), P1(yellow), P3(blue) *Lgr5*-single positive cells, P1 Mitotracker/*Lgr5* double positive cells (green) from control and P3 germ cell defective mutant, *Figla*-KO (light blue) and *Nanos3*-KO (pink). Percentage of variance for PC1 and PC2 is 58 and 23%, respectively. (B) Schematic summary of transcriptome analysis in this study. I used DEGs which shows $\text{padj} < 0.01$ in all transcriptome results. Red arrows show up-regulated genes (fold change > 1) and blue arrows represent down-regulated genes (fold change < -1). To classify the genes whose expression was up- and down-regulated in a germ cell-dependent or -independent manner, DEGs from P1 vs E17.5 of the control embryos (①) were compared with DEGs from *Figla*- and *Nanos3*-KO (② and ③). I, up-regulated genes from E17.5 to P1; II, down-regulated genes from E17.5 to P1; III, genes up-regulated from E17.5 to P1 and down-regulated in germ cell-defective mutants; IV, genes up-regulated from E17.5 to P1 without significant expression changes in germ cell-defective mutants; V, genes down-regulated from E17.5 to P1 without significant expression changes in germ cell-defective mutants; VI, genes down-regulated from E17.5 to P1 and up-regulated in germ cell-defective mutants. This comparison is also shown in Venn diagram in right side. Number in Venn diagram corresponds to DEGs picked up as germ cell-dependent or -independent genes.

Figure 24

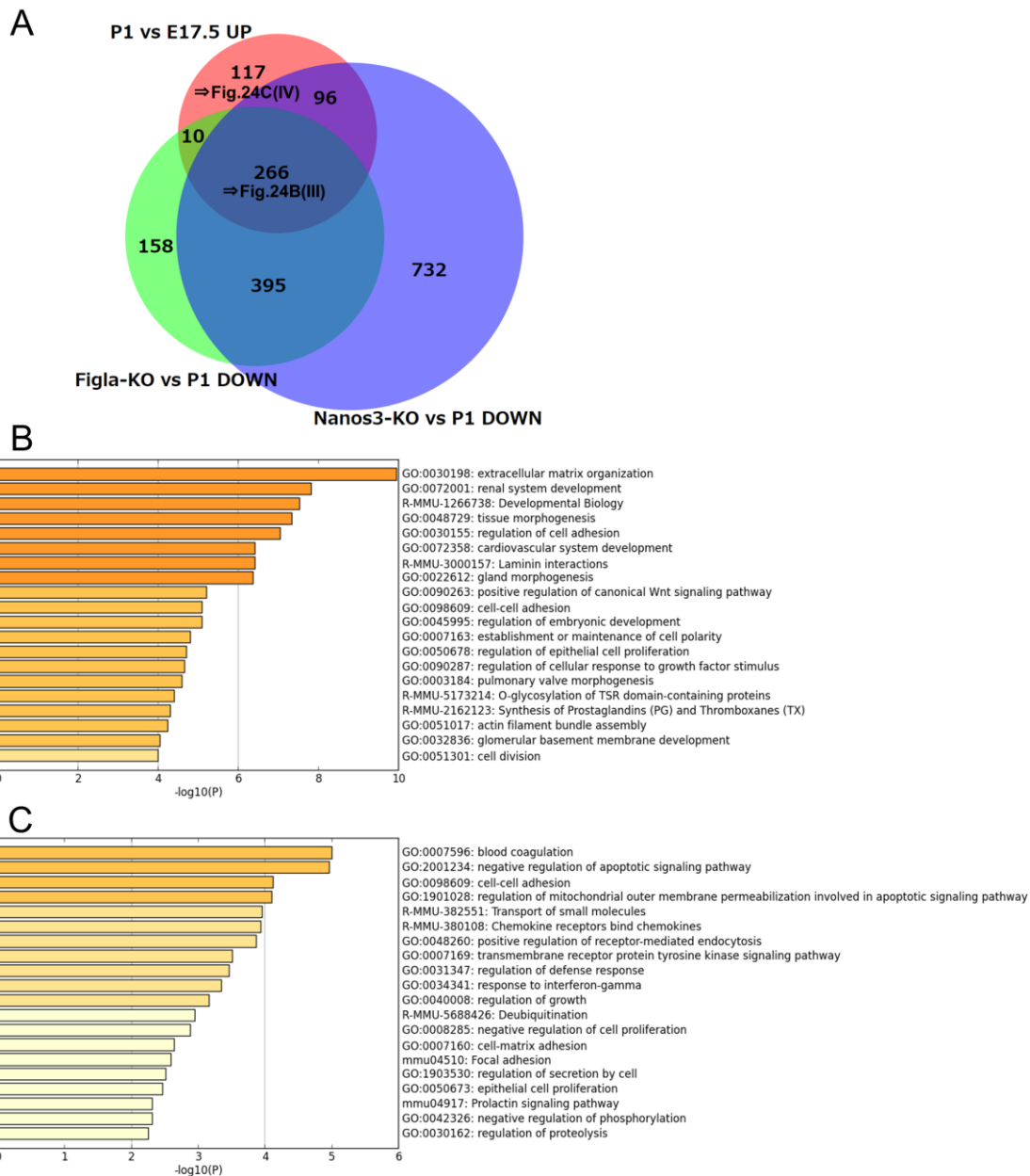
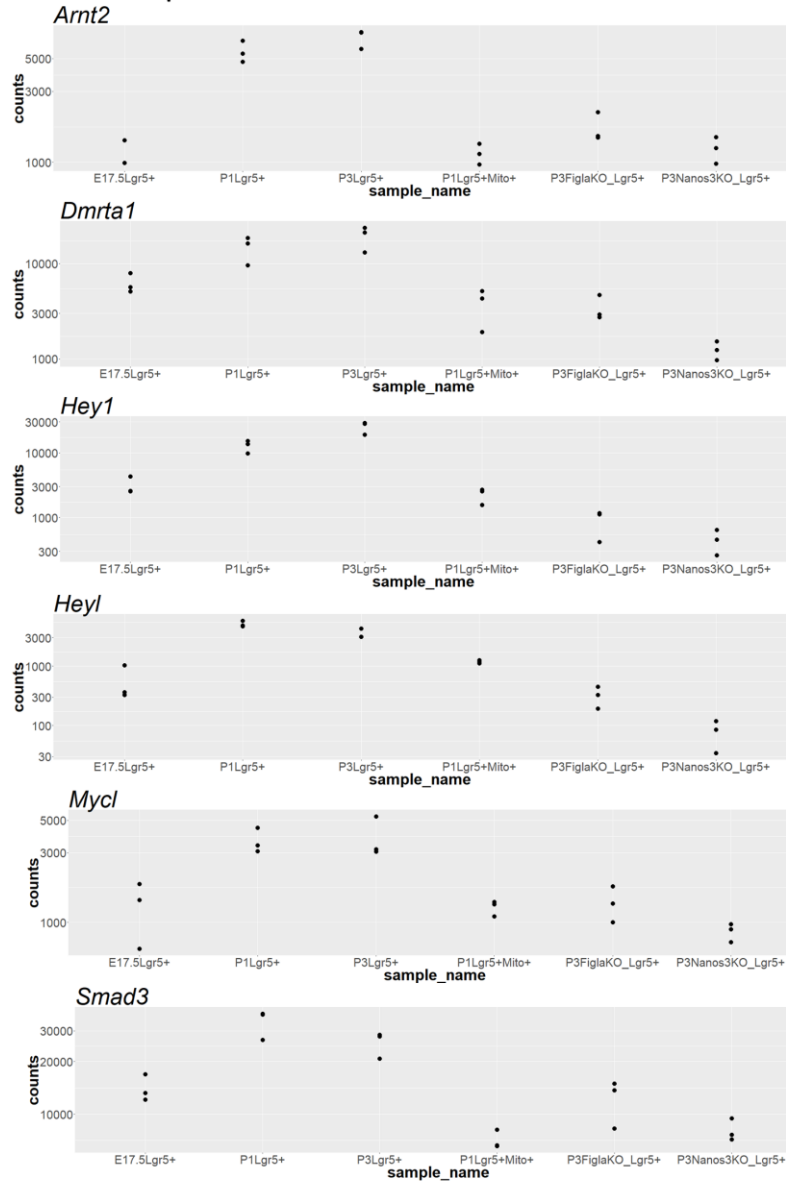


Figure 24. Classification of up-regulated gene in P1 vs E17.5 as germ cell -dependent or -independent candidates

(A) Venn diagram of up-regulated genes in P1 vs E17.5 (pink circle) and down-regulated gene in *Figla*-KO and *Nanos3*-KO (green and blue circle, respectively). Number represent in a diagram represents number of genes contained in each region. (B) Enrichment analysis for germ cell -dependent 266 genes which overlapped all genotypes in Fig. 24A. Horizontal axis of bar graph represents $-\log_{10}(p\text{-value})$. (C) Enrichment analysis for germ cell-independent 117 genes which is only listed in P1vs E17.5 comparison in Fig. 24A. Horizontal axis of bar graph represents $-\log_{10}(p\text{-value})$.

Figure 25

A Germ cell dependent TFs



B Germ cell independent TFs

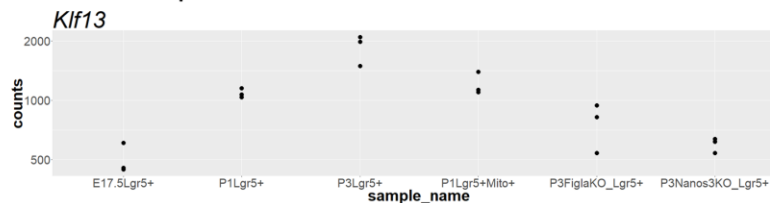
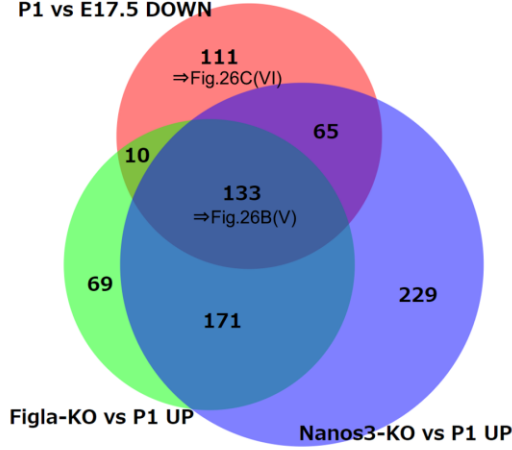


Figure 24. Classification of up-regulated TFs in P1 vs E17.5 as germ cell -depend or -independent candidates

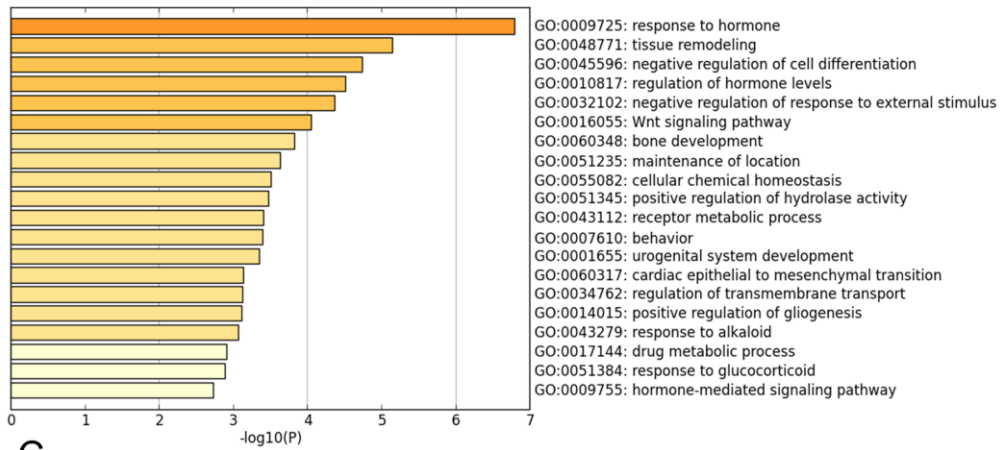
Dot plot showing expression level of TFs which include in germ cell-dependent (A) and -independent (B) candidates of up-regulated DEGs between E17.5 to P1.

Figure 26

A P1 vs E17.5 DOWN



B



C

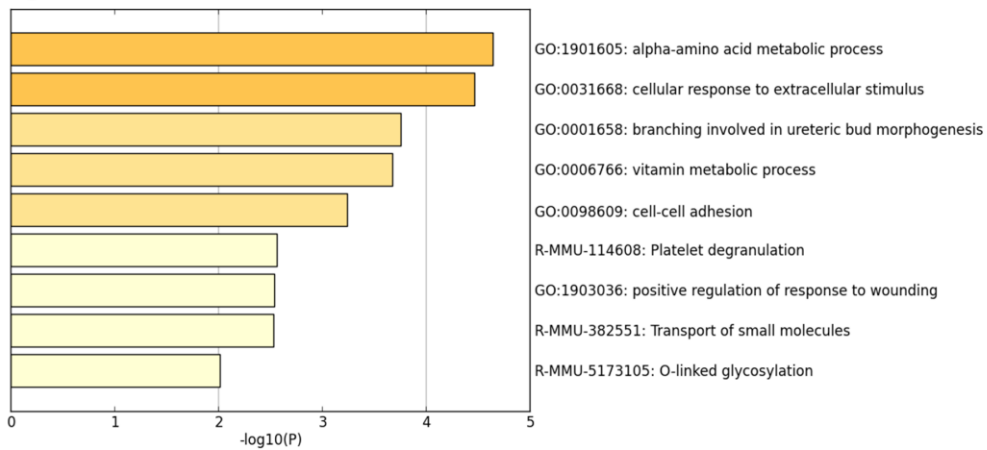


Figure 26. Classification of down-regulated gene in P1 vs E17.5 as germ cell-depend or -independent candidates

(A) Venn diagram for down-regulated gene in P1 vs E17.5 (pink circle) and up-regulated gene in *Figla*-KO and *Nanos3*-KO (green and blue circle, respectively). Number represent in a diagram represents number of genes contained in each region. (B) Enrichment analysis for germ cell-dependent 133 genes which overlapped all genotypes in Fig. 26A. Horizontal axis of bar graph represent $-\log_{10}(\text{p-value})$. (C) Enrichment analysis for germ cell-independent 111 genes which is only listed in P1vs E17.5 comparison in Fig. 26A. Horizontal axis of bar graph represent $-\log_{10}(\text{p-value})$.

Figure 27

A

Germ cell dependent TFs

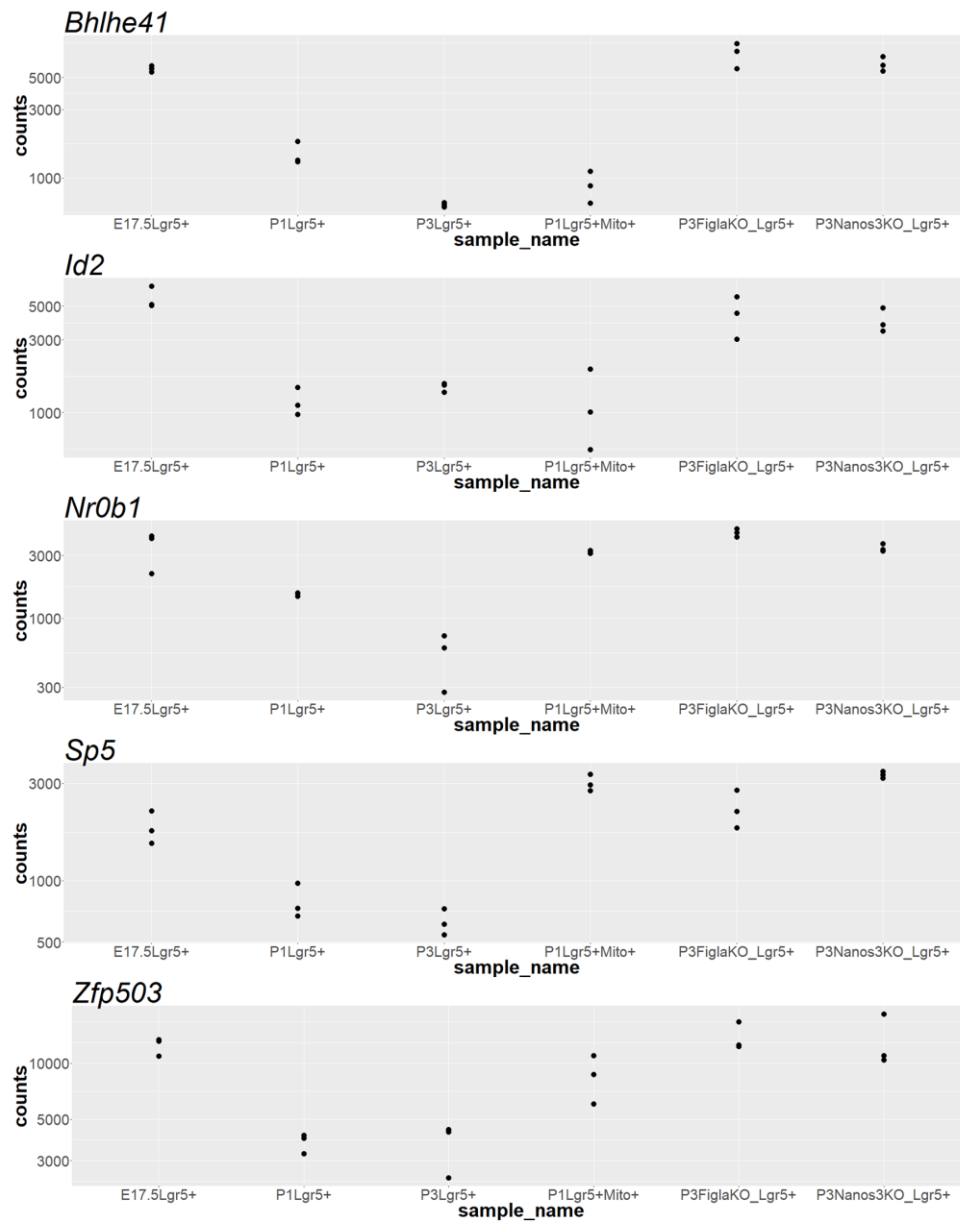


Figure 27 continued

B

Germ cell independent TFs

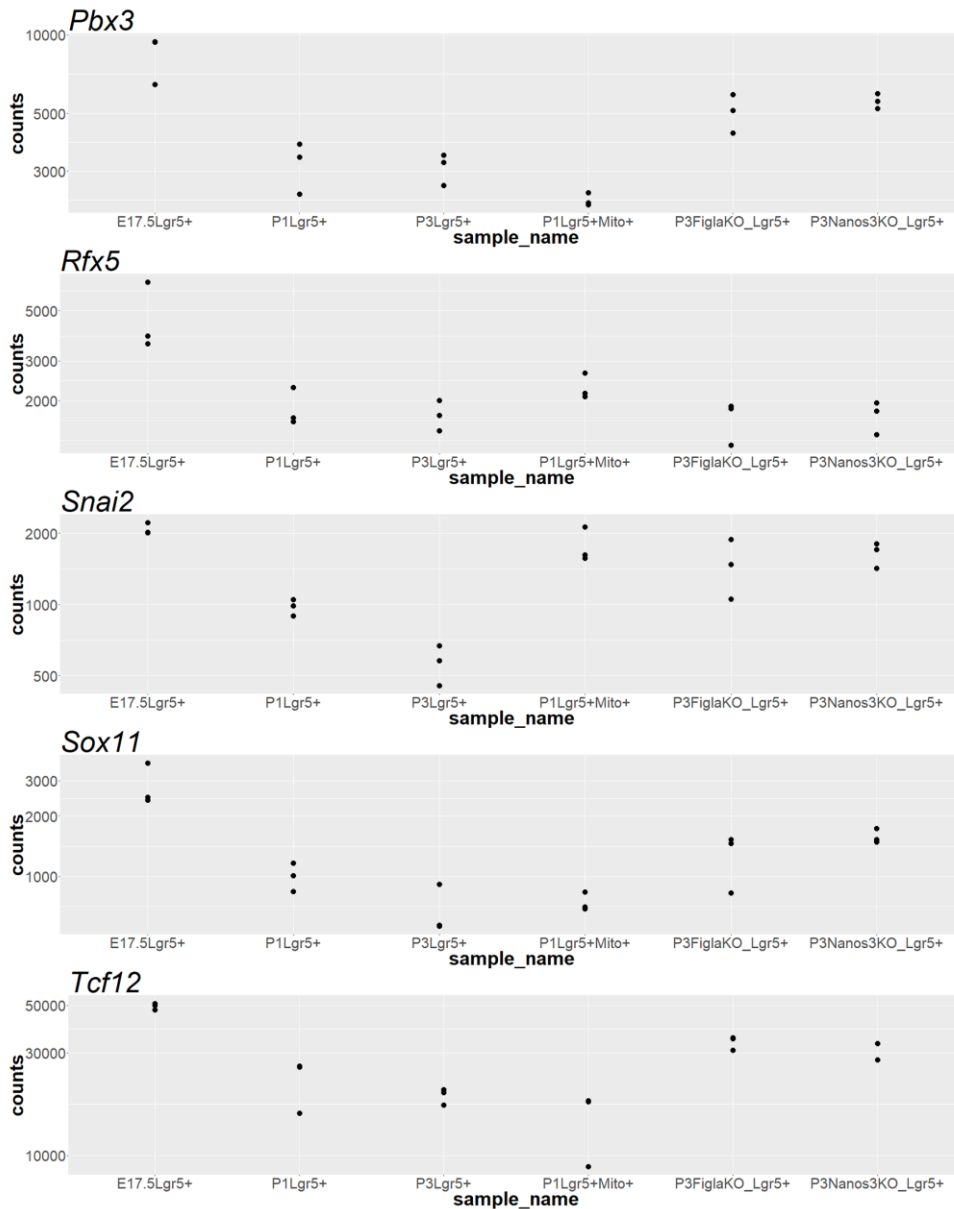


Figure 27. Classification of down-regulated TFs in P1 vs E17.5 as germ cell -dependent or -independent candidates

Dot plot showing expression level of TFs which include in germ cell-dependent (A) and -independent (B) candidates of down-regulated DEGs between E17.5 to P1.

Figure 28

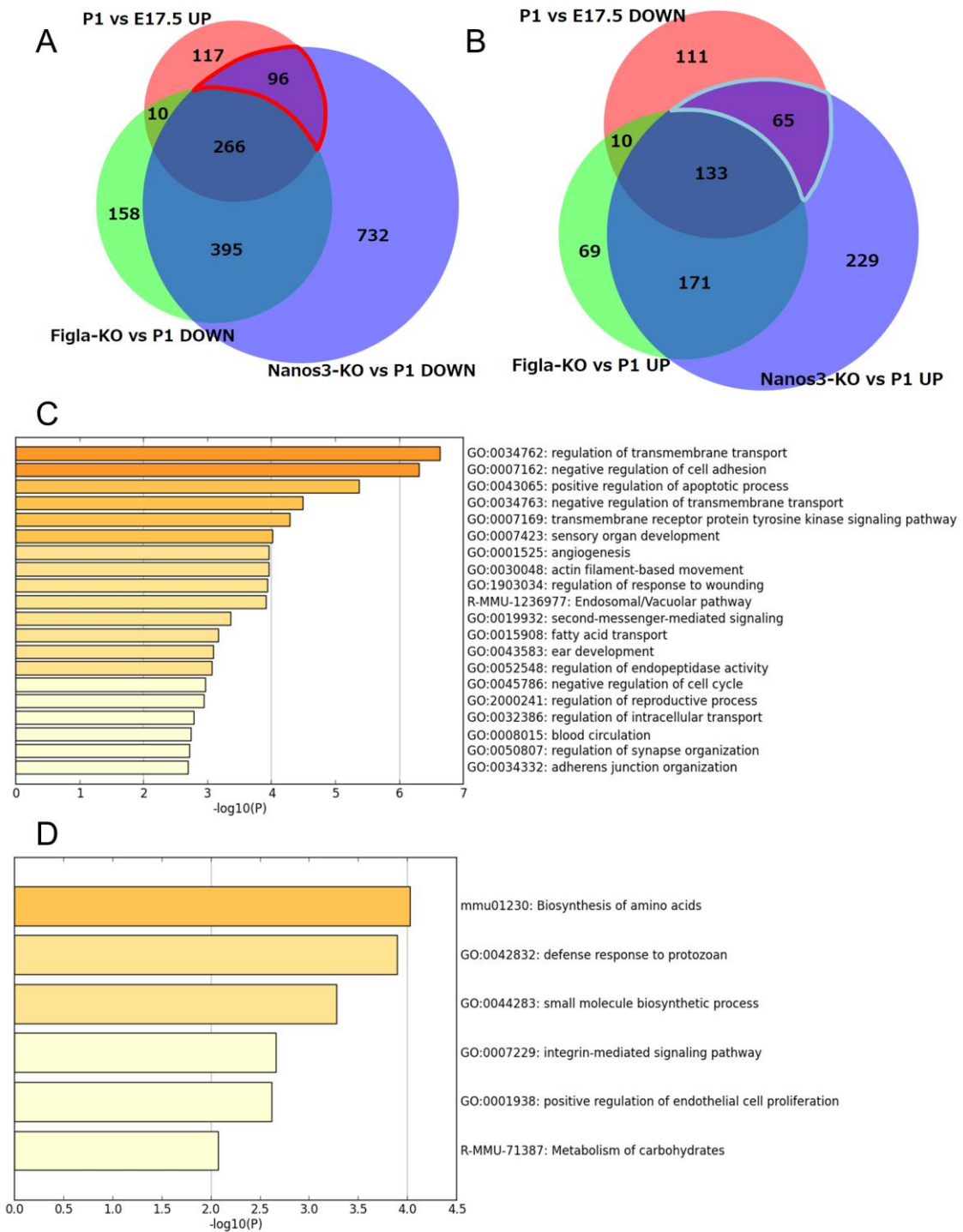


Figure 28. Enrichment analysis for Germ cell-dependent candidates which expression established earlier than PF formation

(A) Venn diagram for up-regulated gene in P1 vs E17.5 (pink circle) and down-regulated gene in *Figla*-KO and *Nanos3*-KO (green and blue circle, respectively) same as shown in Fig. 23B and 24A. Number represent in a diagram represents number of genes contained in each region. Genes which enclosed by red line is thought as Germ cell-dependent candidates which expression established earlier than PF formation. **(B)** Venn diagram for down-regulated gene in P1 vs E17.5 (pink circle) and up-regulated gene in *Figla*-KO and *Nanos3*-KO (green and blue circle, respectively) same as shown in Fig. 23B and 26A. Number represent in a diagram represents number of genes contained in each region. Genes which enclosed by blue line is thought as Germ cell-dependent candidates which expression established earlier than PF formation. **(C)** Enrichment analysis for germ cell-dependent 96 genes which overlapped control and *Nanos3*-KO in Fig. 28A enclosed by red line. Horizontal axis of bar graph represent $-\log_{10}(\text{p-value})$. **(D)** Enrichment analysis for germ cell-dependent 65 genes which overlapped control and *Nanos3*-KO in Fig. 28B enclosed by blue line. Horizontal axis of bar graph represent $-\log_{10}(\text{p-value})$.

Figure 29

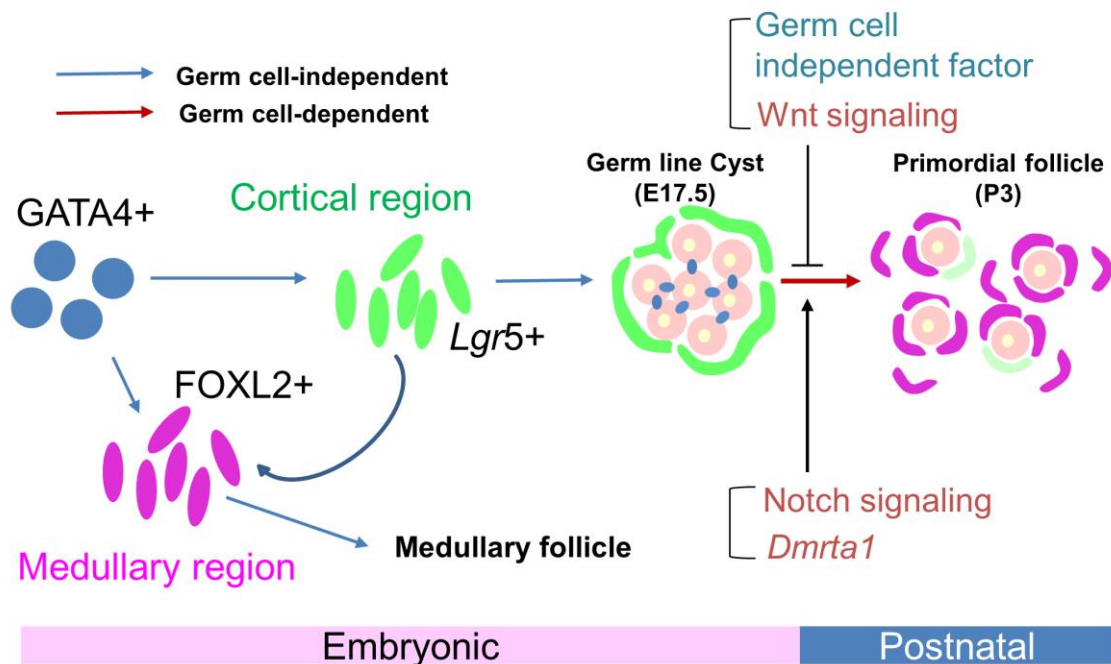


Figure 29. Schematic summary of transcriptome analysis for differentiating pre-G cell.

All pre-G lineage originates from GATA4+ cells (blue cell). Some of them directly differentiate into FOXL2+ cell(magenta) in early embryonic stage, which become medullary follicle and contribute to the fertility in young adulthood (not focused on this study). The other cells localized to cortical region marked by *Lgr5*+ cells (green) contribute to the fertility the rest of the reproductive life. A part of *Lgr5*+ cells differentiate into FOXL2+ during embryonic stage in a germ cell-independent manner. I found other *Lgr5*+ cells retained after differentiate to FOXL2+ cells in a germ cell-dependent manner. In pre-G progenitor, TGF- β (*Fst*, *Bmp2*) and Wnt signaling related factors may suppress differentiation of pre-G and PF formation. On the other hands, Notch signaling genes and *Dmrta1* are known to promote PF formation in a germ cell-dependent manner.